University “Federico II” of Naples, The Center for Advanced Biomaterials for Healthcare @
Istituto Italiano di Tecnologia

Azobenzene-based Biomaterials as Dynamic Cell Culture Systems

PhD thesis

PhD Program in Industrial Product and Process Engineering (XXXI cycle)

Selene De Martino

Tutor
Prof. Paolo A. Netti
Supervisor
Dr. Silvia Cavalli
Coordinator
Prof. Giuseppe Mensitieri

October 2016 − October 2018

AZOBENZENE-BASED BIOMATERIALS AS DYNAMIC CELL CULTURE SYSTEMS

A THESIS SUBMITTED IN PARTIAL FULFILLMENT OF THE

REQUIREMENT FOR THE DEGREE OF DOCTOR OF

PHILOSOPHY IN

INDUSTRIAL PRODUCTS AND PROCESS ENGINEERING

AUTHOR

Selene De Martino

SUPERVISOR

Prof. Dr. Paolo A. Netti

ADVISORS

Dr. Silvia Cavalli

COORDINATOR

Prof. Dr. Giuseppe Mensitieri

COLLABORATION

Prof. Bianxiao Cui of Stanford University, CA (SU).

Table of Contents

Chapter 1

Introduction

1.1 Tissue Engineering

Tissue engineering is a multidisciplinary research area, which involves several contributions from biology, medicine and engineering, all merged in the field of regenerative medicine. Its goal is to develop technologies to repair or replace tissues without the complication of chronic immuno-suppression.[1] More specifically, tissue engineering combines cells, scaffolds and bioactive factors to direct the *in vitro* formation of new tissues or organs. In order to recreate synthetic scaffolds with optimal properties to support cell attachment and tissue growth, tissue engineering is focused on in depth studies of the extracellular matrix (ECM).[2] The native ECM is a complex and dynamic network of proteins that provides both structural and biochemical support to surrounding cells.[3] For a long time, the ECM has been considered as a passive cell support, while recently this concept has been revisited.[4] In fact, the ECM is certainly recognized as an active structure able to promote, guide and sustain cellular functions. The interaction of cells with the ECM plays a key role in the regulation of multiple biological responses of cells. In fact, the ECM provides simultaneously mechanical, topographic, and biochemical cues that can influence cell attachment, morphology, proliferation, migration and differentiation.[5] The field of tissue engineering attempts to translate this knowledge to biomaterial science in order to have a rational control of cell-scaffold interaction. Biomaterials, defined as encompassing natural or synthetic materials that interact with biological systems, serve as the scaffolding upon which cells build tissues.[4] To sum up, tissue engineering research is currently focused on applying knowledge of the biological characteristics of native cellular environment to develop even more innovative and efficient biomaterial-based constructs and cell-instructive platforms.

1.2 Cell-Material Interaction

It is well known that a crosstalk occurs at the cell-material interface and it has a profound influence on the cell behavior.[6] Thus, revealing the basic role of each cues is extremely important in biomaterial development, cell biology, tissue engineering and regenerative medicine. Artificial matrixes, in fact, aim to mimic the ECM behavior, interacting with cells and instructing them in order to promote tissue

regeneration events. Understanding the interaction between the cell and its external environment is fundamental for replicating basic cell-ECM functions in biomaterials. As matter of fact, a big part of this field of research is focused on the development of new cell instructive materials (CIMs), as smart engineered environment that can stimulate cells and guide them to express specific biological features.[7] In particular, the possibility to pattern the material surface at relevant length-scales allows to selectively induce diverse cellular responses. Furthermore, the variation of biomaterials' properties such as stiffness, roughness, ligand density, surface charge, hydrophobicity can affect cell responses. In fact, different topographic features can activate certain mechanotransduction processes which are involved in complex biological progressions, such as morphogenesis, tissue repair, and tumor progression.[8-9] The mechanotransduction process can be described as a simple model where mechanical input influences cells' intrinsic mechanical properties which is then transduced into specific cellular outputs.[10] The cell-ECM communication is mediated by membrane receptors – e.g., integrins, laminin receptors and syndecans – or ECM-modifying proteins, such as matrix metallo proteinases (MMPs).[11] Integrins play a crosstalking role during the biological recognition and signaling events between the ECM outside the cell and the cytoskeleton inside the cell. Each integrin consists of a heterodimer made from one α and one β subunit. Both subunits are type I transmembrane glycoproteins with relatively large extracellular domains.[11] The process of integrin-mediated cell adhesion comprises a cascade of four different, partly overlapping, events: cell attachment, cell spreading, organization of actin cytoskeleton and formation of focal adhesion. During these steps, integrins are involved in physical anchoring as well as in signal transduction processes through the cell membrane.[12] In summary, the cell-ECM crosstalk regulates, through integrins, the cell behavior by influencing cell proliferation, survival, shape, migration and differentiation. These processes are dynamically regulated because ECM is constantly undergoing remodeling, assembly and degradation particularly during the normal processes of development, differentiation and wound repair.[13,14] The development of novel biomaterials able to understand this crosstalk, mimicking the natural cell environment and influencing cell functions over time, is the current challenge in the tissue engineering.

1.3 Static Cell Instructive Materials (CIMs)

It is known that cells are sensitive to the chemical composition, physical properties and biologically functional moieties of artificial matrix where they are seeded.[6] These signals modulate cell adhesion, orientation, motility, and intracellular signaling pathways that regulate transcriptional activity and gene expression.[15] Many attempts have been carried out towards controlling the material surface with nano and micromachining approaches aiming to control cell guidance and polarization at the cell-material interface.[16] In particular, material surface properties can be modulated by physical patterning or creating other physical interactions such as chemical binding or charge injection.[17] In the case of surface patterning, micron, submicron and nanoscale topographies of diverse shapes can regulate different cellular response such as proliferation, migration, and differentiation.[18-21] It is interesting to note that different cell types such as fibroblasts, osteoblasts, epithelial cells, neuronal cells, and more recently stem cells have dissimilar responses.[22] One of the main goals in biomaterials' design is to mimic the structure and function of the native ECM. While the chemical factor effects on cell behavior have been extensively analyzed, topographic cues are relatively less explored.[23] Almost a century ago, the earliest surface morphology effect on cells was discovered and it was found that cells topographic cues, independent of biochemistry, may have significant effects upon cellular behavior. The cell response to topographies depends on cell type, cell-cell interactions, and the geometry of the patterns.[6] However, the most relevant effects are observed when topographies exhibit dimensions comparable to those of cells. It is reported that patterns in the range of 70 nm up to 2-5 μm show relevant effects on cells.[6] Furthermore, the presence of nanometric features alter the surface properties of materials (surface energy, wettability) modifying also the preferred protein adsorption. In this way, the geometric characteristic of topographic patterns creates also a chemical pattern making some surfaces more accessible (i.e. the top of ridges and pillars) than others (i.e. bottom of grooves and pits) for cell lamellipodia and filopodia adhesion.[6] With the development of advanced materials, surface patterning affords a unique and powerful tool to understand cell–material interactions.[24] Many studies have been conducted on features in the micrometer range but recently nanoscale topography has received major attention because of its resemblance to *in vivo* surroundings.[25] For instance, the investigation of the native basement membranes from a variety of animal sources has demonstrated that ECM layers possess a complex topography consisting of intertwining fibers mixed with meshwork of pores, ridges and other features of micro-nanometer sized dimensions.[26] [21] Reproducing the linear pattern *in vivo*, generally results in significant alterations to cell morphology and cytoskeletal arrangement, specifically cells align along the long axis of the groove with actin and microtubules also organized parallel to grooves.[27-28] Hamilton *et al.* investigated the adhesion,

spreading and migration of human periodontal ligament (PDL) fibroblasts in response to continuous and discontinuous topographic cues in the nanometric range. They showed that PDL fibroblasts adhered to and spread on all tested surfaces, with initial spreading and focal adhesion formation slower on discontinuous nanogrooves while they appeared highly elongated on both types of nanogrooves after 24 h post seeding.[29] Ahn *et al.* investigated topographies constituted by nanopots with variable nanopost densities able to guide hMSCs making different cell fate decisions.[30] In particular, osteogenic differentiation was favored by greater distance between posts, whereas smaller post-to-post distances were associated with adipogenesis.[30] In general, a variation of topographic features such as shape, size, distribution, height can differently instruct cells. For example, it was reported that expression of osteogenic markers of human mesenchymal stem cell (hMSCs) enhanced both on nanopits randomly placed (50 nm holes),[31] nanotubes (100 nm diameter) and ridge/groove with 400 nm pitch.[25] Until now, a large number of studies have fabricated substrates that contain microscale and nanoscale features on otherwise 2D surfaces. It is important bear in mind that these substrates only provide cues to the portion of the cell that is in contact with the surface and essentially limit cell motility to two dimensions. This property, for example, induces to polarize only a segment of the cell's membrane that can interact with the ECM and neighboring cells, leaving the rest of the cell exposed to a different environment. Biological processes analyzed on 2D substrates can bring to imprecise results because they are limited in their complexity compared to the native tissue environment.[32]

Effectively, also if 2D cell constructs have provided the base for our nascent interpretation of complex biological phenomena, we can agree upon insufficiency of examining hierarchical biology in just two dimension. Therefore, realization of the well-defined 3D artificial ECM is important from the perspective of tissue growth for systematic studies of fundamental aspects of 3D cell–cell and cell–matrix interactions *in vitro*. As a result, biologists and bioengineers alike have investigated many three-dimensional scaffolds that recapitulate aspects of the native cellular microenvironment for *in vitro* cell culture. For example, Liu *et al.* reported a study where they compared how various biomaterial-based culture conditions, e.g., 2D vs. 3D scaffolds and static vs. dynamic, were able to influence the global gene expression profile of differentiated embryonic stem cell (ES).[33] They reported a higher expression level of extracellular matrix (ECM)-related genes on 3D dynamic scaffolds compared to 2D scaffolds and 3D static scaffolds. Effectively, a 3D scaffold possesses major characteristics resembling those of the 3D-cell environment. Fibrous collagen or matrigel matrices have been commonly used to study 3D cell behavior, but these matrices have a random pore size and are structurally and chemically ill-defined. So much attention has been focused on materials that can demonstrate a distinct efficacy as matrices for 3D cell culture.[34] Hydrogels are an important

class of soft materials that can be fabricated in the form of 3D microperiodic structures.[35-37] Bioprinting of 3D hydrogels has emerged as a powerful alternative for the fabrication of 3D structures (typically collagen, HA, alginate, photocured acrylates, or modified copolymers) with faithfully mimic the structures of native tissue.[38] Furthermore also the direct laser writing (DLW) is shown to be an advantageous and versatile technique to fabricate tailored 3D cell-culture scaffolds.[39] In particular, the two-photon polymerization (2PP) technique allows the realization of arbitrary 3D structures with submicron spatial resolution.[40] Ovsianikov et al. combined 2PP to fabricate highly porous 3D scaffolds of acrylated poly(ethylene glycol) and laser-induced forward transfer (LIFT) as a cell-seeding tool to produce arbitrary multicellular 3D constructs with unprecedented flexibility and precision.[41]

1.4 Dynamic CIMs

An ideal platform for the *in vitro* study of cellular response should include the fabrication of tridimensional structured platforms that are able, at the same time, to deliver biochemical, topographic and mechanical cues with a fine spatial-temporal control.[42] In order to unravel the complex mechanisms at the basis of cell-material interaction, many reports in the literature make use of advanced microfabrication techniques to structure both synthetic and nature-derived materials in complex 3D architectures with "smart" functionalities. We define smart, biomaterials able to change one or more of their properties when exposed to an external electrical, thermal, optical, and mechanical stimulus. So these responsive materials also defined as "Dynamic Cell Instructive Materials" have attracted considerable attention due to their potential to attain unprecedented levels of space/time control over biomolecular processes at engineered interfaces, including the control over reversibility of the signaling/cue. Therefore, *in vitro* platforms that recapitulate dynamic *in vivo* signaling can lead to an enhanced understanding of fundamental biological processes. For this reason, in the last years the scientific community has recently shown an increased effort to design dynamic substrates that can communicate active physical cues to cells in a more biomimetic context. Among different cues, as introduced above, topography plays an integral role in influencing cell behavior. Takayama and co-workers reported the first application of dynamic topography to cultured cell using reversible poly(dimethylsiloxane) (PDMS) surfaces. The C2C12 myoblast cell morphology was dynamically altered using surface array transitions. The initial wavy micropattern was obtained by plasma oxidizing, it was introduced and removed in the presence of cells applying and releasing compressive strain (Figure 1.1 a-d).[43] Also Guvendiver *et al.* reported a strain-responsive buckling

patterns on PDMS substrates used to dynamically and spatially control hMSCs organization. Preferential alignment of hMSCs was completely eliminated after the topography switch from patterned to flat, and could be reversibly repeated for several cycles.[44] Furthermore, also if these preliminary findings are innovative, these materials are not suitable for dynamic *in vitro* analysis because the pattern complexity and versatility are relatively limited. Kirschner and Anseth demonstrated the possibility to control *in real-time* cell morphology through the controlled erosion of a photolabile PEG-based hydrogel system with tunable microtopography. [45] hMSCs were initially seeded onto smooth surfaces, which were in turn patterned using photolithography into an anisotropic channel pattern and then an isotropic square pattern. Cells exhibited a round morphology on the smooth pattern, an elongated shape along the channels, and again a round morphology on isotropic squares.[45] An alternative approach to fabricating reversible surface features is by exploiting the unique properties of shape-memory polymers (SMPs). They are one of the most important examples of systems that can exposing a changing topographic signal by an external heat trigger. SMPs are a class of active materials that have the ability to memorize a permanent shape through crosslinking. They are manipulated and then fixed to a temporary shape by an immobilizing transition and later, they can recover the permanent shape by a triggering event. This behavior allows a change of superficial properties of materials. In the context of dynamic CIMs, the challenge is developing engineering biocompatible surfaces enable to strict regulate the shape-memory effect in terms of well-defined geometry and biologically relevant surface transformations under physiological conditions.[46] Henderson and coworker presented SMP substrates able to change surface topography during cell culture in order to control cell behavior.[47] They embossed on initially flat SMP substrate a temporary topography of parallel micron-scale grooves and successively, the shape memory was triggered through a change in temperature activation that allowed topographic transformation back to the original surface in the presence of mammalian cells.[47] Similar, Le *et al.* proposed a dynamic topographic control of mesenchymal stem cells by culture on responsive Poly(ε-caprolactone) surfaces. The cell morphology was switched from highly aligned to stellate shaped in response to a surface transformation between a 3 μm × 5 μm channel array and a planar surface at 37° C (Figure 1.1 ef).[46]

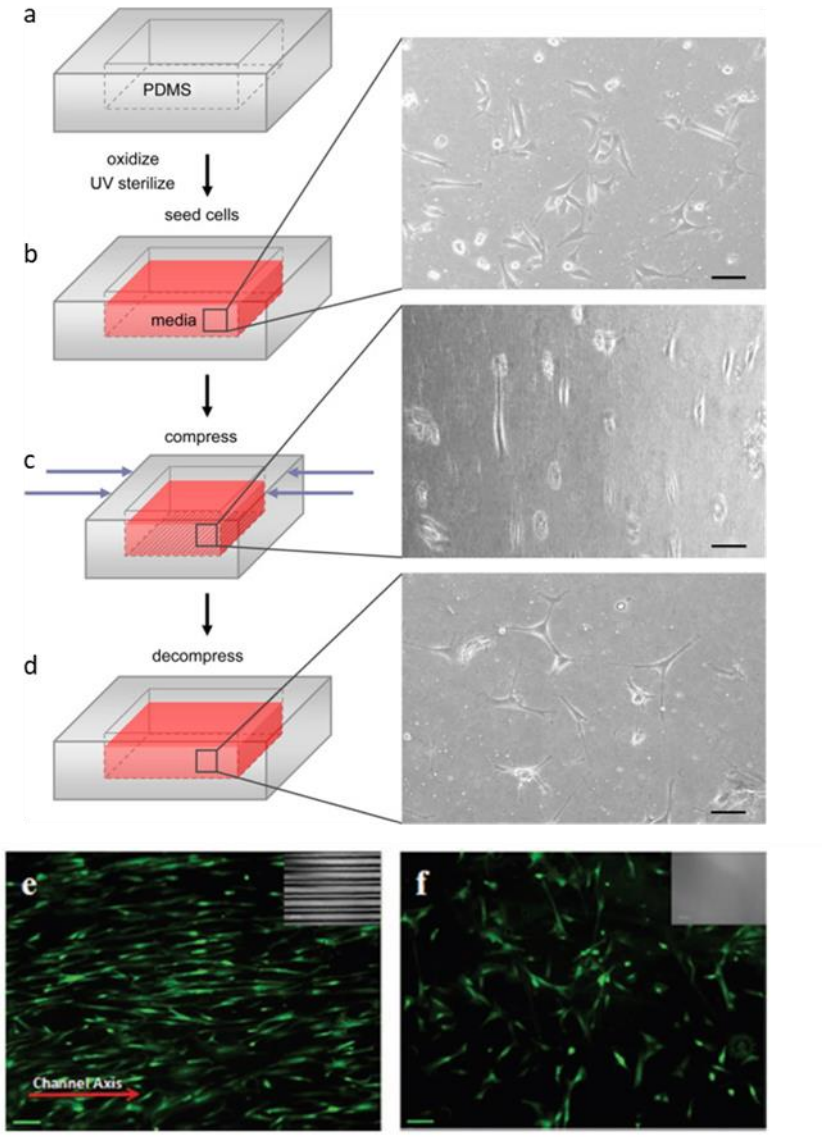

Figure 1.1 a-d (Left side) Schematic of the process of reversibly introducing microfeatures into the substrate surface; after being prepared for cell culture, substrates are compressed to obtain wavy features and uncompressed to remove the features. Micrographs (on the right) show cell behavior on the reconfigurable surface b) before c) during and d) after compression – cells orient from random to aligned and back to random. e) GFP-hMSC cells cultured on temporary 3 μm × 5 μm channel SMP arrays demonstrated significant alignment along the channel axis. f) The cell morphology changed to stellate shaped in response to the surface transformation, switching the patterned surface to flat by heat. (Reprinted from *Biomaterials* 2008, reference 43, and *Advanced materials* 2011 reference 46)

Some distinct advantages of the shape memory process are the ability to program complex shapes in many length scales (from the nano- to macroscales) but despite the promising results obtained with these materials, this shape-memory activity is often not reversible, or not suitable for biological applications.[48] In general, the external stimuli capable of regulating the 'on-off' features of surface properties are not limited to temperature alone. For example, light arises much interest among

possible external triggers (electric or magnetic field, heat etc.) because beyond its unique spatial and temporal controllability, it is a kind of clean energy, which can be manipulated conveniently and controlled *in situ.* In this context, interesting is to fabricate scaffolds with photoresponsive molecules include reversible photoresponsive azobenzene, spiropyran and irreversible photocleavable and photolinkable compounds.[49] Their photochemical reactions can be used to induce switching in surface physicochemical properties involving different mechanisms: photo dimerization, photo-induced intramolecular bonds or photo-isomerization. Nowadays, azobenzene is the most widely used molecule in light-controlled systems.[50-52] It has undoubtedly attracted most attention due to its strong photo-switching effect, simple molecular structure, reversibility, speed and simplicity of incorporation.[53] In fact, when illuminated with a specific type of light, the azobenzene molecules undergo to isomerization process from the more stable *trans* isomer to the less stable *cis* isomer, that can significant changes optical, geometric, mechanical and chemical properties of azobenzenes. Furthermore, these photo-induced variations can be often transferred from molecules to large host systems containing azobenzenes. In fact, interesting photo-mechanical effects come out when azobenzenes are incorporated into biopolymers and other polyelectrolytes.[54]

1.5 Azobenzene

Azobenzene is an aromatic molecule in which an azo linkage (-N=N-) joins two phenyl rings. It undergoes a rapid and reversible photoisomerization, converting between the stable trans configuration and a meta-stable cis form (Figure 1.2).

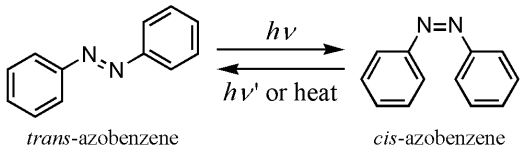

Figure 1.2 Photoisomerization of azobenzene

This photoisomerization is completely reversible and free from side reactions. *Trans* azobenzene is near planar with a dipolar moment around zero. It shows a n-π* band at 440 nm and a strong π-π* transition near 320 nm. *Cis* azobenzene adopts a bent conformation with a dipolar moment different from zero. It also has a strong n-π* band near 440 nm and shorter wavelengths bands at 280 nm and 250 nm. Upon irradiation, a fraction of the trans azobenzene is converted to the cis form, which can thermally revert to the more stable trans state on a timescale dictated by the particular substitution pattern of molecules. Thermal *cis-to-trans* relaxation, however, produces essentially 100% of the

trans isomer. This isomer can be regenerated also by irradiation at 450 nm on a picosecond timescale. Photophysical and photochemical properties of azobenzene derivatives strongly depend on the substituents on the azo groups.[48] As described by Rau *et al.*[55], the azo chromophores are typically divided into three classes, based upon spectroscopic characteristics: 1) azobenzene type molecules, which are similar to the unsubstituted azobenzene with a low-intensity n-π* band in the visible region and a much stronger π-π* band in the UV; 2) aminoazobenzene-type molecules, which are ortho or para substituted with an electron-donating group, with the n-π* and π-π* bands much closer; 3) pseudo-stilbene, which are substituted at 4 and 4' positions with an electron-donating group and electron withdrawing group (Figure 1.3).

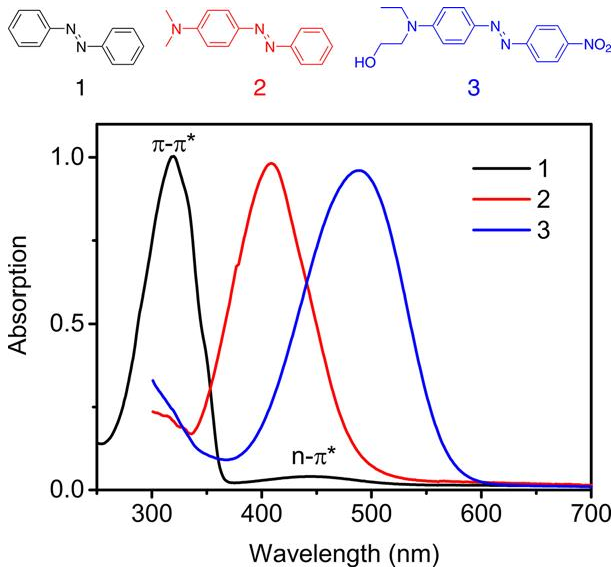

Figure 1.3 Chemical structures and UV/Vis absorption spectra of (1) azobenzenetype, (2) aminoazobenzene-type and (3) pseudo-stilbene-type azo compounds. (Reprinted from *Chemistry-A European Journal* 2017, reference 65)

In the latter case, the strong π → π * absorption with charge-transfer (CT) character is a dominant feature in the visible spectrum, and the n→ π * transition is hidden by this strong band. Substituents on the phenyl rings may strongly influence the position and shapes of the azobenzene absorption bands and the rate of thermal cis to trans relaxation. Azobenzenes with para donor substituents can show strongly red-shifted π-π* bands but at the same time faster thermal relaxation process. This behavior derived by similar dipolar character between the thermal transition state and the excited state. Azobenzenes can be synthetized with spectroscopic properties particularly appropriate for specific applications. Actually, substitutions at ortho position on the phenyl rings introduce steric effects able to slow the thermal relaxation process of cis-trans isomerization. This effect is not observed with para or meta substituted molecules on phenyl rings. In summary, by varying the nature of ortho substituents, together with the number and nature of meta and para substituents, it is possible

to tune spectroscopic properties of azobenzene (longer wavelengths, good thermal stability). Exploring the wide possibilities of chemical modifications of the azobenzene unit, open up a wide range of investigations with new azoderivatives that can be triggered by visible or even IR light. The choice of an azobenzene is strongly related to the properties necessary for a certain application and its introduction in a polymer can have a wide range of possible macroscopic effects.[56]

1.5.1 Azobenzene Photoswitching without UV Light

As introduced, one emerging issue in biomaterial science is the elaboration of bistable molecular switches that can be controlled with visible light only. The majority of applications of azobenzene as a molecular switch uses UV light to trigger trans to cis isomerization. In biological systems, UV light is highly scattered and can induce toxicity effects. For instance, the need of using UV light to induce the switching processes implies serious limitations in living systems. In the light of biological applications, it has been of considerable interest to design azobenzene photoswitches with particular aspects concerned the cis/trans ratio in the photostationary state, the lifetime of the two isomers and the stability over time.[57] A variety of azobenzenes with high conversion efficiency isomerizable in the visible range have been identified. Substitution of all four ortho positions of azobenzene with methoxy groups or Cl or Br atoms, or C2 bridged compounds allowed to obtain azobenzenes with slow thermal cis to trans relaxation facilitating production of large fractions of the cis isomer.[58-59] Following a related strategy, Knie et al. designed a new family of azobenzenes fully addressable in the visible region by introducing fluoro substituents ortho to the N=N bond.[60] Ortho-fluoroazobenzenes showed high photoconversions, and unprecedented robust bistable character. Furthermore, particularly interested was also the introduction of Sulphur at the ortho positions of azobenzenes that leads to a >20 nm red shift as well as a significant increase in the intensity of the longest wavelength absorption bands of the trans isomers.[61] Woolley and co-workers reported the synthesis of azobenzene with methoxy groups in the *ortho* positions of the two phenyl rings in which long switching wavelengths are combined with relatively slow thermal relaxation rates and high cis-state yield (Figure 1.4).[62]

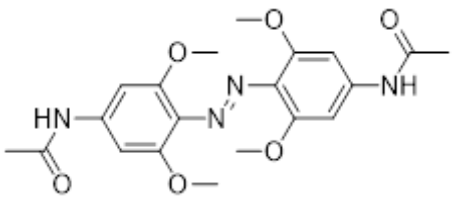

Figure 1.4 Azobenzene with methoxy groups in the ortho positions.

In trans state, it shows a strong π-π* band around 320 nm while a slight bathochromic and hyperchromic effect for the n-π* band relative to parent compound (same structure without orto-substituted). In cis state, the absorption bands are not subjected to spectroscopic variation. This means that the n-π* transition of the cis isomer occurs at significantly lower wavelengths (36 nm) compared to the analogues transition of its trans isomer. The split between n-π* bands of trans and cis isomers allows the switching of this azobenzene completely in visible range, *trans-to-cis* isomers using green light (530-560 nm) while reverse *cis-to-trans* photoswitching with blue light (460 nm) (Figure 1.5). In addition, this azobenzene shows interesting properties: the half-life of the cis isomer is longer that parent compound so that an intense light source is not required in order to maintain a substantial fraction of the cis isomer; very good solubility in aqueous solution for use in a biological application; multiple rounds of photoisomerization; and even constant high-intensity irradiation with green light (70 mW/cm^2) for ∼1 h, without evidence of photobleaching or photo-oxidation.[62]

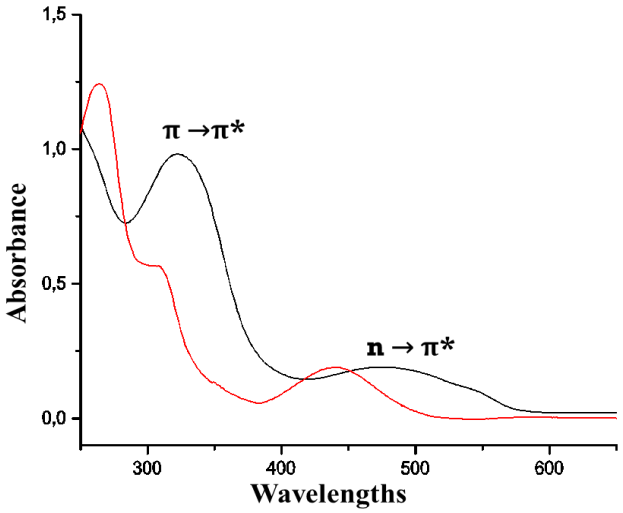

Figure 1.5 Photoisomerization of the 4,4'-diacetamidoazobenzene bearing o-methoxy groups measured in ACN at 25°C

1.6 Azobenzene-containing Polymer

The azobenzene moiety, incorporated in different materials either doped into a matrix or covalently attached to a polymer (amorphous and liquid-crystalline (LC) systems), can be used as a "probe" to induce light driven changes of material properties.[52] In fact in azopolymers, the photoisomerization induces conformational changes of azobenzene and consequently of the polymer chains that in turn lead to macroscopic variations in the chemical and physical properties of surrounding.[63] Furthermore, in the azobenzene-containing polymers, the photo-responsive behavior of the azo groups is combined with the inherent stability of polymers to obtain stable and tunable materials.[64] Azobenzene

functionalized monomer can be attached to the side chain, main chain and end chain of the polymer, or it can be used as cross-linker. The point of attachment to a polymer chains, the size, the shape and the conformation of chromophore play an important role in determining the effective free volume available during the isomerization.

1.6.1 Photo-orientation

Azobenzene chromophores can be photo-oriented by linear polarized light (LPL). This behavior is typical of pseudo-stilbene-type azo compounds characterized by a rapid *trans-cis-trans* isomerization upon light illumination. The constant and fast cyclic photoisomerization activity results in series of motions that can take place at molecular, nanoscale and micrometer levels.[63] Only azobenzene groups orientated with a transition dipole axis along the polarization of the light will absorb and consequently photo-isomerize. The probability of absorption varies as $\cos^2\phi$, where ϕ is the angle between the light polarization and the azobenzene dipole axis. Thus, azo-molecules orientated parallel to the light polarization will absorb, while the chromophores with dipole axis perpendicular to the light will not. For a given initial angular distribution of chromophores, many will absorb, convert into the *cis* form, and then revert to the *trans* form with a new random direction. Thus, there is a net depletion of chromophores aligned with the light polarization, with a concomitant increase in the population of chromophores aligned perpendicular (Figure 1.6).[65] Thus, optical dichroism as well as birefringence is induced in polymer films.

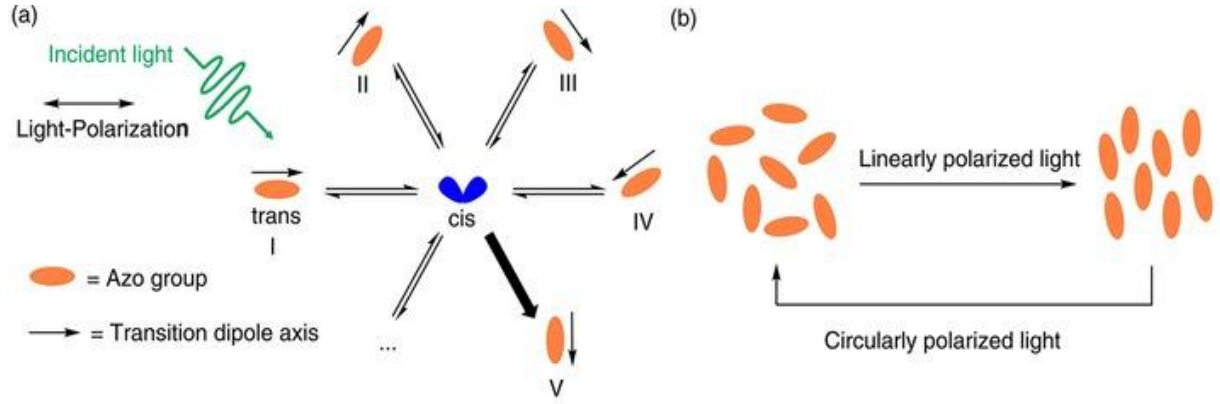

Figure 1.6 Photo-induced orientation of azo compounds in solid state. a) The azo compound aligned along the polarization direction of the incident light (I) absorbs light and isomerizes. The azo compounds aligned in other directions (e.g., II, III, and IV) can absorb the incident light with a lower probability than I and can be photoisomerized. Azo compounds aligned perpendicular to the polarization direction (V) cannot absorb light and remain fixed, because their transition dipole axis and the light-polarization are perpendicular to each other. b) Irradiation of an isotropic azo-containing sample in solid state induces orientation of azo compounds in the direction perpendicular to the polarization direction. Circularly polarized light removes the orientation. (Reprinted from *Chemistry-A European Journal* 2017, reference 65)

1.6.2 Macroscopic Motion

The photoisomerization at micrometer scale level is observed in an organized environment such as liquid crystal (LC), Langmuir-Blodgett films and monomolecular films. Azobenzenes are robust and anisotropic molecules that with suitable substitutions can show liquid crystalline behavior.[66] Instead of amorphous materials where there is not a preferential direction for photo-deformation, liquid crystalline elastomers (LCEs) with anisotropic physical properties allow a precise control in two and three dimensional motions. LCEs in particular are promising materials for artificial muscles because coupled both properties of LC (order) and that of elastomers (elasticity).[52,67] The incorporation of azobenzene mesogenes into LCEs can induce a reduction in the nematic order and causes a contraction of the films upon exposure to UV light as a result of a photochemical reaction of the photochromic moiety.[68] Furthermore, by their incorporation, it also possible observes three-dimensional movement (bending, oscillating, twisting and swimming) of LCE films by irradiation with light.[69] Finkelmann *et al*. reported a pioneering work on large contractions of liquid crystalline networks (LCNs) containing azobenzene moieties by light.[70] Successively, Ikeda *et al*. reported an anisotropic bending and unbending induced by light of LCGs and LCNs, cross-linked polymer films containing an azo- benzene moiety and a diacrylate-azobenzene moiety. The absorption of photons occurs only in the surface of the film due to the high absorption coefficient of azobenzene so the volume contraction is induced only in the surface region of the cross-linked LC polymer film upon

irradiation.[70] Furthermore, R. Yin *et al.* proposed an interesting crosslinked liquid crystalline polymers containing azotolane moieties in side chains which show a photoinduced bending and unbending behavior upon irradiation with sunlight, according to the trans–cis photoisomerization of the azotolane moieties.[71] At micrometer level, we can observe the massive movement of the polymer material because it is not limited only to the mesogenic chromophore but involves polymer chains. This kind of isomerization usually occurs in polymer containing pseudo-stilbene azobenzene type. Currently, there are different approaches on the mechanism of light induced polymer deformation. Upon light illumination, the cyclic azobenzene isomerization induces a macroscopic and anisotropic deformation of the solid azobenzene-containing polymers (azopolymers). Additionally, the direction of the deformation is parallel to the polarization direction of the incident light. Saphiannikova and coworker proposed a re-orientation model, assuming that the light-induced re-orientation of the azobenzene side chains induces a re-organization of polymer backbone and so generating a mass migration.[72-73] This theory claims that the material stays solid during photoirradiation. For this reason, it is described with the term "moving" or "mass transport". While the group of prof. Karageorgiev supports an athermal directional photo-fluidization model claiming that the cyclic isomerization of azobenzenes may cause an athermal transition of the glassy azobenzene containing polymer into a fluid state.[74] Here, the repeated *trans-cis-trans* cycles, "photosoften" or "photoplasticize" the polymer matrix and enhance polymer chain mobility. This phenomenon is described as "flowing", highlighting that *trans-cis-trans* cycles decrease Tg of azopolymers and drive azopolymers to "flow".[65] The exact mechanism that occurs at microscopic scale is being studied by different research groups and still under investigation, but in the meantime this interesting azomaterial behavior is already exploited in a variety of applications. In this Thesis, we will adapt the wide used term photofluidization for describe this phenomena, knowing that the photo-induced deformation or softening theories are still under debate. Furthermore, Pheis *et al*. reported also a third type of photoinduced liquefaction of azopolymers defined as "photoinduced reversible solid-to-liquid transitions". In this last case, the photoinduced flow is non-directional and associated to a cyclic isomerization. In fact, the azobenzene is not a pseudo stilbene type but one with a long lifetime in the cis form and a high cis content.[65] Furthermore, the trans and cis isomers have different Tg values. Once that a trans azopolymer (solid) is converted to the cis azopolymer (liquid), the cis azopolymer stands in the liquid state even when UV light is switched off.

Taking advantage of azobenzene isomerization at micrometer level of azo-materials, different kind of surface reliefs can be fabricated:

- Regular surface reliefs by holographic light irradiation;

- Regular surface reliefs by 1D Gaussian laser beam;
- Randomly-distributed surface reliefs by one-beam irradiation.

1.6.2.1 Regular Surface Reliefs by Holographic Light Irradiation

In 1995, it was discovered by Natansohn *et al.*[75] and Kumar *et al.*[76] the capacity of thin films of the azopolymer Poly(Disperse Red 1 acrylate) (pDR1a) to generate spontaneous surface deformations as a consequence of light irradiation through an interference pattern that reproduced the intensity and polarization gradient of any incident light field. These types of polymers are able to induce the formation of sinusoidal surface patterning, a surface relief grating (SRG), in the form of topographic arrays that trace out the light intensity profile. The Lloyd mirror is the set-up used by original investigation in this area. It is generated by an interference pattern caused by intersecting two coherent laser beams with a wavelength in the azo-absorption band. Figure 1.7 shows a representative set-up example of SRG formation.[77]

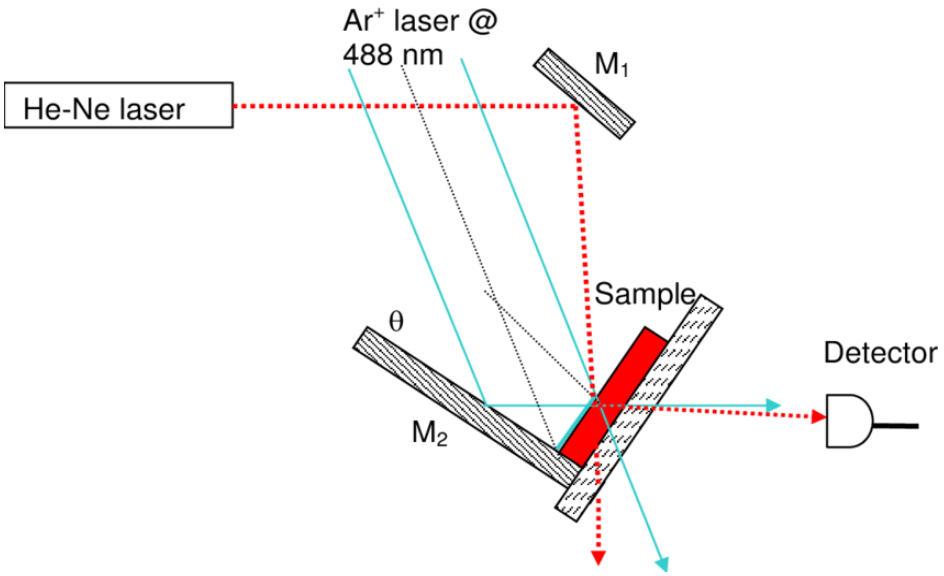

Figure 1.7 Experimental setup for the SRG formation. M1 and M2 are the mirrors. (Reprinted from International Journal of Optics and Photonics (IJOP) 2010, reference 77)

This phenomenon has been used to realize micro− and nano−grooved polymer films, suitable in many applications, such as optics and photonics.[52,78] The surface mass transport involves repeated *trans-cis-trans* photoisomerization of azobenzene, and the transmission of molecular motion to polymer material that being to move over nano to micron length scales, at temperatures well below the

material's glass transition temperature (Tg).[79] This is a reversible phenomenon, where topographic features embossed can be erased by heating the sample above Tg, and by a circular polarized light or an incoherent light source that can also revert the surface to its initial flat profile by a randomization of azobenzenes.[66] After the erasing, the azofilms show no evidence of degradation or charring of the polymer films. As discussed previously, despite considerable research, this complex phenomenon is not completely understood yet. Hurduc *et al*, proposed a new mechanism of SRG formation directly observed the fluid state formation by optical microscopy. They highlighted the importance of polymer chemical structure in the softening/fluidization.[80] The SRG formation is based on three different processes that can take place simultaneously: the polymer photo-fluidization in illuminated regions; the mass displacement from illuminated to dark regions and the inverse mass displacement, from dark to illuminated regions (Figure 1.8).

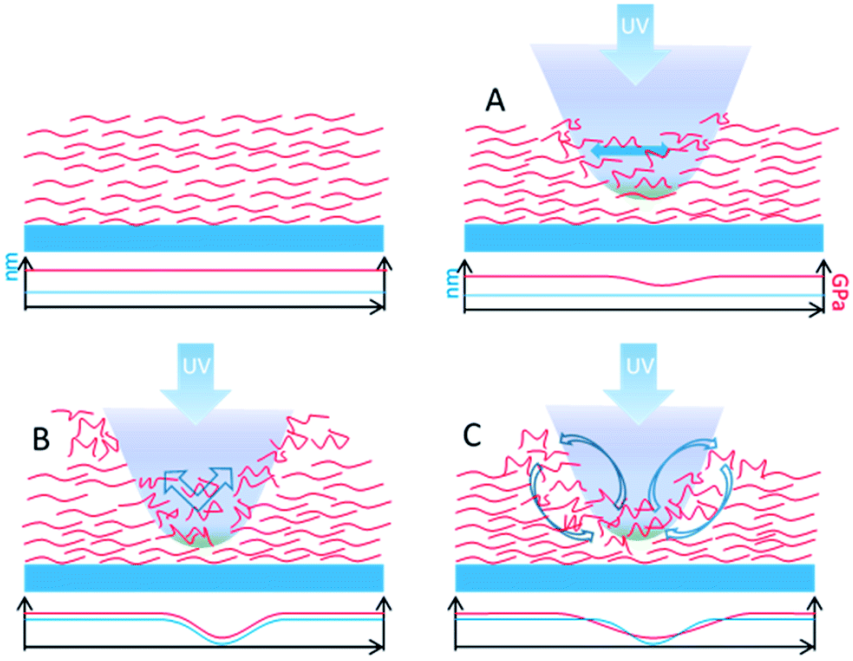

Figure 1.8 The proposed mechanism for SRG formation during laser irradiation, involving at least three processes: A) the polymer photo-fluidization in illuminated regions, B) the mass displacement from illuminated to dark regions and C) the inverse mass displacement from dark to illuminated regions. (Reprinted from *Soft Matter* 2014, reference 80)

1.6.2.2 Regular Surface Reliefs by 1D Gaussian Laser Beam

Interference lithography in Lloyd's mirror configuration is commonly used to emboss surface relief grating (SRG) on azopolymer films. Furthermore, a single focused laser beam allows for embossing linear pattern on azopolymer surfaces by moving the sample consistently to the light polarization direction.[81] A single Gaussian laser beam can induce an azosurface deformation, by aligning the azobenzene groups in the direction perpendicular to the polarization of the incident light.[79] In accordance to the observations of polarization-dependent formation of the SRGs, Bian *et al*. reported a single Gaussian beam-induced deformation on different azopolymer materials.[82] It is known that the mass migration process depends on the light polarization, intensity and wavelength.[56] In fact, they demonstrated that the photoinduced surface deformation occurs in the direction of the light polarization. In fact, the exposure with a polarization perpendicular to the direction of the light intensity does not produce appreciable surface variation. Furthermore, the presence of an intensity gradient by itself does not lead to surface deformation. The focused beam is able to make a hole in correspondence to the center of the laser spot and the resulting surface deformation is influenced by the polarization and intensity of the laser beam. A dip is formed in the center while the polymer chains moved out from the central region and piled up at the wings where the intensity is small, when the surface deformation is induced by a linearly polarized Gaussian beam focused on an azopolymer film (Figure 1.9 a). In contrast, the polymer surface deformation results completely different when induced by a higher-intensity linearly polarized Gaussian laser beam. In this case, a peak in the surface profile appeared in the center of the exposed spot (Figure 1.9 b). This behavior at higher intensities can be explained by some photochemical reactions in addition to photothermal and photobleacing effects that can occur in polymeric matrix.[81] When the surface deformation is induced by a circular polarization Gaussian beam, the polymer moves from the center to the outside of the focused laser spot, thus forming a doughnut-shaped pattern (Figure 1.9 c). A symmetric dip on the surface was formed because of the polarization direction of the optical field sweeping in all radial directions which always causes an intensity gradient.[82]

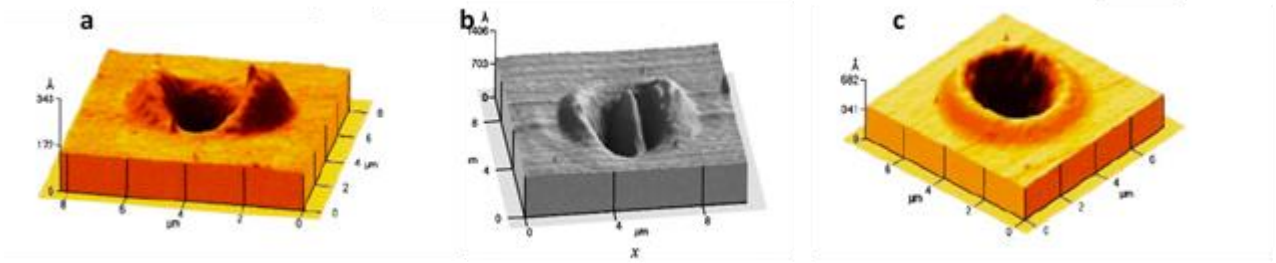

Figure 1.9 a) Surface deformation induced by Linear polarization Gaussian beams with low intensity and b) with high intensity. c) Surface deformation induced by circular polarization Gaussian beams with low intensity. (Reprinted from *Soft Matter* 2014, reference 81 and *Applied Physics Letters* 1998, reference 82)

There are few reports on surface deformations that are induced by a single focused laser beam.[81, 83] Noga *et al*. with optical technique produced topographic features of different shapes on the surface by controlling the position of the sample with respect to the focalized laser beam. They analyzed the changes of embossed topographies by tuning the thickness of the polymer layer, the temperature and the wavelength of laser beam.[84] A symmetric groove was formed when the surface deformation was induced by a cylindrical Gaussian beam along the direction of the light intensity gradient. The central bottom of the groove corresponds to the position of maximum light intensity (Figure 1.10). In contrast, no appreciable deformation was observed when the laser beam had a polarization perpendicular to the direction of the light intensity gradient.[81]

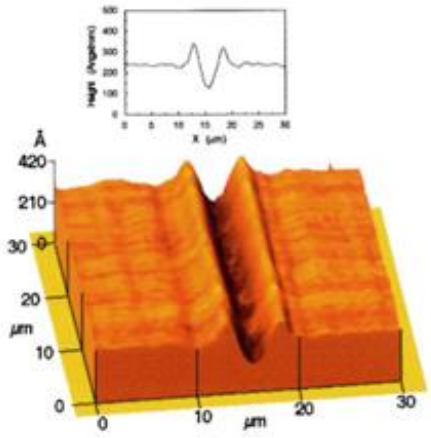

Figure 1.10 Surface deformation induced by a one-dimensional Gaussian beam. (Reprinted from *Applied Physics Letters* 1998, reference 81)

For all kinds of polarization of Gaussian beam, the polymer migrates in the direction of the polarization of the light from high to low light intensity regions. Effectively, the resultant polymer deformation is strongly dependent on many parameters. Tanabe *et al.* discussed the effect of the incident light polarization and the position of the laser focus on the deformation pattern.[85] In particular, they found that the deformation pattern was strongly dependent on the z- position of the focused laser spot. When the z-position was exactly on the film surface the polymer moved along the polarization direction from the center to the outside of the focused spot, thus producing two side lobes

along the polarization direction and a pit at the center (Figure 1.11 a). If the z-position was above the film surface in air, the polymer formed a protrusion coming out towards the center of the laser focus (Figure 1.11 b). The polymer movement was blocked by the substrate and so the protrusion was not formed, when the laser was focused into the glass substrate, (Figure 1.11 c).

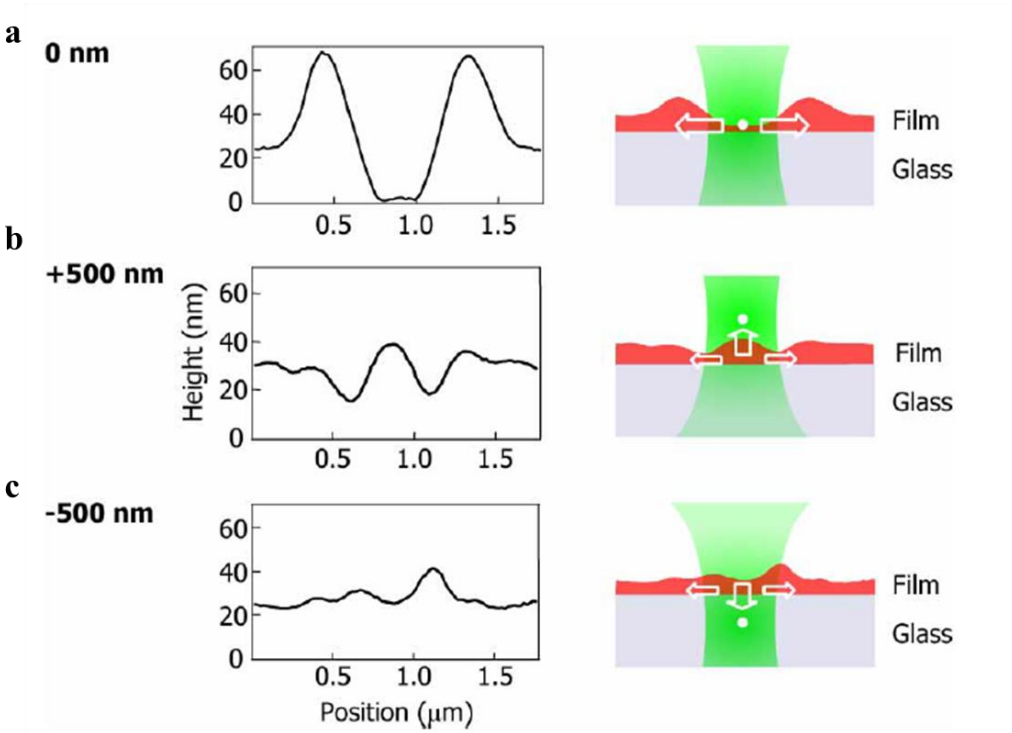

Figure 1.11 (Left column) Line plots of the surface deformation and (right column) schematics of the relationship between the Z-position of the focus and the film surface at a) Z = +500 nm, b) Z = 0 nm, and c) Z = -500 nm. (Reprinted from *Optics express* 2007, reference 85)

Recently, different kind of sources have been used to induce an azopolimer mass migration. Ishitobi *et al.* presented the first report of two-photon induced plastic surface deformation in azopolymer films.[86] In their work, they reported on the deformation induced by a gradient of light intensity depended by the wavelength, polarization direction of the incident laser light and z-position of the focused spot with respect to the plane of the polymer film. In this last case, divergent results respect one-photon absorption has been reported. When the z position of the focus was below the film surface, the polymer always moved from the outside to the center of the focused laser spot along the direction of the polarization of the excitation light and formed a protrusion at the center and two dips, one at each side of the protrusion along the polarization direction (Figure 1.12). However, no deformation was induced due to the intensity of the light spot at the film being not large enough to induce two

photon isomerization and polymer movement, when the distance between the focus and sample surface was larger than 5 μm.

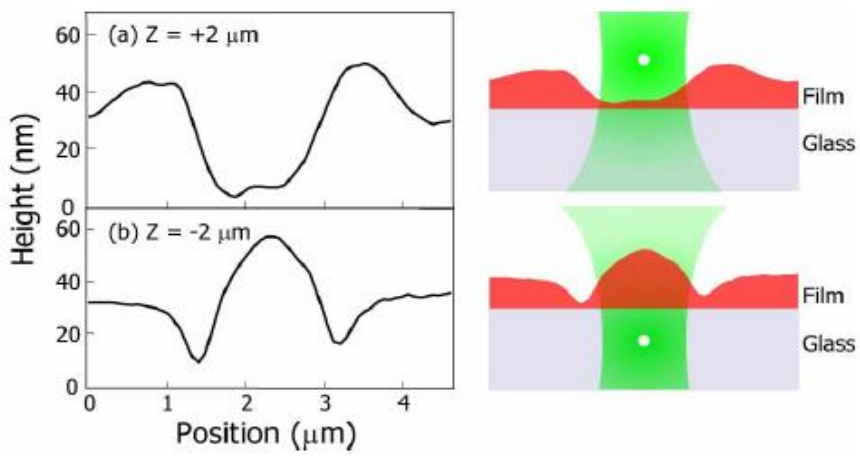

Figure 1.12 (Left column) Line plots of the surface deformations and (right column) schematics of the relationship between the Z position of the focus and the film surface at a) Z = +2 μm b) Z = -2 μm. (Reprinted from *Optics Express 2008,* reference 86)

Moreover, it is extremely interesting the possibility, independently proposed by the groups of prof. Ambrosio and Netti, to emboss photopatterns on azomaterial with a confocal microscope.[87-88] Ambrosio *et al.* realized different topographies (i.e. trenches and bumps) by changing the mutual orientation of the light polarization direction with respect to the sample scanning direction. In more details, they observed the formation of channels when the sample was moved perpendicularly to the light polarization direction, while they obtained ridges when the sample was directed along the polarization direction.[88] In Netti's group, C. Rianna *et al.* used the confocal microscope for embossing patterns in the presence of cells. The mass transport induced by the azobenzene isomerization was activated only inside drawn regions-of-interest (ROIs) by a confocal microscope, scanned by means of galvanometric mirrors. This method allowed to have a great versatility to emboss pattern with

different shape (concentric squares, triangles, sphere-like geometries) realized by simply changing the geometry of the irradiated regions (Figure 1.13).[87]

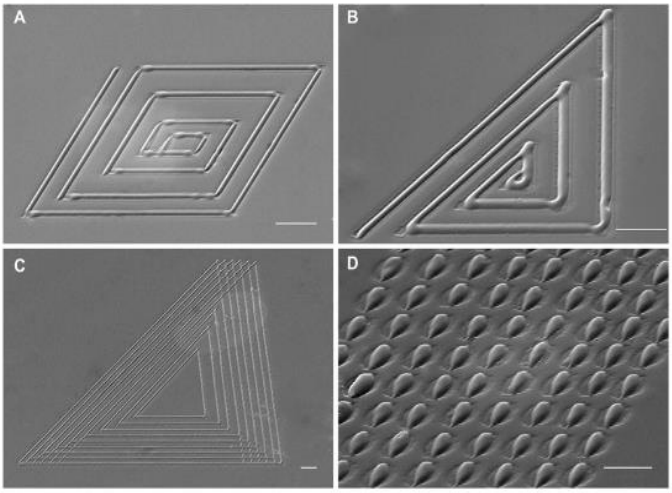

Figure 1.13 Different patterns on pDR1m. SEM images of several patterns realized on pDR1m films by using a confocal microscope, drawing several ROIs and irradiating the sample with 514 nm Argon laser wavelength. A) Concentric squares, B, C) triangles, and D) sphere-like geometries realized by simply changing the features of the irradiated regions. (Reprinted from *Advanced Functional Materials* 2016, reference 87)

1.6.2.3 Randomly-distributed Surface Reliefs by One-Beam Irradiation

In 2002, Hubert *et al.* reported for the first time a spontaneous self-organization of the flat surface of a thin azofilm into ordered hexagonal bumps by a one-beam irradiation. The material creates a diffraction structure in order to optimize the light dissipation.[89] Furthermore changing the irradiation conditions, also parallel stripes, or turbulent structures can be generated in azobenzene-based materials (Figure 1.14).

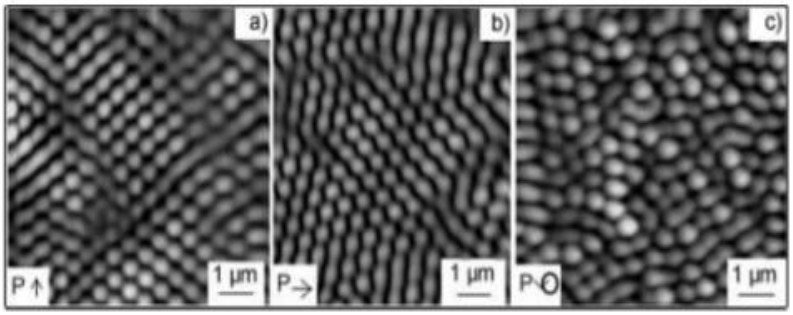

Figure 1.14 AFM images of hexagonal structures for a) vertically, b) horizontally, and c) circularly polarized incident laser beam. (Reprinted from *Advanced Materials* ***2002***, reference 89)

Several attempts have been carried out to understand the underlying physics that controls these various forms of pattern formation. The dependence of photoactivated pattern formation on both the light's intensity and polarization has been extensively investigated, but its physical explanation is still incomplete. Galinski and co-workers, for examples, explained the pattern formation entirely based on principle of phase separation in the polymer.[90]

1.6.3 Directional Photofluidization Lithography (DPL)

An interesting effect can be observed when the mass migration does not interest a flat film but a more complex 2D topography. Coupling the properties of azomaterials with other fabrication techniques allows for the realization of micro/nano structures of different shape and size (e.g., pillars, wives, bars). In particular, the combination of soft lithographic methods and light-induced mass migration leads to topographies tunable after the fabrication. For instance, anisotropic movement of 2D structures under light illumination has provided significant opportunities for the fabrication of complex micro/nanoarchitectures. Main examples include reshaping of funnels, circular or ellipsoidal holes and pillars. This process is known as directional photofluidization lithography (DPL). There are many examples in literature of azopolymer patterns subsequently modified by irradiation.[91,92] Kang *et al.* fabricated a linear azopolymer array by soft lithography and successively photo-reconfigurated it by holographic photofluidization, tuning the polarization of the interference patterns (Figure 1.15).[91] In particular, the use of holographic photofluidization in a monolithic evolution of hierarchical SRGs could be useful both for exerting unprecedented control over structural features by adjustment of the polarizations and for modulation height of the SRGs by light irradiation time. Also Lee *et al.* reported the reconfiguration of line arrays obtained with a single beam irradiation that evolved in ellipsoidal hole array when irradiated perpendicularly to the array by two beam interfering.[92]

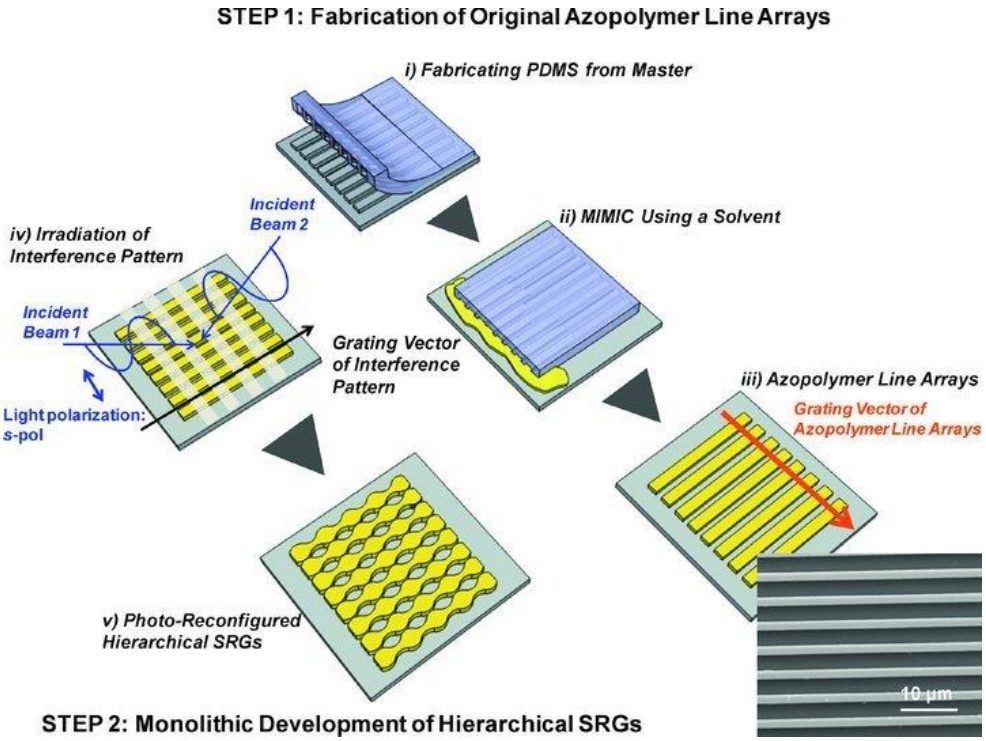

Figure 1.15 Monolithic evolution of hierarchical SRGs by holographic photofluidization of azopolymer line arrays: (step 1) fabrication of original azopolymer line arrays by MIMIC using a solvent; (step 2) monolithic evolution of hierarchical SRGs by interference pattern irradiation. The SEM image indicates obtained original azopolymer line array. (Reprinted from *Advanced Functional Materials 2011*, reference 91)

To sum up. the coupling of DPL and soft lithography leads to the fabrication of a plethora of 2D arrays. These complex structures could be reshaped by light after their fabrication, allowing for creating of 3D complex structures (e.g., domes, mushrooms, lemons, canoes) from a regular array. The advantage of this technique is the possibility to obtain structures not easily fabricated by conventional methods.[93] Lee and co-workers produced for the first time a set of pillars containing-azobenzene using a PDMS negative master.[59] The profile of the pillars were reshaped after the fabrication using polarized light by directional photofluidization of azobenzene materials. Under irradiation with a linearly polarized light, azo-materials became fluidized at room temperature and their direction flow was parallel to the light polarization. This behavior led to shape transition from an initial circular pillar shape to ellipsoidal. However, this process was hardly reversible on isolated azopolymer micro-objects, as an excessive photofluidization resulted in a material flow outside the initial volume, created mushroom-like structures.[45, 94] In order to avoid that the light irradiation brings the azopolymer to flow down on a substrate, different approaches have been adopted. Lee and coworkers confined the light-driven mass-migration inside the edge of the posts putting an extra PDMS capping layer on the posts.[92-93, 95] Pirani *et al.* increased the mechanical response to light of

pillars using a polymer blend (polymethylmethacrylate (PMMA) within a PAZO-PMMA mixture), so avoiding the polymer overflow outside the initial volume. This blend formulation allows a reversible and controlled deformation of the micro-pillars by periodically tuning the laser polarization in time reducing also the degradation of the structure morphology over several cycles (Figure 1.16 a-d).[96] In this way, it is possible to obtain a reversible process and a back and forth transition from pillar to elongated pillar by alternating LPL and CPL irradiation.[96] During this process, many interface properties (shape, phase, and wettability) can be affected. Illuminating the pillar array, Oscurato *et al*. analyzed how the superficial wetting properties are tuned, elongating the three-dimensional geometry of soft-lithographic imprinted micropillars. They showed the ability of the light-induced pillar reshaping of tuning the wetting anisotropy of the surface in a reversible way **(**Figure 1.16 e).[97] Recently Pirani *et al.* have showed a directional reversible change of hydrophobicity of pDR1m pillars with a locally anisotropic topography induced by light irradiation. In particular, they obtained a change of contact angle of a water droplet on the structure of roughly 30° due to a precise spatial-temporal control of the light induced deformation of an azopolymer microstructure. Finally, they showed a partially reversibility of the process when the pillar elongation was kept within a roundness larger than about 0.5.[98]

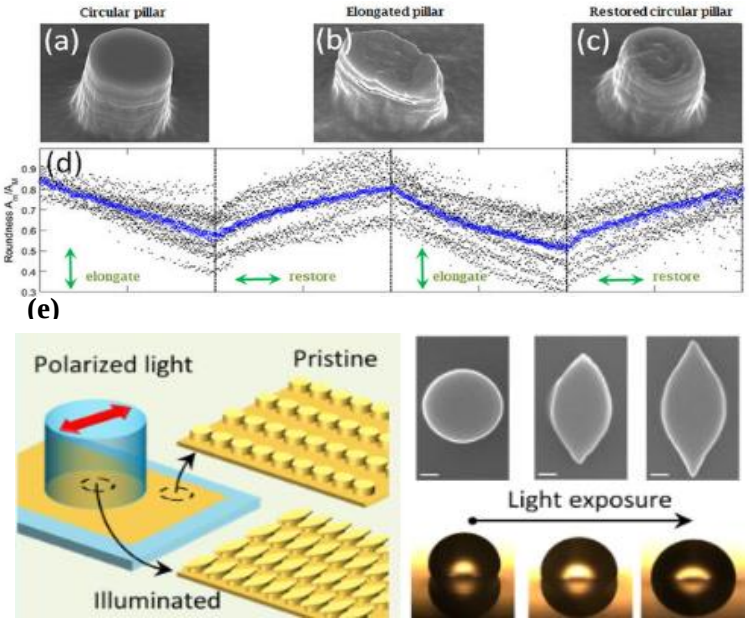

Figure 1.16 Exemplary SEM pictures of individual pillars: A) before laser irradiation, B) after a single laser exposure with LPL, C) after two laser exposures with two orthogonal polarizations (restored circular cross section). D) Time-resolved roundness values for pillars during laser irradiation with time-varying polarization state (black dots: roundness of individual pillars, blue circles: mean value over pillars in each frame). E) Light induced superficial asymmetry and directional wetting anisotropy. (Reprinted from *Scientific reports 2016, reference 96* and *ACS applied materials & interfaces 2017*, reference 97).

As mentioned previously, the initial pillar array is usually fabricated by soft lithography. A more innovative approach uses the photo fluidization properties of azobenzene to fabricate nanostructures and not only for modifying already existing arrays. Choi *et al.* reported the possibility to obtain directly patterned superficies from micrometer to sub-100 nm range by vertical-directional photofluidization of azobenzene materials. They showed the advantage of obtaining structures into a range which is typically not feasible by soft lithography technique. In particular, they focused on vertical directional movement of azobenzene materials instead on, largely investigated, lateral directional movement of azobenzene materials. Submicrometric structures were fabricated by two-step illumination, first a slantwise- circularly polarized light was directed onto azo material film in contact with patterned elastomeric molds (*i.e.*, PDMS), followed by a perpendicular irradiation. Under illumination, the polymer drifted upward along the cavities of the molds resulting in pattern formation. This light-induced fabrication was defined directional photofluidization imprint lithography (DPIL) and provided also a facile way to fabricate complex hierarchical multiscale structures.[99]

1.7 Azopolymers as Dynamic CIMs

In the last years, a variety of structures containing azobenzene have been fabricated in order to obtain photo-tunable surfaces able to change their properties when illuminated by light at a certain wavelength. The most common examples of azo-materials are based on amorphous polymeric chains, for instance, poly (disperse orange 3) (PDO 3), and polydisperse red1 methacrylate (pDR1m).[95] Their extraordinary ability in photofluidization leads to additional flexibility in the micro/nanofabrication techniques.[95] This tunability represents another strong advantage for the production of light-responsive materials in different fields such as microfluidics, tissue engineering[50] and optoelectronics.[100] In this thesis, we have focused on the advantage of azomaterial properties in biological field, to obtain dynamic scaffolds for *in vitro* study of cell behavior. Cell attachment, proliferation, migration, differentiation have been usually analyzed in static environment, which led to results sometimes not complete and difficult to interpret.[101] Baac *et al.* were the first to use SRGs imprinted with interference lithography in Lloyd's mirror configuration on an azopolymer film to culture primary human astrocytes (Has). Cells respond to the underlying pattern and appeared oriented and elongated along the direction of holographically formed SRGs.[102] Successively, Hurduc *et al.* proposed an interesting work in which, highlighted the advantages to use azo materials as support in cell cultures. They introduced a new class of materials with azo-polysiloxanic structures, chemically modifiable due to the presence of the chlorobenzyl groups in the polymeric side-chain.[101] This allowed to precisely tune the chemical signals transmitted

to the cellular membrane with immediate consequences on the cell fate. Berille *et al.* investigated the effect of writing and erasing pattern on an azopolymer-based platform in the presence of PC12 cells. They proposed a direct inscription of a pattern in the presence of cells, while the sample was immersed in a phosphate buffered saline (PBS). For their investigation, two different azo biocompatible nanopatterns were fabricated, the first with an optical interference pattern and the second by self-organization of azopolymer under single laser beam irradiation (Figure 1.17). Their technique could be used to fabricate on demand platforms for controlling surface topography in real-time and in biocompatible condition.[103]

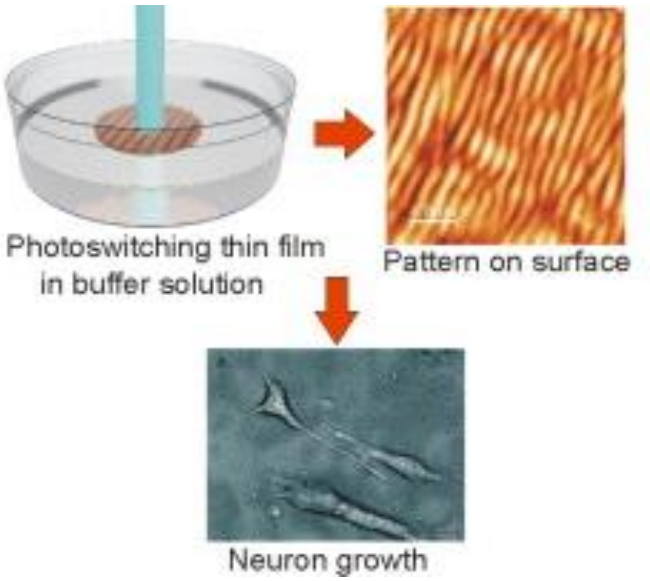

Figure 1.17 Inscription of a pattern on the surface with a laser when the biopolymer thin film is immersed in a buffer solution. (Reprinted from *Colloids and Surfaces B: Biointerfaces 2011, reference 103)*

Also our group has mainly focused on using mass migration displacement of azopolymer to write and erase specific patterns in the presence of cells. Rianna *et al.*, showed the possibility to write a linear pattern on an azopolymer thin film in the presence of cells with a confocal microscope, analyzing the cell response *in real-time*.[87] As mentioned earlier, the confocal set-up equipped with a cell incubator allows to emboss different patterns on the same cell-populated azosubstrate in biocompatible conditions to evaluate different cell response simultaneously (Figure 1.18).[87]

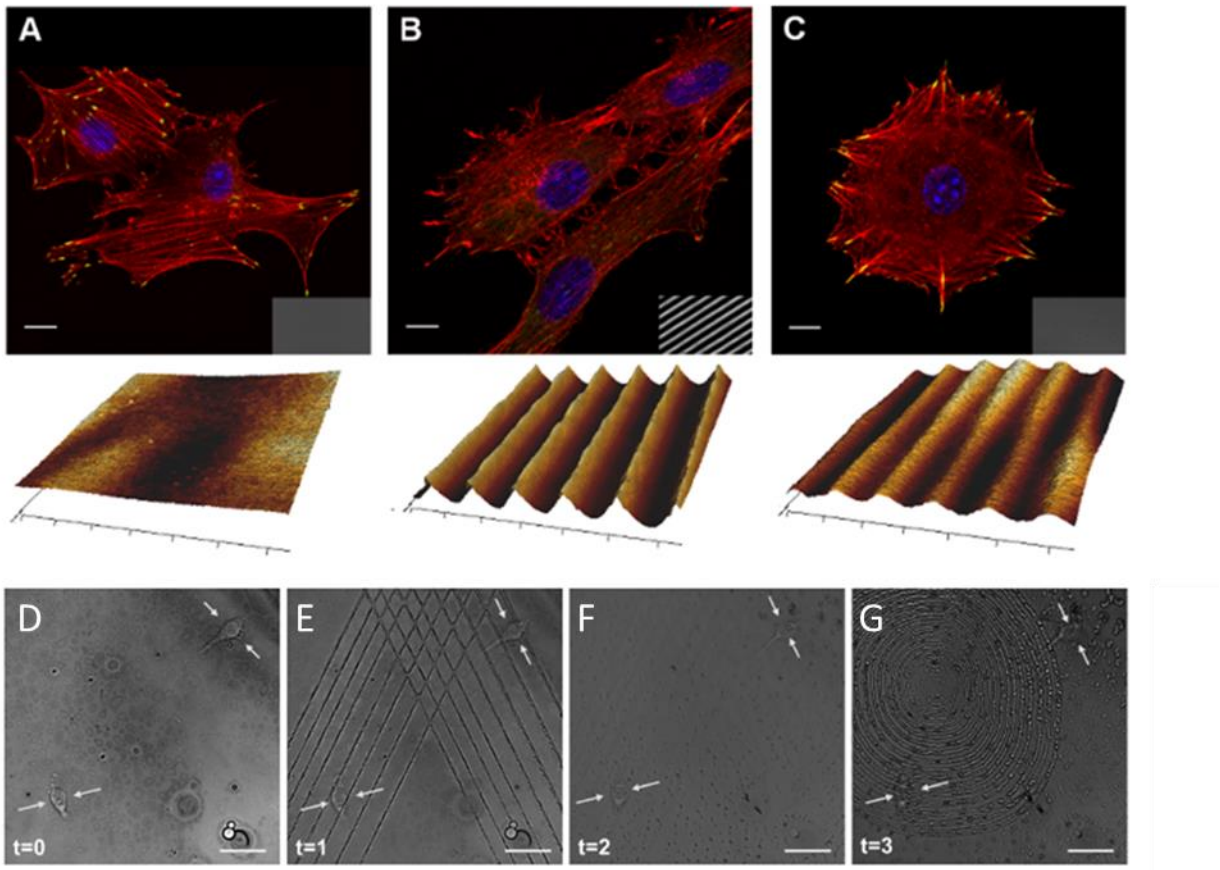

Figure 1.18 Confocal images of NIH-3T3 cells cultivated on A) flat pDR1m substrate, B) SRG grating, and C) pattern erased with circularly polarized light. Transmission images of the substrate are reported in the bottom right of each confocal micrograph and AFM scans are shown below them. Confocal images of write/erase/write pattern. NIH-cell on D) flat pDR1m E) triangular inscription embossed with confocal set-up F) erased pattern with incoherent light G) second pattern inscription. (Reprinted from *Advanced Functional Materials 2016, reference 87)*

Recently, also liquid crystalline elastomers (LCEs) are earning more attention as dynamic cell scaffolds. The macroscopic motion of LCP containing- azobenzene upon light illumination suggests that they could be a valid approach for future biological applications. Typically, the use of liquid crystalline polymers as biomaterials have been limited by high temperature required for nematic-to-isotropic transition. Instead, the presence of azobenzene in LCP can drive a transition between liquid crystalline phases with light, avoiding the use of high temperature for cell culture. For example, Jonkheijm *et al.* analyzed the cell migration on light-induced surface change of LCE *in situ*.[104] Martella et al. explored the biocompatibility of acrylate-based LCN film by testing their ability to promote cell differentiation and maturation for different murine and human cell lines, demonstrating an amazing contribution of LCN films in human induced pluripotent stem cell-derived cardiomyocyte (hiPSC-CM) growth, speeding it up in respect to common substrates.[105]

1.8 The role of Topography in the Regulation of Stem Cells

Adult stem cells such as human mesenchymal stem cells (hMSCs) are multipotent cells that contribute to tissue regeneration.[106] In response to a stimulus such as a trauma or disease, hMSCs circulate away from their niche and engraft in mechanically diverse environments to renew bone, cartilage, muscle or fat. Adult stem cells *in vivo* are found in specific locations of a tissue (niches) that are responsible of different functions such as maintenance of stem cell populations, control of their proliferation and differentiation into multiple cellular lineages.[85] The ECM in these microenvironments is a complex network that presents to cells both nano- and micro-topographic features. They have a direct impact on cell behavior and cells are able to sense surface patterns ranging from 10 nm to 100 μm.[37, 107] Smart surfaces have been fabricated with controlled stiffness, different micro-nanoscale topographies and chemistries to recapitulate the topographic landscape of native cellular niche. The physical properties of biomaterials have been shown to directly influence stem cell fate acting alone or in combination with chemical cues.[45,108,109] Various signaling pathways have been implicated in the regulation of hMSCs differentiation; however, complexities of pathway interactions are still under debate. Numerous works reported topographically patterned arrays including posts, pits, ridges, grooves, or gratings with different geometries and sizes to control the stimuli on stem cells. As mentioned above, this mechanosensitive interaction initiates a cascade of signaling pathways within the cell leading to inner cytoskeleton rearrangements. In particular, ridges/grooves are deeply investigated resembling the native collagen structures of ECM. As example, Wagner and coworker generated micro- and nano-patterns in polyimide with ridge ranging from 2 μm to 15 μm and analyzed the differentiation of MSCs towards specific lineages. They reported that 15 μm ridges increased adipogenic differentiation whereas 2 μm ridges enhanced osteogenic differentiation. Notably, the comparative analysis indicated that the size of the ridges is more important than the size of the grooves to support lineage specific differentiation of MSCs.[37] In particular, hMSCs differentiated into osteoblasts when allowed to spread and flatten, whereas restricting the surface area upon which to grow promoted adipogenic differentiation of hMSCs.[108] While nano-patterns with a periodicity of 650 nm increased differentiation towards both osteogenic and adipogenic lineages. Concluding that grooved surfaces did not induce differentiation *per se,* but by supporting the differentiation processes initiated by induction media. Instead, Watari *et al.* demonstrated that a specific size scale of topographic cues (400 nm pitch) promote osteogenic differentiation with or without osteogenic agents. They used topographically-patterned substrates containing anisotropically ordered ridges and grooves to investigate the effects of topographic cues on mesenchymal stem cell morphology. They attributed

their results to a greater average cell area of hMSCs cultured on 400 nm pitch instead of 4000 nm to promote osteogenic differentiation.[25] Initially, hMSCs were believed to be restricted to mesenchymal lineages. Successively, the pioneering study of Woodbury *et al.*[110] demonstrated the differentiation of rat and human bone marrow stromal cells into neurons, and so many other groups investigated neuronal differentiation of hMSCs. The mechanism responsible for the transdifferentiation of mesenchymal stem cells to neurons can be induced by neuronal induction medium and/or cell contact with neurons, but it is not well understood yet. Also, Genetos and co-workers differed from previous studies, that induced only osteogenic markers on topographic ridges and grooves, instead, showed a number of neuronal markers on pattern with 700 nm pitch.[111] Furthermore, micro- and nanostructured surfaces, in particular grooves, have been also used to study the role of mechanical cues in cell self-renewal or reprogramming.[107] Strikingly, microsized alignment "wrinkles" were observed to increase significantly the efficiency of reprogramming of mouse fibroblasts.[112] Numerous works have reported the effect of surface topography in stem cell differentiation. Furthermore, multiple combinations of materials with several physical characteristics were used to assess the role of topographic features in cell fate. In fact, a proper utilization of stem cells for clinical applications requires an integrated understanding of multiple signal inputs that control maintenance of stemless, proliferation, commitment and differentiation.

1.9 Aim and Outline of the Thesis

The aim of this Thesis is to fabricate dynamic light-switchable biomaterials as scaffolds to study cell behavior in a more complex environment than the one generated by the use of static systems. We take advantage of compelling properties of azobenzenes to engineer photoresponsive 2D and semi-3D platforms to investigate different biological processes from adhesion up to differentiation. *In vivo*, in addition to the chemical and mechanical properties, the topographic cues play a main role to guide cell response. The ECM is filled with nano- to micro-meter scale landscapes (e.g., ridges, pores and fibers) in continuous remodeling. However, the topography of the most widely implemented *in vitro* platforms is static and difficulty mimics the dynamicity of ECM. Thus, we propose platforms, which can dynamically tune on demand their topographic properties upon external stimulation. In particular, azobenzene-containing systems can tune their properties under light illumination, recapitulating the spatial-temporal changes of the physiological cell environment. In **Chapter 1**, we will discuss about important properties of azobenzene molecules and present different applications of a variety of materials containing azobenzenes from amorphous materials to highly organize liquid crystal polymers. In particular, we will focus on the recent use of azopolymers as dynamic cell instructive materials. As of now, there is a lack of knowledge on the role of dynamic topography and, even more on its effect on stem cell differentiation. In the light of this, in **Chapter 2** we will present a technique to photo patterning azopolymer thin films *in situ* by means of a laser-based confocal microscopy. Further, we will analyze the human mesenchymal stem cell (hMSC) response after the spatial-temporal dynamic topographic changes. In more details, a mass migration phenomenon of azopolymers elicited under light irradiation allows to emboss a variety of patterns on cell-populated azopolymer films. We will investigate the stem cell response on a switchable topography from a linear pattern to a grid both in term of cell cytoskeletal re-organization and cell differentiation. Our aim is to investigate the impact of dynamic remodeling of cell environment on hMSCs gene expression profile, in comparison to static surfaces. In order to achieve our goal, we will investigate the cell behavior over time, changing the topographic aspects of the substrate and analyzing the effect of dynamic cues in modulating cell morphology and osteogenic gene expression profile. In particular, we will investigate whether epigenetic effect induced by changes in the biophysical properties of the substrate over time would redirect the expression of lineage specific markers. In **Chapter 3**, we will discuss about an athermal photofluidization process that can directly reshape an azopolymer pillar array in the presence of cells to investigate the dynamic reassemble of F-Actin on deformed pillars. We will show that pillar arrays can be reshaped along the direction of laser polarization, resulting in elongated structures with controllable eccentricity.[94, 98] This light-driven phenomenon, permits to use

such type of systems as platforms to analyze cell membrane curvature remodeling in respond to dynamic pillar reshaping. The plasma membrane wraps around the pillars, which generate local curvatures on cell membrane and trigger the F-actin accumulation. Human bone osteosarcoma epithelial cells (U2OS) will be used to investigate the reorganization of F-Actin during the platform transition from pillar to ellipsoidal-shape structures over time. In **Chapter 4,** we will focus on designing semi-3D hydrogel platforms containing azobenzene to engineer and manipulate culture systems in order to develop photoactuable cell confining systems. Acrylamide-modified gelatin containing azobenzene-based cross linkers will be used to microfabricate well-defined semi-3D photo-responsive structures by means of two-photon lithography (2PP). As proof of concept, we will show an example of an array of squared structures, where cells are physically confined between the adjacent gelatin blocks, which can be remotely stimulated. The light irradiation can be converted in a local mechanical stimulation able to deform the nucleus at a single-cell level. **In Conclusion and Future Perspectives,** a summary of the main results achieved in this thesis is presented and future applications are proposed.

Chapter 2

Dynamic Topographic Control on Mesenchymal Stem Cells by Photoresponsive Azopolymers

Abstract. Material surface properties affect the strength and the nature of the cell–material interaction at biomaterial interface.[8] In particular, topographic properties influence cell behavior at different levels: from adhesion up to differentiation.[6, 113] Of particular relevance in tissue engineering and regenerative medicine, is the control of stem cell fate by topographic cues. Many micro- and nanopatterning techniques have been employed to create patterned surfaces to direct stem cell lineage specification.[2, 109, 114] More challenging, our group has developed a method for the fabrication of azopolymer-based devices that can dynamically tune their topography under illumination with a laser-based confocal microscope in presence of cells.[87] This is possible because the light interaction with an azopolymer film induces a mass migration phenomenon that allows to emboss a variety of topographic patterns on the polymeric film.[87-88, 115-116] Taken together the intrinsic light-responsive properties of azopolymers and the versatility of our technique, we can control topographic changes of azopolymeric platforms *in situ* during cell culture. The dynamic topographic signal can thus effectively regulate the shape and the cytoskeletal arrangement of human mesenchymal stem cell (hMSCs) in time. The morphological variation of hMSCs on dynamic micropatters lead to a modulation of cytoskeletal tension that can regulate signal transduction of stem cells and subsequently guide their differentiation. In particular, we analyze how dynamic cues with or without soluble induction factors can promote stem cell differentiation into an osteogenic lineage. These platforms pave the way to investigate the effect of dynamic cues on stem cell behavior from cell shape to lineage commitment.

*The work described in this chapter is part of a manuscript in preparation: De Martino, S.; Cavalli, S.; Netti P.A. "Dynamic Topographic Control on Mesenchymal Stem Cells by Photoresponsive Azopolymers".

2.1 Introduction

Classically, the control of stem cell fate, has been attributed principally to genetic and molecular mediators.[117] Recently increasing evidence has revealed that the topography can contribute to the overall control of stem cell activity.[117-118] Developments in advanced micro and nanomachining techniques have enabled the fabrication of substrates that recapitulate the structure and length scale of native topography in two-dimensional substrates.[18] The interaction of mammalian cells with these scaffolds has proven to be an important signaling modality in controlling cell fate. Stem cell differentiation mediated by topographic cues is currently largely debated in literature, but in the meantime the physical gene regulation pathway is not completely clarified yet. Various signaling pathways have been implicated in the regulation of stem cell differentiation; however, complexities of pathway interactions, create an often confusing and contradictory results.[119] In fact, cells may encounter different sizes of topographies (ranging from nano to macro) and shapes (pit, groove, needle, pillar), each of which has the potential to influence cell fate.[20] After an accurate literature study and in accord with our fabrication technique, we chose to focus on submicron ridge/groove topography to control the cell shape and to investigate stem cell differentiation. Many studies have demonstrated the potential to modulate stem cell differentiation only by topography, nevertheless the information that is possible to obtain are only partial because a patterned topography can reproduce only static cues at cell-material interface. In fact, although conventional techniques for physical structuring of surfaces offer precision, miniaturization and reproducibility of fabrication processes which allow to recapitulate the topographic setting of the native tissue, they inadequately mimic the active and dynamic cell environment. Recently, of great interest is the possibility to move away from traditional "static" biomaterials towards new "dynamic" platforms that provide specialized cell behavioral cues in temporally defined manners. Thus, in order to have a more complete information from cell–microtopography interaction to control cell behavior including stem-cell differentiation, we have focused on the use of dynamic surfaces.[120-121] In the light of this, "smart" or "stimuli-responsive" materials have emerged as powerful tools for basic cell studies as well as promising biomedical applications.[122] These materials, through the fabrication of structured surfaces, are able to change their morphology upon external stimuli. Recently, many examples of smart materials have been introduced, including principally temperature-responsive polymer-surfaces (SMP) where the surface energy can be controlled with temperature.[123,124] The advantage of our approach compared to others, is the possibility to use the light as the external trigger so having a major control on timescale of topography switch and flexibility on fabrication of embossed topographies. The use of light-

responsive materials, such as azopolymers, has opened interesting perspectives for triggering specific surface properties upon proper light irradiation.[50] Azopolymers are polymeric compounds containing azobenzene groups that can undergo a reversible isomerization upon photon absorption.[53, 55-56] Photoisomerization induces conformational changes both at molecular and macroscopic scale resulting in light-induced variations of shape, phase, and wettability.[125] Furthermore, polymers containing stilbene type azobenzene, such as poly−disperse red1−methacrylate (pDR1m) used in this work, are unique and attractive materials in which the azobenzene photo−isomerization can lead to a macroscopic material motion, also named light−induced molecular displacement or mass migration.[63] Starting from this physical phenomenon, we employed a confocal microscope to realize precise and complex topographic patterns on azopolymer substrates. Here, the combination of intrinsic light-responsive properties of azobenzene and the versatility of laser-based confocal microscopy techniques has allowed *in situ* spatial-temporal dynamic topographic changes during cell culture.[87] To sum up, we have engineered patterned substrates containing anisotropically ordered ridges and grooves to investigate the effect of topographic cues on stem cell morphology and differentiation. The topography is examined as a means to guide differentiation, and its application is described for skeletal stem cells. Human mesenchymal stem cells (hMSCs) are a type of clonogenic cells capable of self-renewal and multi-lineage differentiation into mesoderm-type cells (e.g., osteoblasts, adipocytes and chondrocytes).[126] We have analyzed if topographic cues in the form of linear patter, mimicking biophysical cues provided by collagen fibers, can promote the differentiation of hMSCs into osteoblast lineage.[25, 127] After a preliminary analysis of cell shape and differentiation under static conditions, we have proposed to investigate the cell development over time, changing the topographic aspects of the substrate and analysing the effect of dynamic cues on modulation of cell morphology and osteogenic gene expression profile.[128] We have shown that hMSCs respond to pattern switch by altering their shape and alignment, leading to reversible changes in nuclear area, profiles and cell differentiation.[129-130]

2.2 Materials and Methods

Poly-Disperse Red 1-methacrylate (pDR1m), Triton X-100, TRITC-phalloidin, were supplied by Sigma. Circular cover glasses were purchased from Thermo Scientific. Chloroform and other solvents were purchased from Romil. Anti-vinculin monoclonal antibody was supplied by Chemicon (EMD Millipore), whereas Alexa Fluor 488-conjugated goat anti-mouse antibody were purchased from Molecular Probes, Life Technologies. Osteocalcin-antibody-oc4-30 and opn-antibody-akm2a1 were purchased by Acam.

2.2.1 Substrate Preparation

Poly-Disperse Red 1-methacrylate (pDR1m, Sigma) was dissolved in Chloroform (Sigma) at a concentration of 5% (w/v). 6 μL of the solution was spin-coated on 5 mm diameter circular cover glasses by using a spin coater (Laurell Technologies Corp.) at 3500 rpm, 1500 acceleration for 30 sec. A flat and homogenous polymer layer was obtained with a thickness of ≈300 nm, measured by A Veeco Dektak 150 profilometer.

2.2.2 Optical Pattern Inscription

Single photon confocal microscopy with an Argon laser (laser intensity 1.3 mW scan speed 400 Hz) with a 25x water objective was used to emboss precise and complex submicrometric patterns on pDR1m thin films. In more details, since the maximum absorption band of our polymer was in the range of 400-600 nm, the laser source with a wavelength value of 514 nm was used to induce the continuous *trans-cis-trans* isomerization of pDR1m molecules, which resulted in surface mass migration.[82,88] The laser beam path was controlled *via* software by drawing specific region of interests (ROIs) with ROI Designer HTML5 Assistant: http://www.ceerk.com/tech/roi0.2.1/. The ROIs Designer is an extension for a more precise and complex ROIs pattern design. Used for selecting accurate area to define the ROIs for Leica Microsystems Microscope Imaging Software, in order to create patterned surfaces on light responsive polymer. It is developed as an HTML5 application using the canvas and object oriented javascript.

2.2.3 Cell Culture Experiments

hMSCs were purchased from Lonza and grown in maintenance medium consisting of mesenchymal stem cell basal medium (MSCBM), L-glutamine and GA-1000 at 37 °C in a humidified atmosphere of 95% air and 5% CO_2. Cells were seeded onto the patterned or planar polymeric substrates using a density of 2.000 cells/cm^2 and the medium was changed twice per week. Prior to cell seeding, pDR1m substrates were sterilized under UV light for 1 h. Additionally, hMSCs were grown in osteogenic medium (dexamethasone, L-glutamine, ascorbate, penicillin/streptomycin, MCGS, β-glycerophosphate) and the medium was changed every three days. Stem cells at passage 5 and 7 were used in these experiments.

2.2.3.1 Immunofluorescence

Cells on surfaces were fixed with 4% formaldehyde for 20 min, permeabilized in 0.1% Triton X-100 in PBS for 3 min and blocked with 1% bovine serum albumin (BSA) for 30 min. Actin filaments were stained with TRITC-phalloidin. Samples were incubated for 30 min at room temperature in the phalloidin solution (1:200 dilution). Focal adhesions (FAs) were stained with vinculin. Briefly, cells were incubated in an anti-vinculin monoclonal antibody solution (1:200 dilution) for 2 h and then marked with Alexa Fluor 488-conjugated goat anti-mouse antibody (1:1000 dilution) for 30 min in a humid chamber. Finally, cells were incubated for 15 min at 37 °C in a DAPI solution (1:1000 dilution) to stain cell nuclei. Primary antibody labeling was performed in 1% BSA in PBS for 2 h at room temperature (20 °C) with rabbit anti- RUNX2 and anti-Osteocalcin (anti-BGLAP). Secondary antibody labeling was performed using the same procedure with Tetramethylrhodamine-conjugated anti-rabbit IgG antibody along with Alexa Fluor 488-phalloidin (1:200 dilution), Alexa647-conjugated anti-mouse and DAPI for 20 min in a humid chamber. Cell and FA morphometry measurements were performed by using Fiji software with the procedure previously described by Ventre *et al.*[21] Immunofluorescence microscopy was achieved using a TCS SP5 confocal microscope (Leica Microsystems). Briefly, cell elongation was assessed by phalloidin-stained cells that were analyzed with the MomentMacroJ version 1.3 script (hopkinsmedicine.org/fae/mmacro.htm). We evaluated the principal moments of inertia (i.e., maximum and minimum) and defined the cell elongation index as the ratio of the principal moments (I_{max}/I_{min}).[115] High values of I_{max}/I_{min} identify elongated cells. Cell orientation was defined as the angle that the principal axis of inertia forms with a reference axis. The reference axis was considered as the x-axis. Statistical significance was assessed through t-test (Origin).

2.2.3.2 rt-PCR analysis

Total RNA was collected from hMSCs at 7, 14 and 21 days. RNA was isolated with E.Z.N.A. Total RNA Kit I (Omega, biotec). It was purified with homogenizer mini column (HCR003). Total RNA was reverse-transcribed with M-MuLV-RH First Strand cDNA Synthesis. Proprietary primer and probe sets for BGLAP (Osteocalcin,), RUNX2 (runt-related transcription factor 2) and GAPDH (Glyceraldehyde 3-phosphate dehydrogenase) were purchased from Biorad. Amplification conditions were 95 °C for 3 min, followed by 40 cycles at 95 °C for 3 s and 60 °C for 30 sec. ΔCt was calculated relative to the loading control (GAPDH) for each sample; ΔΔCt was calculated by normalizing ΔCt of target conditions to that of control conditions (i.e. planar surface at the same time point). Relative expression was subsequently calculated using the formula $2^{\Delta\Delta Ct.}$ All experiments were performed in triplicate.

2.3 Results and Discussion

2.3.1 Pattern Fabrication

In this thesis, a confocal microscope was employed to dynamically and reversibly modulate the topography of Poly-disperse red 1-methacrylate (pDR1m) thin film to control *in situ* cellular and nuclear alignment of hMSCs. In more details, an Argon laser at 514 nm was used to induce a continuous *trans-cis-trans* isomerization of disperse red 1 molecules (DR1), triggering a surface mass migration of azo-material according to the polarization of a proper illumination light. The laser stimulation allows to emboss complex topographies on the entire area of the pDR1m thin film. As a matter of fact, most of the confocal software allows to define specific regions-of-interests (ROIs) in which the laser irradiation is activated with a high spatial resolution (nm order). In our approach, by using a single photon confocal microscope with a ROI-designer extension (ROI-designer HTML5 Assistant), multiple and accurate ROIs evenly spaced were drawn in order to allow the activation of the laser only inside these regions. The extremely versatility of the technique was proved by the possibility to design ROIs of various shapes (e.g., circle, grid, bar, linear pattern, triangle etc.) (Figure 2.1).

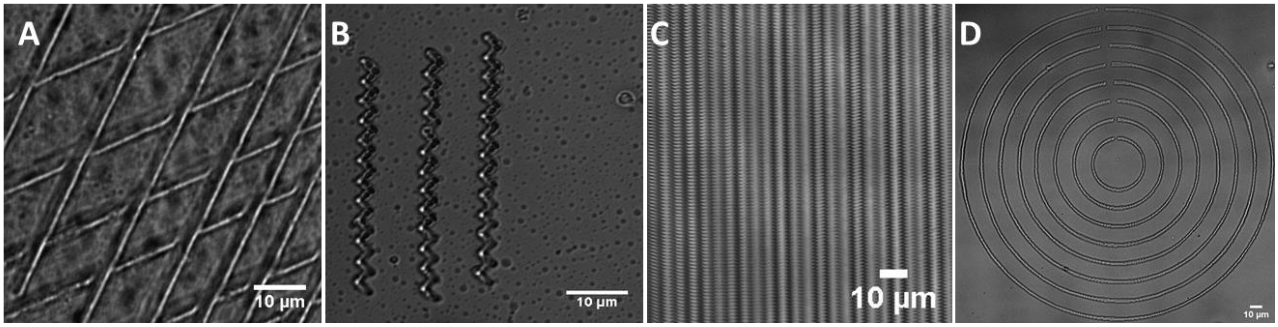

Figure 2.1. Topographic patterned surfaces of pDR1m obtained drawing different ROIs with a confocal microscope. A) Grid, B) zig-zag structures, C) linear pattern and D) circle.

In fact, the innovation of this approach is not only the extensive topographic versatility possible during the pattern fabrication that allows us to made-up different kind of arrays, but also the possibility to change the topography after the fabrication, switching between different patterns.

In this work among a plethora of possible patterns, we chose to focus principally on ridge/groove structures because they could recapitulate some features of native cell environment resembling the collagen structures of ECM, and because they were easy fabricated by our optical set-up.[82, 88] In more details, the Gaussian laser beam of a confocal microscope induced a material displacement in the direction of the linear polarization of the laser light, with the result of a central groove with a lateral

ridge along the light polarization direction. So, preliminary experiments were performed to set the optimal conditions to inscribe topographic patterns on azopolymer material which could be suitable for our biological experiments. Because our purpose was to fabricate a homogeneous array for stem cell culture, we embossed patterns onto the entire pDR1m film which was spin coated on a 5 mm diameter glass. We used an objective magnification 25x, that allowed to pattern for every scanning an area of 495 μm x 495 μm. Successively, we drew rectangular ROIs (2.5 μm x 495 μm) spaced of 2.5 μm and irradiated the sample for 42 seconds at 514 nm, generating easily parallel gratings. We selected this ROI size because the most relevant biological effects at cell-material interface are observed when the topographies exhibit dimensions approximate those of cells (from 70 nm to 2-5 μm).[6] The resultant topographies obtained by this method, relied strongly on confocal microscopy parameters. For this reason, it was reasonable to expect that the embossed topographies were affected by both laser illumination properties (e.g., intensity, polarization states and wavelength) and processing parameters (e.g., laser speed, beam scanning, laser direction). So, because potentially a great variety of topographies could be fabricated, we performed a preliminary screening to understand the relation between microscope parameters and pattern features. For example, the ROIs position relative to the scanning direction profoundly affected the resultant topography. In particular, by drawing rectangular ROIs arranged horizontally (O) to the scanning direction, we observed linear ridges with longitudinal fringes along the grooves (Figure 2.2 a). Conversely, when we fabricated rectangular ROIs, orthogonal to the scanning direction (V), we observed the presence of high needles on the top of ridges (Figure 2.2 b). In this way, we could finely fabricate pattern with different features in x and y planes. Along the axis x, the pitch was defined from the ROI size while in y plane, the pitch and depth of needles that protruded from the top relied on confocal parameters (i.e. format). To sum up, vertical arrangement of ROIs led to a needles-grating pattern with a height of about 300 nm, while horizontal ROIs position brought about a linear ridges array (height = 120 ± 10.7 nm) with parallel fringes. We could also obtain a variety of topographies embossing consecutively patterns with different orientation on the same surface. For example, grids (G) were obtained with 2-steps illumination, initially obtaining a linear pattern (O) and subsequently overlapping the same array rotated of 90° on the first one (Figure 2.2 c).

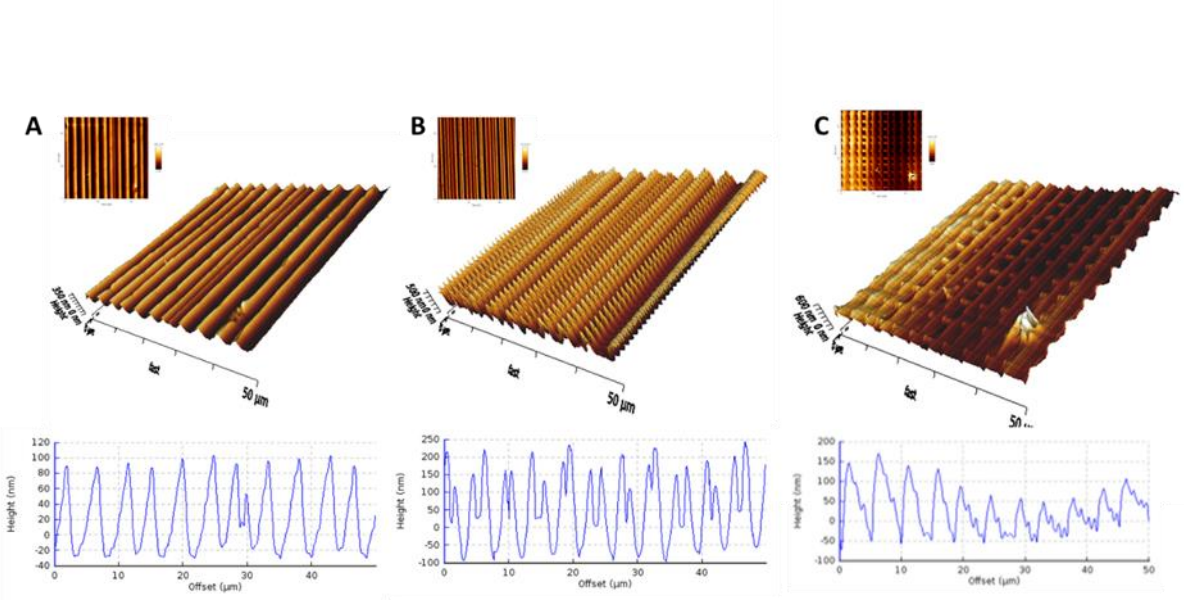

Figure 2.2. Three-dimensional AFM images and cross-section of A) linear pattern (O); B) needle-grating V realized with ROIs arranged in opposition (orthogonally) to scanning direction, and C) 2D grating obtained by two-step illumination.

Maintaining some parameters fixed -*i.e.*-the wavelength (514 nm), the dwell time on a pixel, the scan speed (400 Hz) and the ROIs size (2.5 µm x 495 µm)-, we changed the ROIs position relative to laser scanning direction, the scan direction (mono or bidirectional mode) and scan format (1024 x 1024, 2048 x 2048).[115] In Figure 2.3, we report the comparison between topographies obtained changing the scan direction and the format. When ROIs were perpendicular to scanning direction (V), the height and periodicity of fringe protrusions on the ridges were strictly correlated with scan format. The format dictated how many pixels were used to cover the scan field and as result, the size of the pixel changed with the selected format. In our condition, the scan format defined the features of fringes that protruded off on the ridges. For a scan format of 1024 x 1024, every pixel was 0.48 x 0.48, while if the scan format was of 2048 x 2048, the pixel size was reduced to 0.24 x 0.24 µm. The bigger was the number for pixels for line, the minor was the height and periodicity between fringes. Fringes fabricated with a pixel number equal to 1024 x 1024, were deep about 100 nm with a periodicity of 1200 nm (Figure 2.3 a), while increasing the pixel number (2048 x 2048) the height decreased of roughly 50 nm and the periodicity was reduced to 600 nm (Figure 2.3 b).

As explained previously, the format defined the pixel size and consequently the amount of azopolymer displacement during the illumination, so it was reasonable that the pixel size affected the pattern features. Furthermore, by modulating the scan of the object area in a single− or bi−directional fashion (keeping the same format and the ROIs orthogonal to laser scanning) was possible to obtain a different distribution of fringes on ridges. In a bidirectional mode, fringes protruded off with an

alternate arrangement (Figure 2.3 a,b), while in single-directional mode, a symmetric displacement of azopolymer created aligned needles that protruded off 100 nm from only one side with a pitch of 60 nm (Figure 2.3 c).

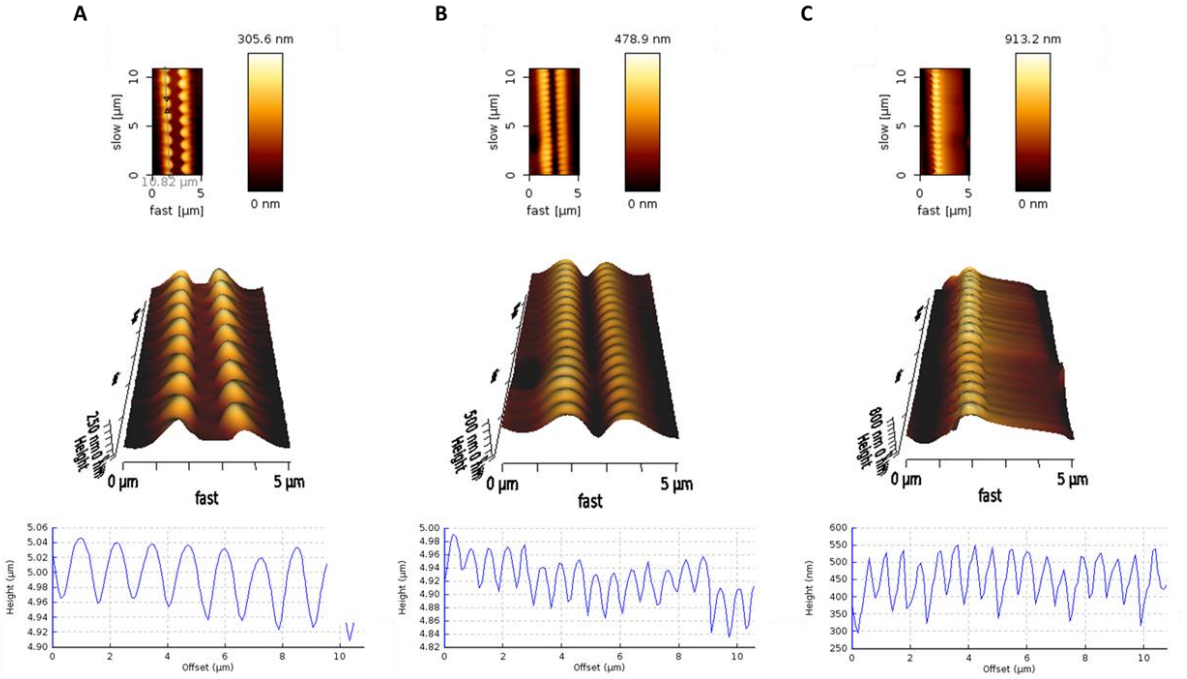

Figure 2. 3. 3D AFM images and cross-section profiles of linear pattern with grooves and ridges of 2.5 µm obtained with an Argon Laser at 514 nm. Different conditions have been tested; A) bidirectional mode, format 1024 x 1024; B) bidirectional mode, format 2048 x 2048; C) monodirectional mode, format 2048 x 2048.

2.3.2 Pattern Erasure

The fabricated patterns could be thermally or optically erased. The azopolymer was globally randomized to the initial disordered state heating the sample above the glass transition temperature (85 °C), or locally randomized by using incoherent and unpolarized light with a mercury lamp or circularly polarized light (CPL) with the confocal microscope.[131] In this thesis, because our aim was to work in biological condition, the molecular orientation of azobenzenes was randomized optically rather than by heating. Furthermore, in order to improve light induced pattern modification or erasure in the presence of cells, the fabrication parameters were set in the presence of cell medium. The laser beam or incoherent light had to pass also through the culturing medium after colliding onto the patterned surface. As analyzed by Rianna *et al.*, the process of pattern erasure was profoundly affected by the presence of an aqueous environment.[87,115] For these reasons, we investigated the

writing/erasure process both in dry and in wet conditions. We employed a mercury lamp, implemented in the Leica confocal microscope (15 mW intensity, 488 nm filter) for 1 min, to erase the pattern. In this case, the illumination of the sample led to a decrease of initial ridge height (120 nm) of about 100 nm (Figure 2.4a). The same condition was tested also in a wet environment, but the formation of bubbles−like structures with a height of 700 nm were observed at the polymer surface (Figure 2.4 d). It is likely that bubble-like structures were due to light scattering or promoting uncontrolled interactions between water and the azopolymer. Furthermore, we tried to erase the pattern used a CPL with a confocal microscope. In a dry environment, we illuminated the embossed linear pattern (h=120 nm) with CPL at 514 nm for 42 sec. The initial pattern height was deleted and the lines of laser scanning generated another highly regular pattern perpendicular to initial array with depth of 40 nm and pitch ~ 1μm. More in detail, the erasure of pattern was obtained setting the scanning direction of CPL laser beam perpendicular to the initial pattern and illuminated the entire scan area without ROIs (Figure 2.4 c). While in a wet environment, the same conditions led to a completely pattern deletion and a surface roughly flat (Figure 2.4 e).

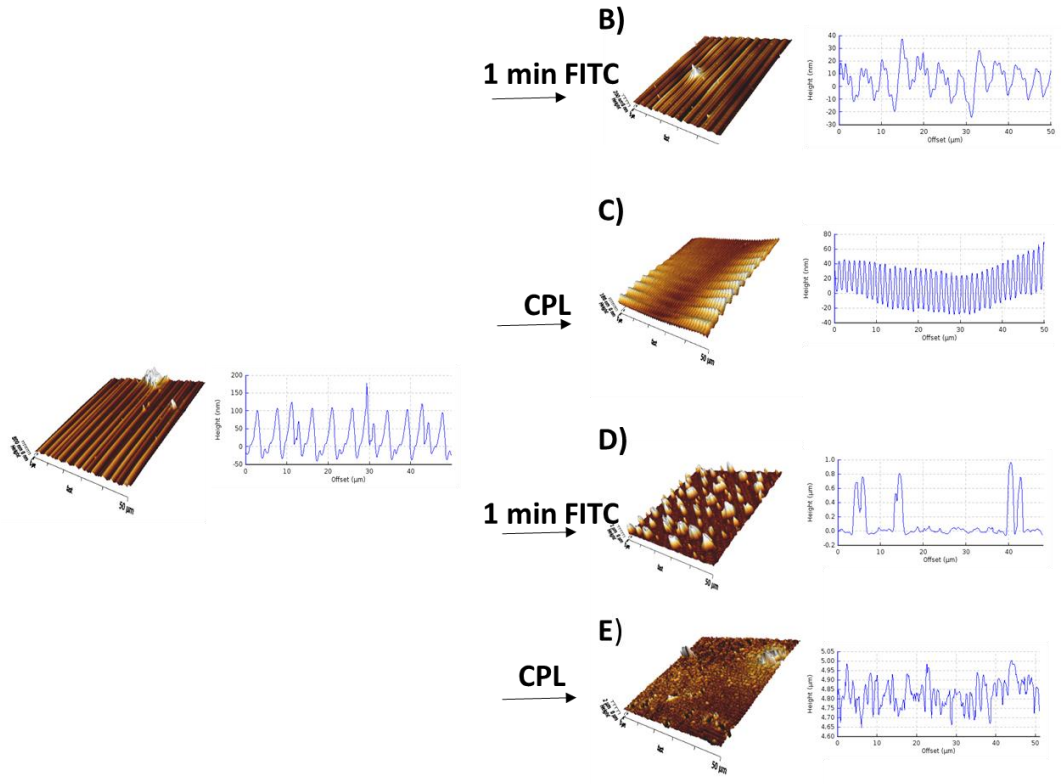

Figure 2.4. A) 3D AFM images of linear pattern as fabricated with a height ~ 200 nm. 3D AFM images of erased patterns in dry condition, B) the initial pattern was illuminated with a Mercury Lamp with a green filter (FITC) for 1 min or C) with a CPL illumination by confocal microscopy for 42 sec. 3D AFM images of erased patterns in wet condition (in presence of the medium), D) the linear pattern was irradiated with a mercury lamp with a green filter (FITC) for 1 min or E) it was irradiated by confocal microscopy with a CPL for 1 min.

2.3.3 Cell Adhesion, Orientation and Elongation on Static Pattern

Recently, cell behavior on static topographic patterns has been widely analyzed and special attention has given to results on groove/ridge topographies.[17] Many topographically patterned arrays with different geometries and sizes have been proposed aiming at controlling the mechanical stimuli on stem cells.[132-133] These studies showed that surface topography directly affects cell adhesion, orientation, elongation, proliferation and differentiation. In particular, on grooved patterns, strong cellular and nuclear alignment due to contact guidance are generally observed in the pattern direction.[44] Abagnale *et al.* reported that MSCs deposited on small surface pattern with 5 μm grooves (2 μm ridges) showed an elongated phenotype and differentiated mainly toward an osteogenic lineage. On the contrary, when MSCs were deposited on larger motifs (15 μm ridges), cells were less elongated and adipogenesis was favored. [37]

In this Thesis, different patterns were fabricated to assess the role of topographic features on hMSCs shape in static condition. Successively, cell shape and alignment were analyzed on dynamic topographies switched *in situ*. We chose to focus on hMSCs response on linear pattern (O), needle grating (V) and grid (G) using flat (F) polymer films as control. Furthermore, we fabricated ridges and grooves (O) of various dimensions by drawing ROIs with different sizes of ridges in a range between 2 to 10 μm and with a ridge/groove ratio equal to one. Preliminary results, in accord with literature, showed that hMSC cells were more elongated on grooves with 2.5 μm width than 5 μm and 10 μm (data not shown). [37] Thus, we focused on topographic pattern with groove and ridge size of 2.5 μm to investigate hMSCs response in terms of cell adhesion (length and orientation of FAs), cell shape and differentiation. Cells were elongated on 2.5 μm linear pattern (O) with a $I_{max}/I_{min} = 24.3 \pm 9.5$ and the majority of stress fibers ran along the entire cell body length being oriented along the pattern direction as it is observed by staining with Phalloidin-543 in Figure 2.5 a. We considered aligned only cells that had an orientation angle within ± 20° with respect to the lamellar pattern orientation, indicating with 0° a perfect cell alignment and with an angle of 45° random orientations. Cells on needle grating (V) were neither elongated on the ridges ($I_{max}/I_{min=}$ 13.5±7.5) nor aligned to the pattern, and displayed a number of thick actin bundles remote from the nucleus (Figure 2.5 b). A very different cytoskeleton structure was formed in cells on the grid pattern and flat surface in which a sparse network of thick and radially assembled fibers was observed (Figure 2.5 c,d). Cells appeared not elongated (~ 10°) and random distributed (~ 45°) on G and F. To sum up, after 24 h from seeding, single hMSC was aligned and elongated on O while randomly spread on F and G surfaces, and not

significantly oriented on V (Figure 2.5 e,g). Furthermore, it was no observed a significantly difference between cell area on different topographic patterns (Figure 2.5 f).

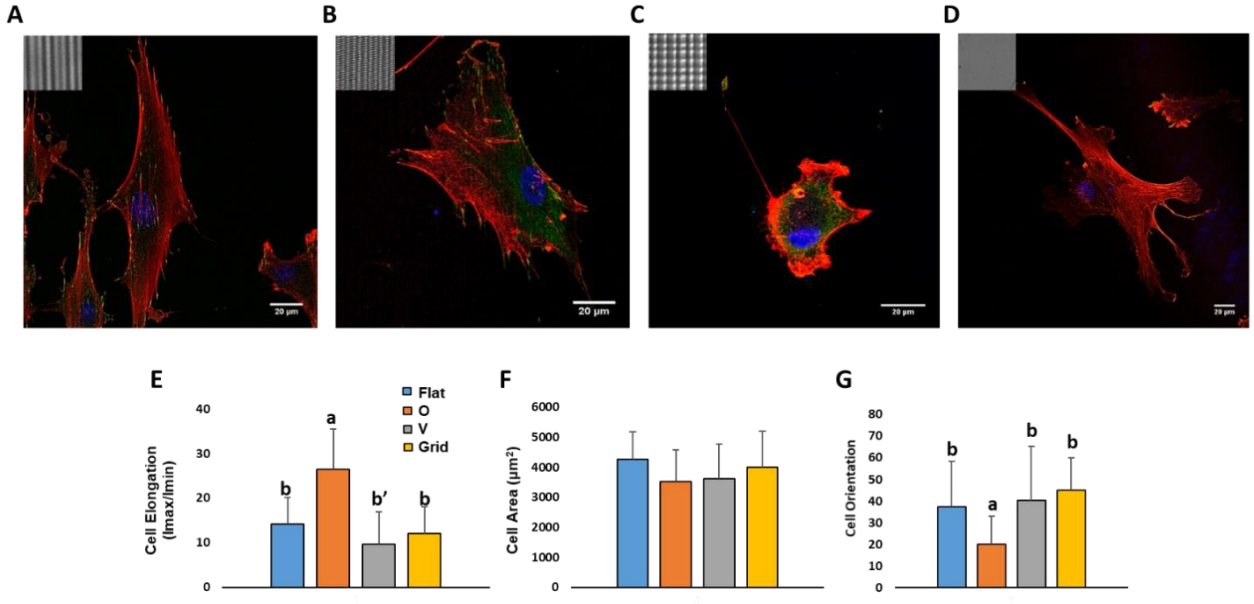

Figure 2.5. Confocal images of hMSCs labelled with rhodamin phalloidin (cytoskeleton), vinculin (focal adhesions) and DAPI (nuclei). Cells were cultivated on A) 2.5 µm linear pattern (O), B) 2.5 µm needles-grating, C) grid and D) flat pDR1m surface. Scale bars are 20 µm. 2.000 cell/cm^2 were seeded on pDR1m substrates so that analyzed cells were not in contact with other cells. Micro-photopattern architecture directed alignment and shape of single hMSCs. E) Cell elongation (I_{max}/I_{min}), F) cell area and G) cell orientation on F, O, V and G. Conditions labeled with different letters were statistically different (ab'' $p < 0.001$, ab' $p < 0.01$, ab $p < 0.5$).

As known, changes in the nuclear morphology are generally regarded as early indicators of cellular differentiation.[134-135] Thus, we also tracked changes of nuclear area and aspect ratio. Nuclei of single cells on aligned patterns (O) (Figure 2.6 b) were found to have higher aspect ratios (mean aspect ratio, AR~3) than on flat surface (AR~2) (Figure 2.6 a) and other patterns (Figure 2.6 g). Furthermore, cell nuclei on O were preferentially aligned with the pattern direction while flat, needle-grating and grid substrates showed no nuclear alignment preference (Figure 2.6 f). It was also observed a lower nuclear area on O pattern then flat topography, but not significantly.

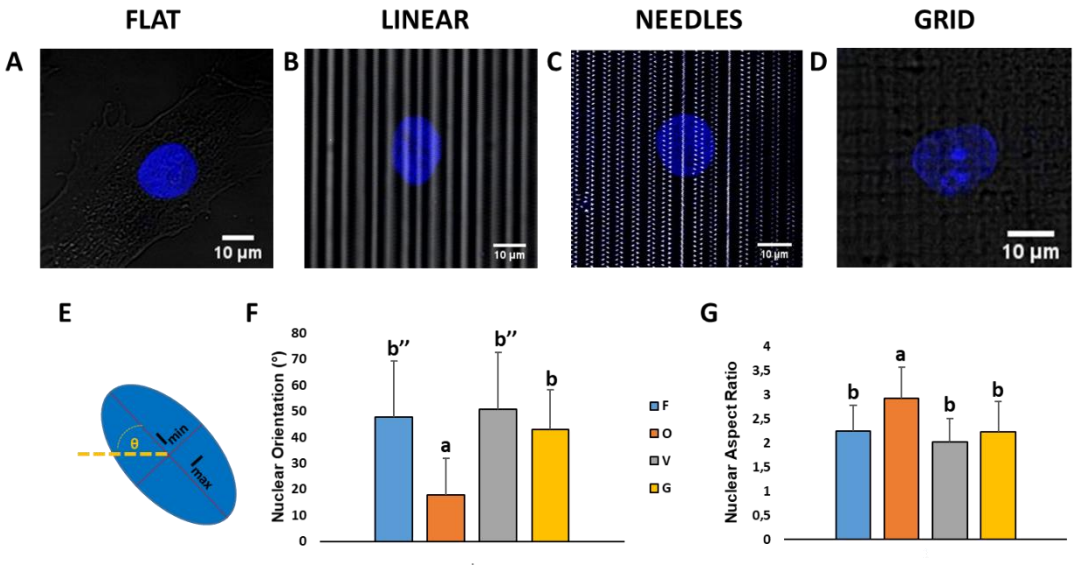

Figure 2.6. Cell nuclei analysis on micro-photopattern architecture. hMSCs nucleus staining with DAPI on A) flat, B) linear pattern, C) needle-grating and D) grid. Scale bar of 10 µm. E) Representative image of cell nucleus, red lines represent main axis of cell nucleus (maximum and minimum). The angle between I_{min} and the reference axis is shown in yellow. F) Nuclei orientation and G) nuclear aspect ratio on O, F, V and G. Conditions labeled with different letters are statistically different (ab'' $p < 0.001$, ab' $p < 0.01$, ab $p < 0.5$).

Recent literature studies, highlight that FA assembly could play a fundamental role on the regulation of cell fate.[136] FAs could tune the cytoskeleton-generated forces employed by the cell at the interface and alter the cell contractility that successively could deform the nucleus and impact on the regulation of cell fate through the cytoskeleton-nuclear axis.[6, 137] The first phase of cell/material interactions depends on adhesion protein (*i.e.* integrins) and the quality of this phase can influence the cell signal transduction, promoting the action of transcription factors and consequently regulate gene expression for differentiation.[136]

We analyzed morphological features of FAs on the different patterned topographies compared to flat samples. The distribution of vinculin patches on flat substrates was completely random (37.5° ± 1.3) (Standard error of the mean, s.e.m), while mature vinculin patches were observed across patterns, which were mostly following the cell alignment (19.3° ± 0.7) on linear pattern (O) (Figure 2.7 a,c) Interestingly, a considerable number of FAs were located at cell periphery and were predominantly co-localized with the pattern ridges on O patterns. Moreover, from the distribution of FA lengths with respect to pattern orientation in Figure 2.7 b-d (right side), was emerged that mature FAs (10-20 µm) were mainly oriented to the pattern, instead, FAs with dimension minor or comparable with the pattern size (2.5 µm) showed a random distribution on any topographies. FAs on linear patterns had length (3.27 ± 0.1 µm) and area (2.65 ± 0.1 µm) comparable with those measured on the flat substrate (length = 3.69 ± 0.1, area = 3.05 ± 0.1) which displayed FAs broadly distributed. On V patterned

substrates, FAs were not alignment to the pattern (~44°) and FAs appeared smaller than others surfaces (2.85 ± 0.1 μm), probably due to needle-grating topography that created unfavorable zones for adhesion plaques to establish and to grow. As expected, FAs also on grid were randomly oriented with a broad distribution (Figure 2.7 d). Our results are consistent with other reports that emphasize the role of FA assembly and orientation on cell shape and elongation.[138] It is reported that surface patterning can control the initial assembly of focal adhesions, hence guiding hMSCs through the process of self-organization and differentiation.[139] Taken all together, these data demonstrate that topographic patterns were very effective in modulating the material−cell crosstalk.

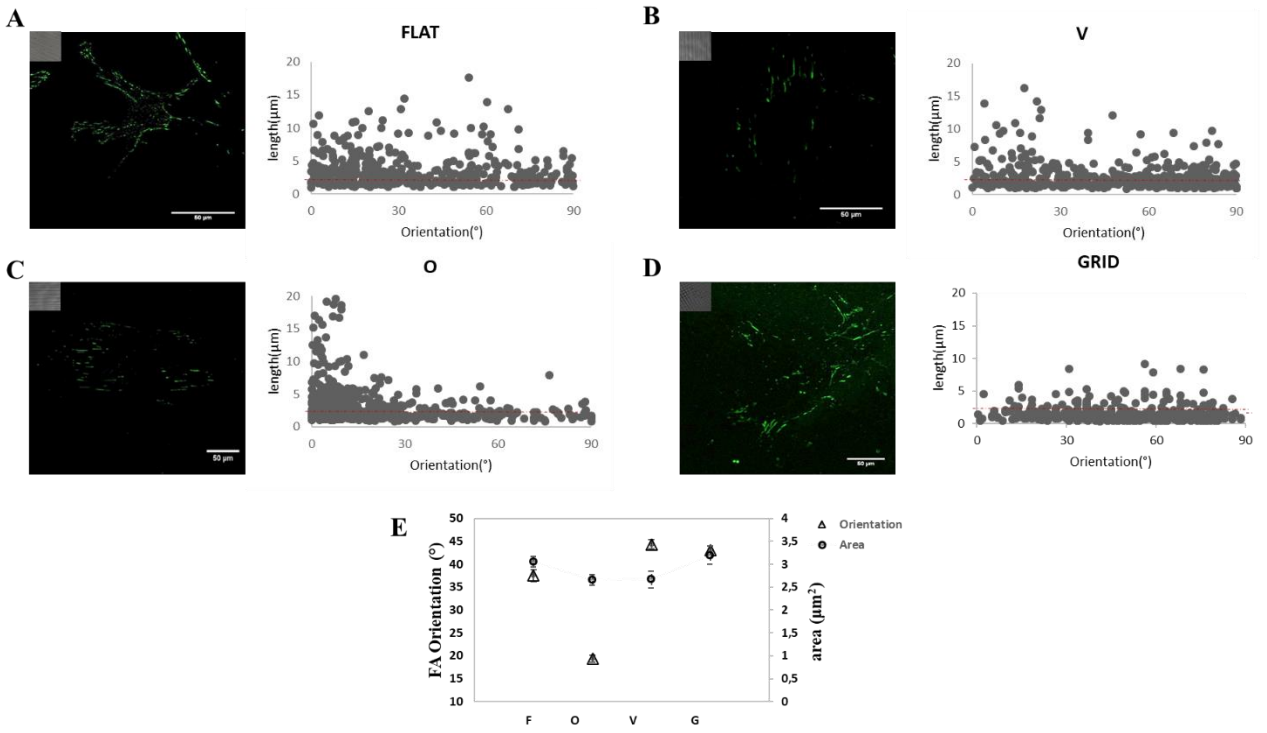

Figure 2.7. Confocal image of focal adhesions (vinculin, green) and distribution of FAs length and orientation on A) flat, B) needles-grating (V), C) linear pattern (O), and D) grid (G). Red dashed line is traced along 2.5 μm. E) Plots of the FAs orientation (triangle) and FAs area (circle). Bars indicates standard error of the mean.

Furthermore, hMSCs alignment was strongly dependent on cell density, such that increasing cell density led to formation of dense cell sheets which strongly hindered cellular alignment on static patterned substrates and cellular response to topography switches on dynamic substrates. Thus, we investigated how cell-substrate interaction could be altered by cell-cell contacts. To examine the effect of micro-scale architecture on groups of cells, hMSCs were plated at low (2.000 cell/cm^2) and high density (20.000 cell/cm^2) on O, to investigate the relationship between alignment and plating density. After 24 h post seeding, the nuclei of hMSCs were stained with DAPI and their orientation

angle was evaluated. At low density (single cell analysis) roughly 70% of cells were aligned along the ridges on linear patter (O), while at high density, the percentage of cell nuclei oriented on the same pattern was decreased of ~ 13% in comparison to lower density. Cell nuclei were equally randomly spread on other surfaces (F, V, G) at both densities. In conclusion, we found that human mesenchymal stem cells cultured on groove/ridge (O) showed greater cell shape, actin cytoskeletal, nuclear and FA elongation and alignment relative to other topographies for single cells and also for groups of cells, but in the last case, the percentage of cell alignment could slightly decrease in relation to cell's density. In fact, in agreement with the literature, cell–cell interactions can overcome cell–substrate interactions at higher density.[44, 140]

2.3.4 Cell Response to Dynamic Pattern

We investigated how cell orientation and adhesion morphology responded to dynamic pattern switching. More in detail, to demonstrate the potential and versatility of the azopolymer surfaces in dictating cell morphology, hMSCs were cultured on flat surfaces for 1 day (Figure 2.8 a), followed by various *in situ* switching surfaces. After 2-day seeding, the polymeric film was patterned embossing a linear pattern O on the flat surface (FtoO) (Figure 2.8 b). The cellular nuclei orientation was evaluated by staining after 24 h from topographic switch. The distribution of nuclear orientations of hMSCs was parallel to linear patter and cells appeared elongated (Figure 2.8 e). After further 24 h (4-day seeding), the linear pattern was overwritten to obtain a grid (OtoG) (Figure 2.8 c) and nuclei of hMSCs appeared randomly oriented on it (Figure 2.8 f). Different patterns could be imprinted several times on a cell populated azopolymer support, influencing cell response without compromising cell viability.

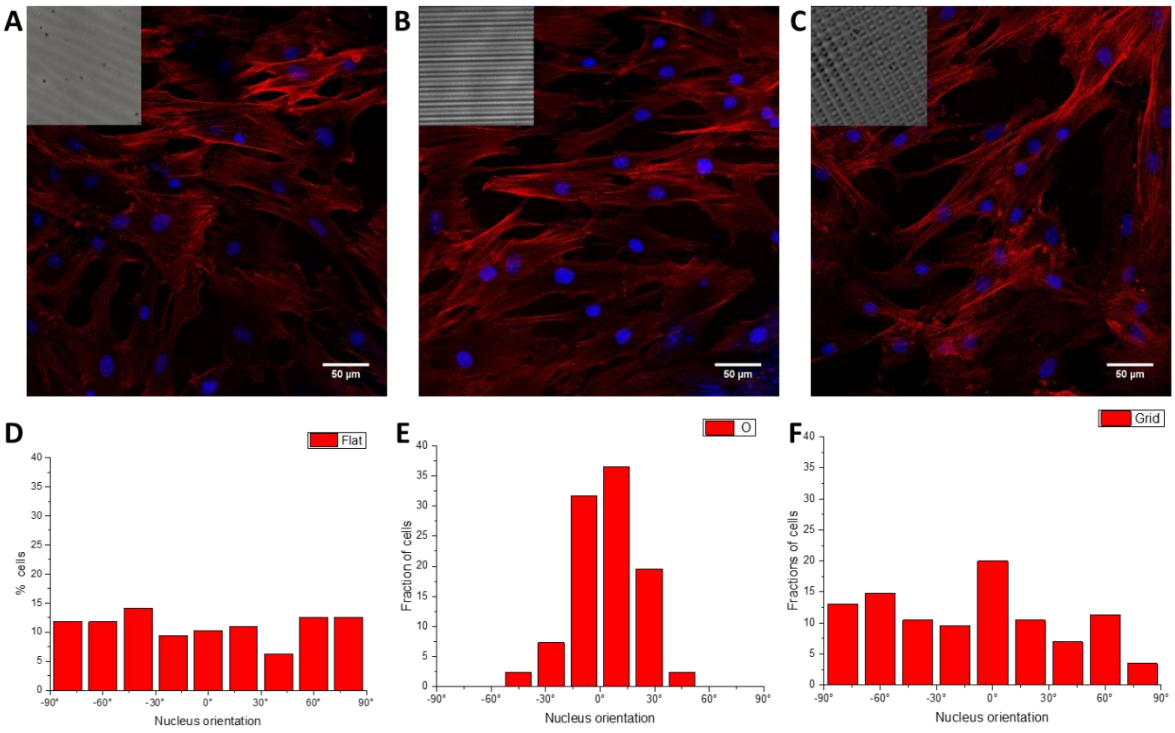

Figure 2.8. hMSCs were seeded on a flat surface of pDR1m and successively the topography was modified in the presence of cells. Confocal images of hMSCs staining the cytoskeleton with Phalloidin (Red) and the nucleus with DAPI (blue) A) on flat surface where cells are randomly oriented, B) on linear pattern, after FtoO switch where cells appear aligned along the ridges and C) on grid after OtoG switch, where cells are again randomly orientated. Scale bar of 50 µm. Statistical distributions of the nuclei orientation angle for hMSCs D) after 1 day of culture on Flat, E) on FtoO at day 2 and F) OtoG at day 4 (n > 200).

We could change the topographic pattern from OtoG or delete the linear pattern and came back to initial flat surface OtoF. We chose to change the topographic pattern instead of erasing it, because previous studies in our group showed that the switch from linear pattern to grid topography (OtoG) reduced cell attachment, involving a faster cell cytoskeleton remodeling and a faster decrease of Young modulus than the deletion of pattern from linear to flat (OtoF). The inscription of topographic patterns profoundly affected the cell mechanics more than the deletion of the linear pattern with regard to Young's modulus (data not already published). For this reason, we expected that OtoG had a major impact on cytoskeleton assembly of hMSC cells relative to OtoF.

The azopolymer platform could be considered as a reversible system because the initial random cell distribution was restored after OtoG switch. hMSCs had an average angle of deviation of 45° on flat surface, after the topography switch from F to O, cells became align in the direction of the lamellar patterns (~20°) and appeared again randomly oriented on grid after O to G (~45°) (Figure 2.9 a). There was no statistically significant difference between nuclei orientations on flat surfaces and grid before and after the light-stimulated topographic change. Static substrates were also used as controls

for each condition at days 1, 3 and 5. Furthermore, whereas cell orientation was very sensitive to switch of the topography, FAs length did not display significant changes on F (3.5 ± 1.1), O (3.0 ± 1.3) and G (2.9 ± 0.9) (Figure 2.9 b). In this experiment, we proved that cells could have a reversible behavior on dynamic platform and it is a crucial aspect within the context of dynamic signal presentation in order to mimic the remodeling of natural ECM.

In our work, we initially focused on cell response in term of orientation and morphology on dynamic surfaces, highlighting that the topographic switch could induce a morphological cell variation on demand. Successively, we proponed to investigate whether a dynamic reshaping of cell environment could also affect the hMSC differentiation. In order to achieve our goal, we first of all analyzed the effects of culture time on the stem cell response on dynamic platform. hMSCs were pre-cultured on flat substrates for 1, 5, 9 and 13 days prior to the topography switch (from FtoO) and cultured for 1 additional day, successively cell nuclei were stained with DAPI to investigate the cell response. As control, hMSCs were cultured on static flat and patterned substrates for a total culture times of 2, 6, 10 and 14 days. The increasing cell density during the culture time, could affect the hMSCs response because a higher cell density and cell-cell interaction could reduce the cell-material crosstalk during the topographic switch. However, for static patterned substrates, the percentage of cells with preferentially aligned nuclei increased significantly from 62 to 93%, between culture day 2 and 6 and it was holding steady until culture day 14. While for hMSCs on dynamic patterns, the percentage of cells with preferentially aligned nuclei decreased significantly from 77 to 63 at day 6 and 10 respectively, further to ≈ 15% at day 14 (Figure 2.9 c). Thus, the cell-topography interaction was still relevant after 10 days from seeding, allowing the cell reshaping on switched surface. At 14 days, cells did not respond to topographic variation, likely due to cell overcrowding.

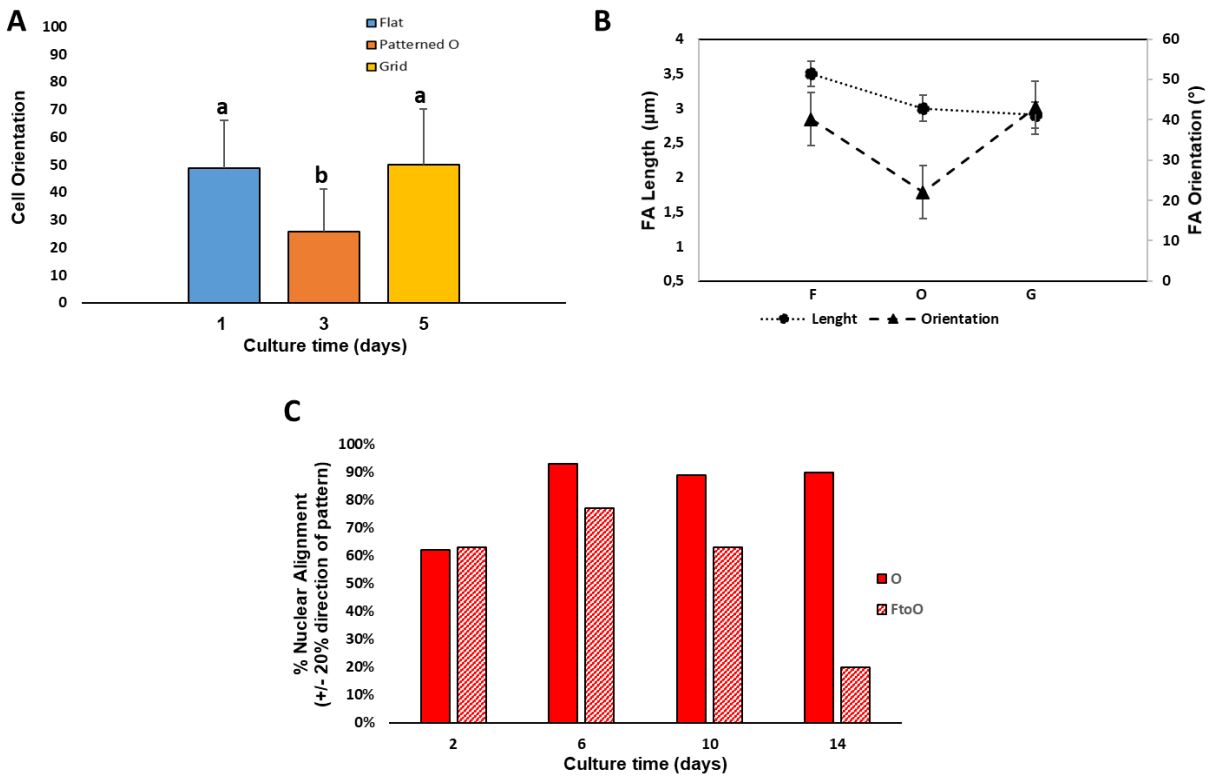

Figure 2.9. A) Cell orientation on pDR1m substrates after topographic switch. hMSCs orientation on flat surface at day 1, on O after FtoO switch at day 3, and on G after OtoG at day 5. The cell analysis was done after 1 day of cell culture on switched surface. Conditions labeled with different letters were statistically different. B) Plot of length (circle) and orientation of FAs (triangles) respect to the pattern direction. For the grid and flat surface, angles were evaluated with respect to the horizontal axis. Bars refer to standard error of the mean. C) Percentage of nuclear alignment on the linear pattern O (red columns) and on switched surfaced from FtoO at 2, 6, 10 and 14 days (red-patterned columns).

This preliminary analysis allowed to define the time-window in which hMSCs were still able to response to switchable topography. It is known that high cell–cell interactions override cell–substrate interactions, showing cellular alignment decrease due to overcrowding.[140] hMSCs alignment was strongly dependent on cell density, such that increasing cell density led to formation of dense cell sheets, which strongly hindered cellular alignment on static patterned substrates.[20] For this reason, we tuned in our experiment the surface properties no later than 10 days from the cell seeding.

2.3.5 Stem Cell Differentiation in Static Conditions

We have presented a system that allowed a switch between two or more topographies in the presence of cells, on which hMSCs rapidly reorganized their morphology in response to surface changes. Furthermore, our approach allowed the maintaining of high cell viability and attachment during the dynamic external stimuli. Nonetheless, before investigating the impact of dynamic cue on stem cells,

we chose to explore the topographic effects on morphologies and differentiation outcome of hMSC in static condition, namely when topography was not altered by external cues. We performed gene expression analysis using quantitative real-time polymerase chain reaction (rtPCR) and fluorescent immunohistochemistry. To literature data, substrates with micro- and nano-topographies, independently of substrate biochemistry, seem to have significant effects on cell fate.[141] In fact, cell shape relies on topography that regulates the switch in the lineage commitment of hMSC by modulating endogenous RhoA activity. When hMSCs are allowed to adhere, flatten and spread, they undergo osteogenesis, whereas unspread, round cells become adipocytes.[108] Apparently, changes in cell spreading alter RhoA-mediated cytoskeletal contractility, focal adhesion assembly and downstream integrin signaling. Effects of substrate topography on cell differentiation cannot well established, due to the multitude of studies, sometimes with contradictory results, found in the literature.[141] Dalby *et al.* reported that random circular nanostructures promoted and directed osteoblast differentiation of mesenchymal stem cells without the need of osteogenic promoter cell culture medium.[31, 114] Even, Oh *et al.* observed that nanotubular-shaped titanium oxide surface structures allowed a specific differentiation of hMSCs into osteoblasts by using only the geometric cues, eliciting a dramatic stem cell elongation, which induced cytoskeletal stress and selective differentiation into osteoblast-like cells. Watari *et al.* showed that topographic ridges and grooves, especially in the smaller biomimetic size scale (400 nm pitch), were feasible ways to improve osteogenic differentiation in hMSCs.[25] Other than material stiffness and geometry also factors such as different culture medium, coating material, seeding density could cue the hMSCs into a different cell path. This explain why many studies reported different results.[111] Nonetheless, we can infer from literature that cell spreading and elongation are components of cell shape that can influence cytoskeletal configuration and in particular osteogenic differentiation.[142] Because we selected topographies on which cells appeared to be elongated as confirmed by morphological cell analysis previously discussed, we investigated mainly osteogenic commitment of hMSCs in our biological analysis. hMSCs were cultured on substrates where cells appeared to be randomly spread (planar, F and grid, G) or aligned and elongated (patterned, O). They were cultured for 21 days without osteoinductive agents and the expression of osteogenic gene markers were determined using rtPCR at 7, 14 and 21 days. To assess the expression of lineage specific markers in response to the topographic properties of our photo-responsive azopolymer substrates, we chose to analyze early and late stage markers associated with osteogenesis (RUNX2, ALPP and BGLAP). Initial analysis of hMSCs for osteogenic lineages showed little change in gene expression profile and immunostaining of common osteogenic markers with topography. RUNX2, also called Cbfa1, is a transcription factor required for osteoblastogenesis. Ducy *et al.* reported that RUNX2 bounds the osteocalcin promoter

and it is expressed in early stage of osteoblastic differentiation.[143,144] In our study, the expression levels of RUNX2 were progressively increased during the culture time from the beginning but there was no statistically significant influence of O topographies on RUNX2 expression compared to planar controls (Figure 2.10 a). While cells on grid did not seem to slightly promote the RUNX2 expression. Alkaline Phosphatase (ALPP), is a marker of mature osteoblasts that initiates and regulates the synthesis of extracellular matrix, which is the core of differentiation. We observed an increase of ALPP expression at day 14 (Figure 2.10 b) but not statistical significant relative to planar control. We also examined the expression of BGLAP marker (osteocalcin) of mature osteoblasts. A major stimulatory effect of topography O upon BGLAP expression was observed comparing them with grid and planar controls at 14 days and 21 days (Figure 2.10 c). These data demonstrate that ridge/groove topography slightly promoted osteogenic differentiation of stem cell relative to other surfaces also without differentiation inducers. Further, to verify our conclusion we chose to immunostaining hMSCs with RUNX2 and BGLAP. In Figure 2.10 c a major expression of BGLAP on linear pattern O (yellow) is shown, while the fluorescent signal is not observed on G or F surfaces.

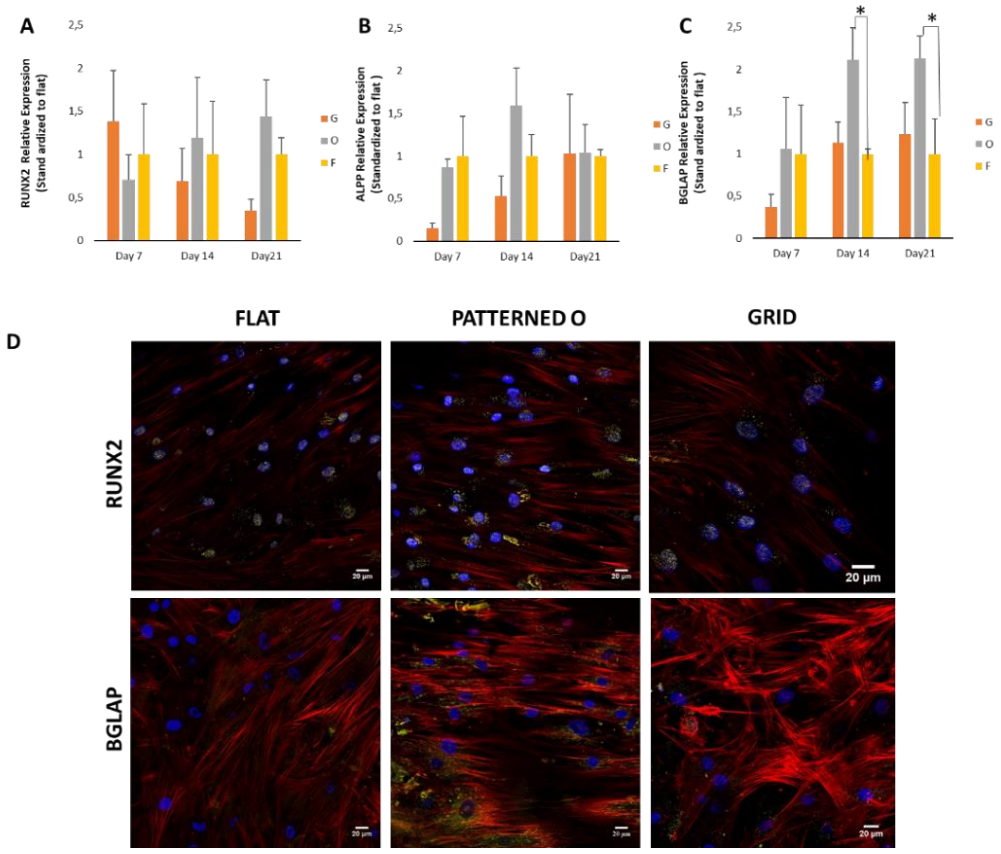

Figure 2.10. A) RUNX2, B) ALPP and C) BGLAP gene expression, were measured by quantitative rtPCR at day 7, 14 and 21 on grid (G), linear pattern (O) and flat (F). The expression of BGLAP and RUNX2 was first normalized to the expression of endogenous control GAPDH and then normalized to the BGLAP and RUNX2 expression of the planar control at each day. D) Representative immunofluorescence images: staining for hMSC nuclei (blue), actin (red), RUNX2 (yellow) (upper part) and BGLAP (lower part). Scale bar of 20 µm.

2.3.6 Stem Cell Differentiation on Dynamic Pattern

Our aim was to tune the cell cytoskeletal tension, switching on demand the topographic pattern underneath stem cells and observing its impact on the gene expression profile during osteogenic differentiation. The cytoskeletal tension induced by topographies, plays a fundamental role in stem cell differentiation or reprogramming.[112] So, we wondered if the modulation of cytoskeleton tension by dynamic topographies during the cell differentiation could regulate the stem cell lineage commitment. In particular, we investigated the expression of osteogenic markers after the change from linear to grid substrates. hMSCs were seeded on pre-patterned linear array O at low density, and after 10 days of culture, hMSCs were undergone to a topographic change *in situ* from O to grid G and cultured for other 11 days with and without osteogenic differentiation media. The choice of 10 days as switching point was guided by our results in static condition that demonstrated hMSCs capability to response to a change of topographic cues up to 10 days and a progressive increase of osteogenic expression on O pattern between 7-14 days after seeding, as confirmed by Wang et al. [145] We observed that in these conditions (OtoG switch at day 10) cells from an elongated and aligned shape passed to randomly oriented and more stretched morphology. In fact, switching the topography, the actin cytoskeleton was reorganized and the elongated stress fibers along the pattern were reassembled in a random way. After 21 days, *rt*PCR was performed to understand whether dynamic changes in surface topography and mechanical forces had influenced and regulated stem cell differentiation. Thus, we quantitatively examined some marker genes in osteogenic differentiation (RUNX2 and BGLAP) of hMSCs cultured on the static and dynamic surfaces with or without the differentiation induction reagent. Comparing the dynamically changing OtoG patterns (D) to the ones on the static microgrooves (O), we observed that the transcription of genes involved in the osteogenic pathway was slightly inhibited (Figure 2.11). Also Gong *et al.* reported a decrease of osteogenic markers with a dynamic change in surface but in their approach, a thermal controlled four-stage SMP led to an increase of aligned cells that promoted myogenic expression and inhibited osteogenic markers.[123] We might speculate that the alignment and elongation of hMSCs on O can promote osteogenic differentiation in contrast with random and not elongated cells on flat or grid surfaces, as confirmed by *rt*PCR *in static* conditions. Under specific contexts, hMSCs specify through different phases from osteoprogenitor to preosteoblasts (initial stage) and finally committing to osteoblast and osteocyte phenotypes (later stage).[146-147] Our results showed that after 10 days, when the differentiation was not at a mature stage yet, the topographic change could tune the gene expression of osteogenesis. Our hypothesis needs to be confirmed by further analysis at different switching points in early and middle differentiation phases to understand the correlation between the time in which the topography is changed and osteogenic gene expression profile. We propone in our future experiments to alter the

topographic cue in the initial stage of stem cell journey and compere the results with ones here reported. Furthermore, we intend to analyze the cell response also in other dynamic surfaces such as from flat to ridge/groove (FtoO) pattern in order to verify if the opposite switch compared to that one tested in this thesis can, instead, lead to an increase of expression of osteogenic markers.

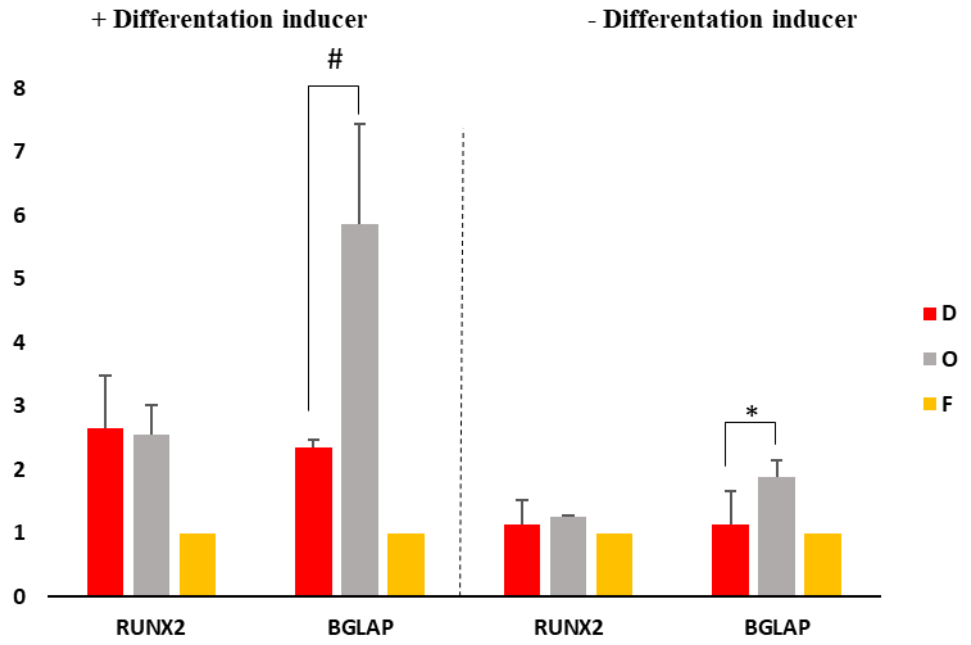

Figure 2.11. rtPCR analysis of osteogenic (RUNX2, BGLAP) markers on dynamic surface (OtoG) (D) linear patterned (O) and Flat (F) topographies, with addition of osteogenic differentiation media (left part) and without inducer (right part). The expression of BGLAP and RUNX2 were first normalized to the expression of endogenous control GAPDH and then normalized to the BGLAP and RUNX2 expression of the planar control at each day (# $p < 0.001$, * $p < 0.05$).

2.3.5.1 Conclusion

In this work, we examined the effect of topographic changes of azopolymer substrates on stem cells behavior, from cell shape to differentiation potential. Taking advantage from the mass migration effect observed after light-stimulation of pDR1m azopolymer, we switched the topography from linear patter (O) to grid (G) in the presence of stem cells. Initially, we evaluated mesenchymal stem cell response after the topographic change of surfaces in term of cell shape, nuclei and FAs orientation. hMSCs were aligned and elongated on O, accompanied by organization of actin and other cytoskeletal elements in an orientation parallel to the grooves. After the OtoG switch, hMSCs appeared randomly spread and their cytoskeleton was observed as sparse network of thick and radially assembled fibers. Successively, we focused on the influence of dynamic cues on cell gene expression profile and lineage specific differentiation. We chose to analyze osteogenic markers expression in dynamic conditions in comparison to static ones with rtPCR. It is known that the ability of cell shape to determine hMSC differentiation is dependent to cytoskeletal cues related to both the actin cytoskeleton and the microtubule skeleton.[118] The elongated cell shape on the linear surface seemed to promote osteogenesis of hMSCs in static condition, while after the topographic switch, the transcription of genes involved in the osteogenic pathway were inhibited. Indeed, from our preliminary results presented here, in accord with recent reports, we can suppose that dynamic microstructure shifting can modify the tension and the arrangement of cytoskeletal fibers (actin and intermediate filaments) affecting signal transduction and, in turn, cell fate.[123-124, 133, 147]

Chapter 3

Dynamic Manipulation of Membrane Curvature by Light-Driven Reshaping of Azopolymer Substrates

Abstract. The interaction between cells and extracellular environment has been largely investigated in order to engineer CIMs able to instruct cells by triggering specific molecular events.[6] A complete understanding of the cell-material crosstalk is highly complex because of the dynamic and articulate cell environment. Topography plays a key role at cell-material interface, in fact various nanostructures have been reported able to influence many biological processes.[18, 121, 148-151] Cui and coworkers proved that local cell membrane curvature induced by nanostructures (e.g., pillars and bars) directly acts as a biochemical signal able to trigger intracellular signaling such as the actin reorganization through membrane-associated and curvature-sensing proteins.[4,152] In collaboration with Cui's lab, we propose here to investigate dynamically the membrane curvature-dependent actin polymerization at microstructure-cell interface, tuning the cell membrane curvature *in situ* through a topographic reshaping process. In fact, our increasing interest in developing surfaces with tunable abilities, pushed us toward the use of light controlled azobenzene-based polymers.[52-53, 65, 82, 95, 153] Thus, we fabricated array of micro pillars, made-up by soft lithography and successively reshaped by light in the presence of U2OS cells, to investigate *in real-time* the effect of the dynamic topographic modification on filamentous actin (F-Actin) accumulation. After the re-shaping, pillars that initially showed a local accumulation of F-actin around them, displayed an F-Actin reorganization at the elongated pillars' ends due to high cell membrane curvature. In this chapter, we analyzed dynamic curvature-dependent actin accumulation over time, and further we propone to investigate the actin re-organization effect on the cell behavior such as migration.

*The work described in this chapter is part of a manuscript in preparation: De Martino, S., Hsin-Ya, Lou., Klausen, L., Zhang, W., Xiao, L., Cavalli, S., Santoro, F., Netti, P.A., and Cui, B. Dynamic manipulation of membrane curvature by light-driven reshaping of azopolymer substrates.

3.1 Introduction

A variety of material surface properties such as topographic cues influence the cell–material interactions at the biointerface. In this context, the possibility to pattern material surface to influence cell behavior, lead to focus on the improvement of biomedical platforms such as cell-instructive materials (CIMs). Biomaterials have the aim to recapitulate the physiological cell environment *i.e.* - the extracellular matrix (ECM)- that is a 3D dynamic surrounding, where biomechanical re-shaping continuously takes place. In the last decades, many attempts have been carried out to mimic ECM conditions, however, creating smart materials, which can be addressed dynamically, still remain a challenge.[87] Towards smart systems, photo-responsive materials have raised major interest as they can change their properties upon light stimulation. For instance, azobenzene-based polymer has attracted considerable attention due to cyclic *trans-cis-trans* isomerization of azobenzene that leads to an athermal photofluidization process when illuminated by light at a proper wavelength.[72,52, 153] As explained in the introduction of this Thesis, the exact mechanism that occurs in azopolymers under light illumination is being studied by different research groups and still under investigation. In this chapter, we adapt the wide used term photofluidization for describe this phenomena, knowing that the photo-induced "mass migration" or "photofluidization" theories are still under debate. [72-74]

Azopolymers can be easily patterned *via* lithography techniques and successively, re-shaped in more complex geometries through light. For instance, micropillars can be deformed parallel to the polarization direction during laser exposure to give ellipsoidal structures.[94, 98] Under these conditions, these platforms can be used to control and modulate cellular processes at the interface over time/space.[125]

Recently, a variety of studies reported that micro- and nano-topographies are able to influence the organization of the actin cytoskeleton inside cells.[18] In particular, the Cui's Lab underlined a correlation between the membrane curvature induced by vertically aligned nanopillars and actin reorganization through membrane-associated and curvature-sensing proteins.[154] The nanopillar arrays induce cell membrane wrapping and thus generate local curvatures on the plasma membrane that affect curvature-dependent cellular processes such as endocytosis.[149-150, 152, 155] Furthermore, they also proved that the nanoscale topography is able to induce a local actin polymerization in a curvature-dependent manner.[37] By tuning the cell-material interface properties (pillar sizes and shapes), they investigated the relationship between nanostructures and F-actin reorganization and the successive effects on cell adhesion and migration.

In this chapter, we present how light-induced deformation of a micro-textured photo-sensitive azopolymer material can exploit the curvature-dependent cellular processes such as F-Actin

accumulation. In our experimental setup, the pillar elongation can be precisely controlled over time by laser irradiation in the presence of U2OS cells. A starting circular-shaped pillar array of the azo-composite can be then transformed into an ellipsoidal-shaped pillar array through photo-reconfiguration (inducing an athermal photofluidization) with linearly polarized light following the polarization direction of the laser beam. In this way, we can monitor the F-Actin assembly and remodeling in respond to dynamic pillar reshaping over time. Furthermore, we propone to investigate other cellular components/proteins which, together with F-actin, are curvature sensitive and can be affected by a dynamic re-shaping of the culture support. In fact, we first investigate how cells adhere on circular pillars (i.e. labelling the plasma membrane) and then monitor the F-actin and the complex Arp2/3 (involved in nucleation of branched F-actin) accumulation on localized regions of interest, while circular pillars pass to an ellipsoidal configuration.

3.2 Materials and Methods

3.2.1 Micro-pillar array fabrication

Silicon Master Fabrication. 4-inch silicon wafer was first cut into 20 mm x 20 mm square pieces. The substrate pieces were cleaned by sonication in acetone and isopropyl alcohol (IPA) for 5 min respectively, prior to dehydration and hexamethyldisilazane coating in YES prime oven. The pieces were spin-coated with CSAR E-beam resist (2000 rpm for 1 min) and an Electra 92 conductive layer (1000 rpm for 1 min). E-beam writing was done with a JEOL JBX-6300FS system, after which the substrate pieces were developed in xylene for 40 sec and cleaned in IPA for 10 sec. The pieces were then blow-dried. The next step was chromium coating with AJA evaporator to generate a 100 nm thick layer. The chromium layer was then removed in lift-off in acetone sonication and IPA cleaning, leaving only circular mask patterns. The 20 mm x 20 mm pieces were cut into 10 mm x 10 mm chips with DISCO wafersaw, and they were placed on a dummy wafer for dry etching. The dry etching was completed with PT-OX using a CF4-based recipe, at a 7 nm/s etching rate. In the aftermath of dry etching, the chips were placed in chromium etchant for 1 h to remove the chromium masks.

PDMS mold fabrication. Poly(dimethylsiloxane) (PDMS, Sylgard 184, DowCorning) pre-polymer was obtained by mixing the elastomer solution and the curing agent in a proper ratio (here 10:1 w/w). The mixture was poured onto a silicon master (pre-treated for 30 min with chloromethylsilane (Sigma-Aldrich)) and then left to cure at 68 °C for 2 h. After curing, the PDMS was peeled off from the master and used as stamp for imprinting the pDR1m structures.

pDR1m film preparation. A commercially available Poly (Dispersed Red 1 methacrylate) (pDR1m) azopolymer formulation (Sigma Aldrich) was used in this work. pDR1m was dissolved in chloroform (7% w/v) and then spin coated onto a glass coverslip in order to produce thin film of pDR1m. In details, 12 mm diameter circular cover glasses were washed in acetone, sonicated three times for 15 min and then dried on a hot plate prior to spin coating process. The pDR1m solution (15µl) was spun over the cover glass by using a Laurell spin coater (WS-400B-6NPP/LITE) at 2500 rpm for 40 sec. The sample was dried in oven until the solvent was completely evaporated (3 h at 60 °C). AFM (BioScope^{TM} Resolve BIOAFM, Bruker) was used to monitor the thickness of the polymer film (about 300 nm).

pDR1m Array Fabrication (2.5 µm pitch). The pDR1m film was patterned by soft-imprinting as an array of square micro-pillars. The pDR1m film was kept in touch with PDMS mold in an oven at 150 °C, above the azopolymer T_g (82°C), for 12 h, leading the pDR1m polymer to fill the inner volumes of the mold. Successively, the stamp was peeled off and an array of well-defined micro-

pillars was finally obtained. Atomic Force Microscopy (AFM) relieved squared pillars array arranged in two dimensions with a height of ~800 nm and a diameter of 1000 nm.

pDR1m Array Fabrication (5 μm pitch). pDR1m pillars with 5 μm pitch were fabricated by vertical-directional photofluidization of azobenzene materials.[99] This fabrication technique is based on vertical directional movement of azobenzene materials. The pDR1m was spin-coated on a glass slide and the PDMS mold was put in contact with the flat polymeric surface at room temperature. This light-induced fabrication defined directional photofluidization imprint lithography (DPIL) was performed by using two-illumination steps. First, a slantwise- circularly polarized light (532 nm, 4 mW) was directed onto azobenzene materials in contact with patterned elastomeric molds (*i.e.*, PDMS). The azo-film stacks with patterned PDMS was positioned at 45° relative to laser irradiation beam and irradiated for 1 min with circularly polarized light. The resulted flow was drifted upward along the cavities of the molds resulting in pattern formation. This first illumination step was followed by a perpendicular irradiation for 30 sec (532 nm, 1.5 mW) for a structural leveling.[99] Successively, the PDMS mold was gently peeled off. The pDR1m pillars-array dimensions were confirmed by scanning electron microscopy (SEM, FEI Nova), revealing circular pillars with a diameter of~1μm and height of ~1μm, arranged as a squared lattice with a periodicity of 5 μm.

3.2.2 Optical Setup

A 532 nm CW (Spectra-Physics) linearly polarized diode-pumped solid state laser with a maximum output power of 200 mW was used to reshape the azopolymer pillars. To coarsely adjust the laser power an absorptive neutral density filter was placed after the laser head. The laser power was finely adjusted by using a 532 nm half-wave plate followed by a polarizing beam splitter. An electronic shutter was used to selectively controlled the dosage of light delivered to the sample. A laser power of 4 mW was used to illuminate the sample located at the focal length of a 50 mm lens.

The laser beam was associated with a wide-field white-light microscope in transmission mode (Nikon Eclipse T*i*), employing a 10x, NA = 0.25 objective such that the spot size on the sample surface was about 210 μm. The beam could be eventually filtered by a circular polarizer placed on a rotational stage to obtain circularly polarized light along arbitrary directions.

3.2.3 Cell culture experiments

Human osteosarcoma cells U2OS were used in this study. Before cell plating, patterned substrates were sterilized by UV treatment for 2 h, washed 2 times with phosphate-buffered saline (PBS, HyClone) and functionalized with 0.1% gelatin (Sigma-Aldrich) in PBS for 30 min. U2OS cells were maintained in high-glucose DMEM medium (Gibco, with L-glutamine) supplemented with 10% fetal bovine serum (FBS) (Gibco) and 1% penicillin-streptomycin (Sigma-Aldrich). The cultures were maintained in 37 °C with 5% of CO_2.

3.2.3.1 Transfection

Electroporation was used for plasmid transfection. U2OS cells were grown to reach 80% confluence in 6-well plates before transfection. Each well of U2OS cells was treated with 0.25% trypsin-EDTA (Corning) for 3 minutes at 37 °C to induce cell detachment. Trypsin was quenched with medium and the cell suspension was transferred into a 1.5 mL microcentrifuge tube (Eppendorf) followed by 1000 rpm centrifugation for 3 minutes. Cells were the re-suspended in 100 uL electroporation buffer II (88mM KH_2PO_4 + 14 mM $NaHCO_3$, pH 7.4) with 2 uL electroporation buffer I (360mM ATP + 600mM $MgCl_2$) and 2 ug plasmid (1ug each if doing double transfection). The following plasmids, Lifeact-RFP (Michael Davidson Lab, Addgene #54586) and Lifeact-GFP (Michael Davidson Lab, Addgene #54610) (F-actin marker) Arp3-GFP (Addgene #8462), CAAX-GFP (K-Ras CAAX motif) were used in this work. Cells were loaded in a 2 mm-gap electroporation cuvette (Fisher) for electroporation (Amaxa Nucleofector). Transfected cells were then recovered by adding 1 mL of culture medium (DMEM + 10% FBS, no antibiotics) for 5 minutes prior to centrifugation. Cells were then plated on the patterned films and further labelling was performed after 1 DIV.

3.2.3.2 Immunostaining

Cells were washed 3 times by PBS and fixed in 4% paraformaldehyde (in PBS) for 20 min at room temperature. After three PBS washing, cells were permeabilized with 0.1% Triton X−100 in PBS for 15 min and blocked with 1% bovine serum albumin (BSA) for 30 min. Cells were stained with 1:200 diluted Alexa Fluor 594 phalloidin (Life Technologies) for 30 minutes at room temperature.
For CellMask staining, U2OS cells cultured overnight on nanostructured substrates were incubated with 0.25 μg/ml CellMask™ Orange plasma membrane stain for 5 min prior to fixation. After three

washes with Phosphate-buffered saline (PBS) the prepared samples were imaged by confocal microscope (Nikon Eclipse 50*i*) with 60x oil immersion objective (NA 1.4).

3.2.3.3 Live/dead cell viability assay

Live/dead ® Viability/Cytotoxicity Assay Kit (Thermofisher) was used to determine the viability of cells during pillar reshaping. It permitted the simultaneous visualization of live and dead cells with two fluorescent probes: Calcein AM and Ethidium homodimer-1 (EthD-1.) We seeded U2OS cells on pillar array, after 24 h the culture medium was removed and cells were washed three times with PBS. Successively, we irradiated the sample for 5 sec, 15 sec and 30 sec with a laser at 532 nm. The Calcein AM and EthD-1 were dissolved in Opti-MEM (Gibco) at the final concentrations of 2 µM and 4 µM respectively. After the illumination, cells were incubated with the staining solution at room temperature for 30 min before imaging. Control samples for viable and dead cells were performed by seeding U2OS cells on glass-bottom petri dish.

3.3 Results and Discussion

As mentioned earlier, recent studies have shown that vertical nanostructure topographies are able to deform cell plasma membrane wrapped around them.[149] The curvature of plasma membrane at the bio-interface can trigger different intracellular processes such as endocytosis and exocytosis.[156] Furthermore, recent studies have shown that nanostructure-induced membrane curvature can affect not only curvature-sensitive protein activity but also actin cytoskeleton organization.[18] Cell shape and function strongly depend on the cytoskeleton organization that regulate cell adhesion, migration and differentiation.[108, 137] Our attention has been focused on dynamic modulation of topographic cues at the bio-interface and its effect on actin organization. In more detail, our work has investigated the reorganization of F-actin accumulation on "dynamic" vertical structures (bar–like) obtained by coupling soft lithographic methods and light-induced mass migration through reshaping effects of azopolymers.[91-92]

3.3.1 Pillars Reshaping by Optical Set-up

Initially the azopolymer pillar array was fabricated by soft-lithography and successively reshaped by directional photofluidization process with linearly polarized light.[95, 157] Under light irradiation, the azopolymer incurs into a cyclic isomerization exhibiting a strong light-induced mechanical effect both at microscopic and macroscopic scale. *Trans-cis-trans* isomerization induces an athermal transition of the glassy azopolymer, so that, the material passes into a fluid state and flows driven by polarized light.[72] To induce the photofluidization process, we irradiated these azopolymer pillars with a linear polarized laser at 532 nm (power 1.5 mW) for few seconds with the optical set-up described in materials and methods. In agreement with previous works,[93, 96, 98] we observed a directional mass migration of the polymer along the polarization direction. The modification of pillar shape due to mass-migration depends on irradiation conditions (e.g., wavelength, intensity and exposure time).[98] In our case, the initial structures were reshaped into ellipsoidal-shaped pillars, still periodic, that were obtained by precisely controlled the illumination time. The relation between the exposure time and pillar deformation in a range from 2 to 10 sec were investigated. Micro-pillars initially with a circular shape were elongated into ellipsoidal-shape structures by linearly polarized light (LPL) when illuminated for not more than 8 sec. A major irradiation time (10 sec) induced an excessive photofluidization that merged pillars together to form linear gratings (Figure 3.1).

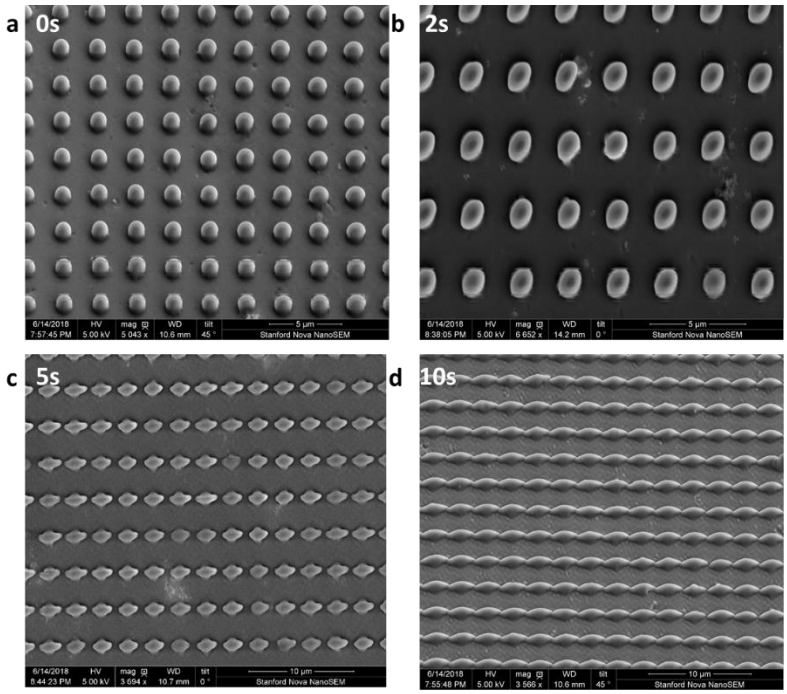

Figure 3.1. SEM images of pDR1m textured surfaces: a) as-fabricated; b) irradiated for 2 sec, c) 5 sec and d) 10 sec at 532 nm.

The ellipsoidal-shape of structures resembled those of domes. In fact, the softening of pDR1m pillars due to the athermal photofluidization caused a leakage of polymer out of the initial confined volume. The polymer flowed from the edges toward the substrate so obtaining 3D-structures such as domes, hardly obtainable by conventional fabrication methods. On the other side, as reported in literature, a more controlled deformation was possible avoiding the polymer overflowing with two different approaches: 1) Lee *et al*. avoided that the material flowed down to the substrate, introducing an extra PDMS capping layer on top of the cylinder array in straight contact with azopolymer,[93] 2) Pirani *et al.* improved the polymer mechanical response making an azopolymer and polymethyl methacrylate (PMMA) blend, avoiding the material overflowing and allowing a reversibly micro-pillars deformation over several cycles.[96] We propone to adopt one of these solutions in future experiments to promote the accumulation of proteins on highly curved membranes obtained by a well-defined reshaped structures. As introduced, we were interesting to take advantage of these phororesponsive platforms for biological investigation. The azostructures *i.e.*-pillars and ellipsoidal-shape structures- can induce membrane wrapping and thus generate local curvatures on the plasma membrane and F-actin accumulation. In particular, the reshape of pillars led to a variation over time of cell membrane curvature at the interface. So, we preliminary tested cells response in term of F-Actin accumulation on ellipsoidal-shape structures with major axis (AM) in the range of 1 μm to 3 μm. Structures with the AM ~2 μm and the minor axes (Am)~ 1 μm, obtained by 5 sec of illumination were selected for further investigation (Figure 3.2).

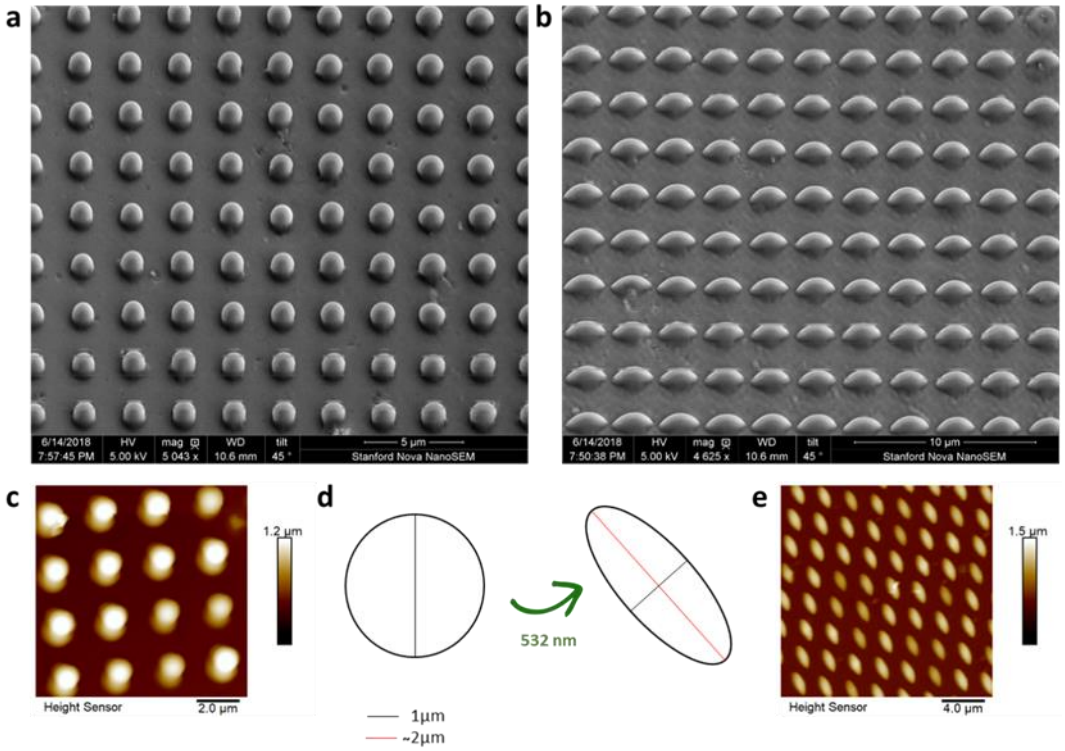

Figure 3.2. A) SEM and C) AFM images of pillar with 800 nm height, 2.5 µm pitch and diameter 1000 nm. B) SEM and E) AFM images after pillar reshaping under green laser illumination for 5 sec, with 600 nm height, pitch < 500 nm, Am ~1 µm and AM 2 µm. D). Representative image of pillar deformation upon light-induced deformation with a laser at 532 nm that induces pillar elongation along the polarization direction of an incident laser radiation.

During the transition of structures from circular to ellipsoidal-shape, the inter-pillar distance significantly decreased from 1.5 µm to less than 500 nm and moreover, also a reduction of pillar height of 200 nm was revealed by AFM. For a quantitative analysis, the mean roundness parameter ε was evaluated as the ratio between the minor (Am) and the major axis (AM) of reshaped pillars averaged over 200 structures. Initially, pillars were almost circular, with a mean roundness (Am/AM) of about 0.95. This value decreased after linearly polarized irradiation leading to a deformation into an elliptical shape to 0.4-0.5. In this way, we could obtain a manipulation of prefabricated azopolymer structures driven by polarized light from pillar to ellipsoidal-shape structures for characterizing the dependence of F-actin accumulation on two different curvatures - high curvature at the ellipsoidal-shape structures ends and low curvature along the side walls.

3.3.2 Pillar Reshaping by Confocal Microscopy

Here, we report an alternative method to modulate the pillar shape by using the focused single laser beam of the confocal microscope that allowed the *real-time* photoreshaped of the pattern in the presence of living cells. In fact, thanks to the microscope equipment, it was possible to precisely localize the focal volume at the polymer surface, avoiding unwanted phototoxicity effects. Moreover, since our confocal microscope was equipped with a temperature- and pH-controlled chamber, the biological environment was preserved. Furthermore, this set-up allowed to precise control the shape of deformed pillars by confocal parameters (*e.g.*, wavelength, scan speed, scan area). In Figure 3.3, AFM images show pillar shape before and after the stimulation with Argon laser at 514 nm for 3 min.

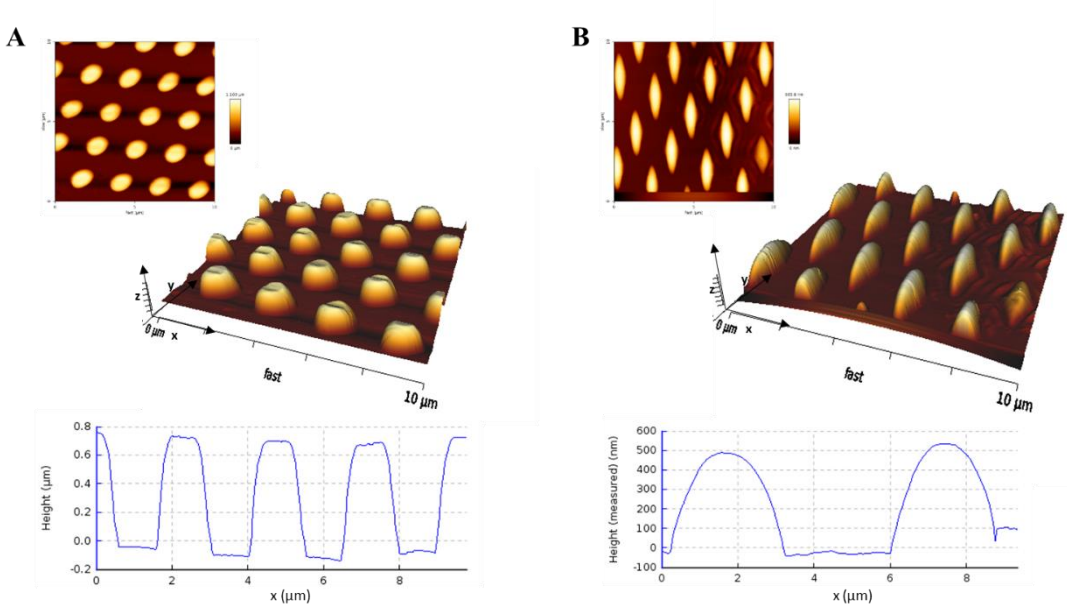

Figure 3.3 AFM bi−dimensional topographic images, three−dimensional images and cross section profiles of pillars along z with 2.5 µm pitch A) before and B) after stimulation with Argon laser at (10%) 514 nm for 3 min.

In the first experiment, we tuned the exposure time from 1 to 3 min, maintaining all other parameters fixed (irradiation with Argon laser and scan area 150 µm x 150 µm) (Figure 3.4 a-d). As expected, increasing the exposure time the *AM* of ellipsoidal structures linearly increased while the height decreased, as possible observe in Figure 3.4 e. Successively, we verified the effect of scan area on pillar deformation, maintaining all other parameters constants (exposure time of 2 min). Decreasing the scan area (100 µm x 100 µm), the pillar deformation was more pronounced, in particular, the length of AM increased of 500 nm and the height was shorter of the 100 nm than with a scan area of 150 µm x 150 µm.

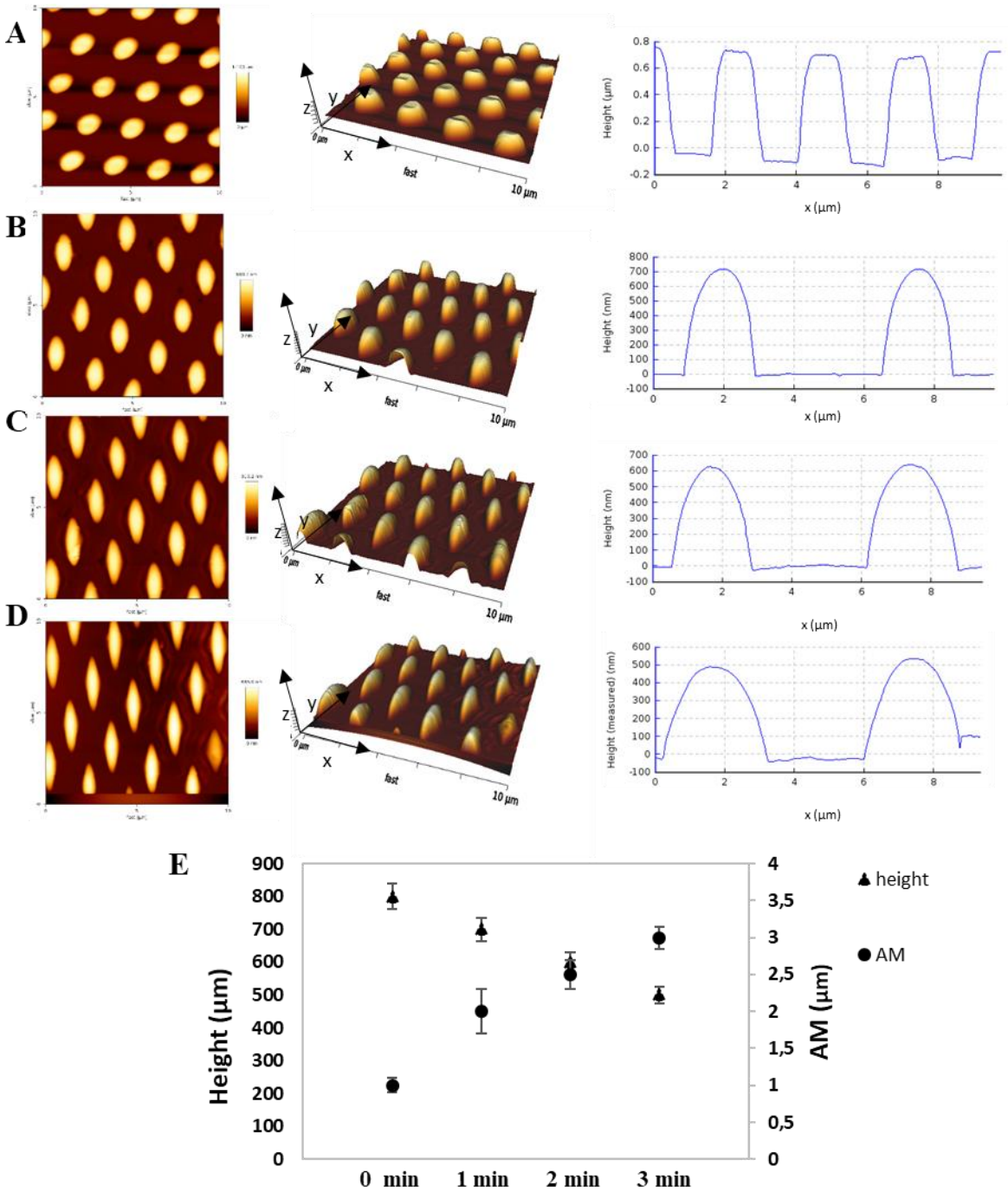

Figure 3.4. AFM bi−dimensional topographic images, three−dimensional images and cross section profiles of pillars. A) Before the stimulation and after the irradiation with an Argon laser for B) 1 min, C) 2 min and D) 3 min. E) Plot of height (triangle) and major axes (circle) of elongated pillars over time (0-3 min).

3.3.3 Pillar Reshaping with Live Cells

The topography manipulation after molding-based fabrication allowed to manipulate the pillar shape *in real-time* in the presence of cells. The pillar array was located up-side-town on the bottom of the petri avoiding the excessive absorption of azopolymer during the imaging. Before stimulation, we acquired a confocal cell image on pillar array. During the imaging, live cells in DMEM medium with 10% FBS were maintained at 37 °C with 5% of CO_2 *via* an onstage incubator. We observed ring-like F-actin accumulation of U2OS cells transfected with lifeAct-GFP, around pillars. In fact, vertically aligned micropillars can induce plasma membrane curvatures and consequently F-actin accumulation around the structures. Successively, the azopolymer array was stimulated with a laser at 532 nm for about 5 sec with the optical set-up described in the materials and methods. A wide-field white-light microscope in transmission mode was employed to visualize the pillar array during the stimulation. The laser spot illuminated homogeneously a circular area of roughly 210 μm diameter. This approach allowed for 1) creating a dynamic platform where the laser spot could be precisely localized, 2) modulating the platform behavior over time and 3) limiting toxicity effects on cells. In Figure 3.5, is reported the live/dead analysis after 5 sec, 15 sec and 30 sec of illumination. U2OS cells were still alive after 15 sec of illumination but, increasing the exposure time, the live-dead ratio decreased. This analysis revealed that the azopolymer reshaping with a solid state laser at 532 nm with a power 1.5 Mw for 5 sec was not cytotoxic and allowed to examiner the F-actin reorganization just after the light stimulation.

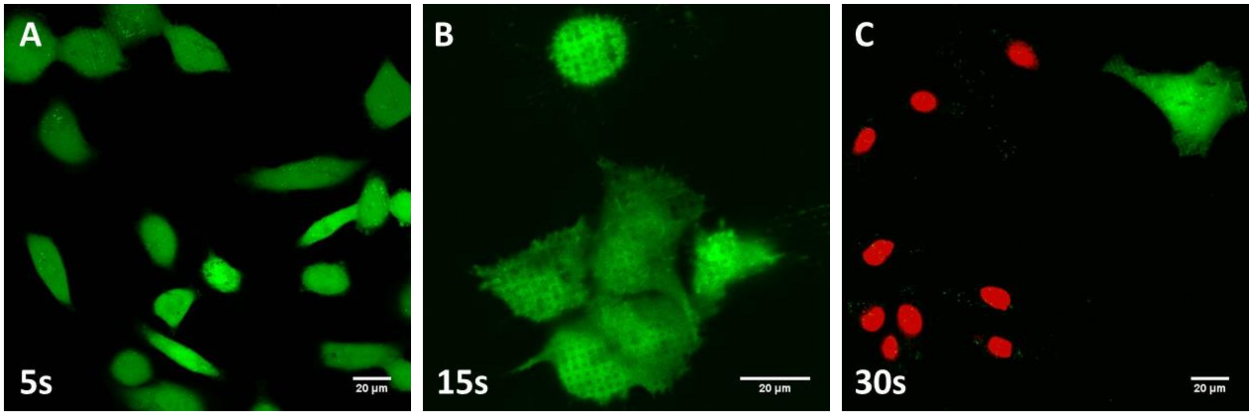

Figure 3.5. Cell viability (live/dead) assay during stimulation with a laser at 532 nm for A) 5 sec, B) 15 sec and C) 30 sec. In the figure the green channel (live cells) and red channel (compromised/dead cells) are merged. Scale bar of 20 μm.

Furthermore, as reported also in Chapter 2, the light interaction with azopolymer in an aqueous media, could sometimes generate some bubbles-like structures in the micrometer range on the azosurface due to light-azobenzene and medium interaction. The bubbles structures on the polymer surface were arranged in a sort of aligned pattern whit an angle roughly of 45° relative to polarized light direction. This interesting response of the azopolymer materials in wet condition is still under investigation but in any case it has not altered the cell response in our experiments.

3.3.4 Membrane Curvature-Dependent Actin Polymerization on Static Azopolymer Array

First, we examined whether the cell membrane wrapped around the azo-pillars inducing the F-Actin accumulation at high curved reshaped pillar ends in static condition. Transfected LifeAct-RFP U2OS cells were plated both on 1) azopillar-array fabricated by soft-lithography and 2) reshaped structures obtained by directional photofluidization process. In the case of pillars, cell membrane wrapped tightly around circular structures and rings morphology were formed, while in the case of re-shaped (elongated) structures the accumulation was mainly observed at the structures' edges. In more details, F-actin accumulated all around the structures when the pillars were irradiated for less than 3 sec; it started accumulating preferentially toward the bottom ends for light irradiation up to 8 sec while there was only a slight accumulation on regions where pillar merged together to form a linear grating after 10 sec of irradiation. In Figure 3.6 a, it is possible to note the F-Actin ring-like accumulation on pillars until 2 sec of illumination, while increasing the exposure time F-Actin dots are observed at the reshaped pillar ends, these dots disappear when pillars are combined together after 10 sec of illumination. In former studies in Cui lab, the molecular mechanisms of nanostructure-induced F-actin accumulation has been investigated. [150, 152] Analyzing the distribution of actin nucleation factors on nanostructures, they reported that branched actin, rather than linear actin, accumulated on nanostructures in a curvature-dependent manner. In fact, one of the key factors that created an actin curvature-dependent effect was the presence of the Arp2/3 complex, known to induce the formation of branched F-actin. To validate their hypothesis also on this platform, we transfected U2OS cells with Arp3-GFP, a subunit of the Arp2/3 complex, to verify its co-localization with F-actin that could prove the branched actin mechanism. The Arp3 expression at structures' edges confirmed that the branched actin mechanism took place in F-Actin accumulation (Figure 3.6 b).

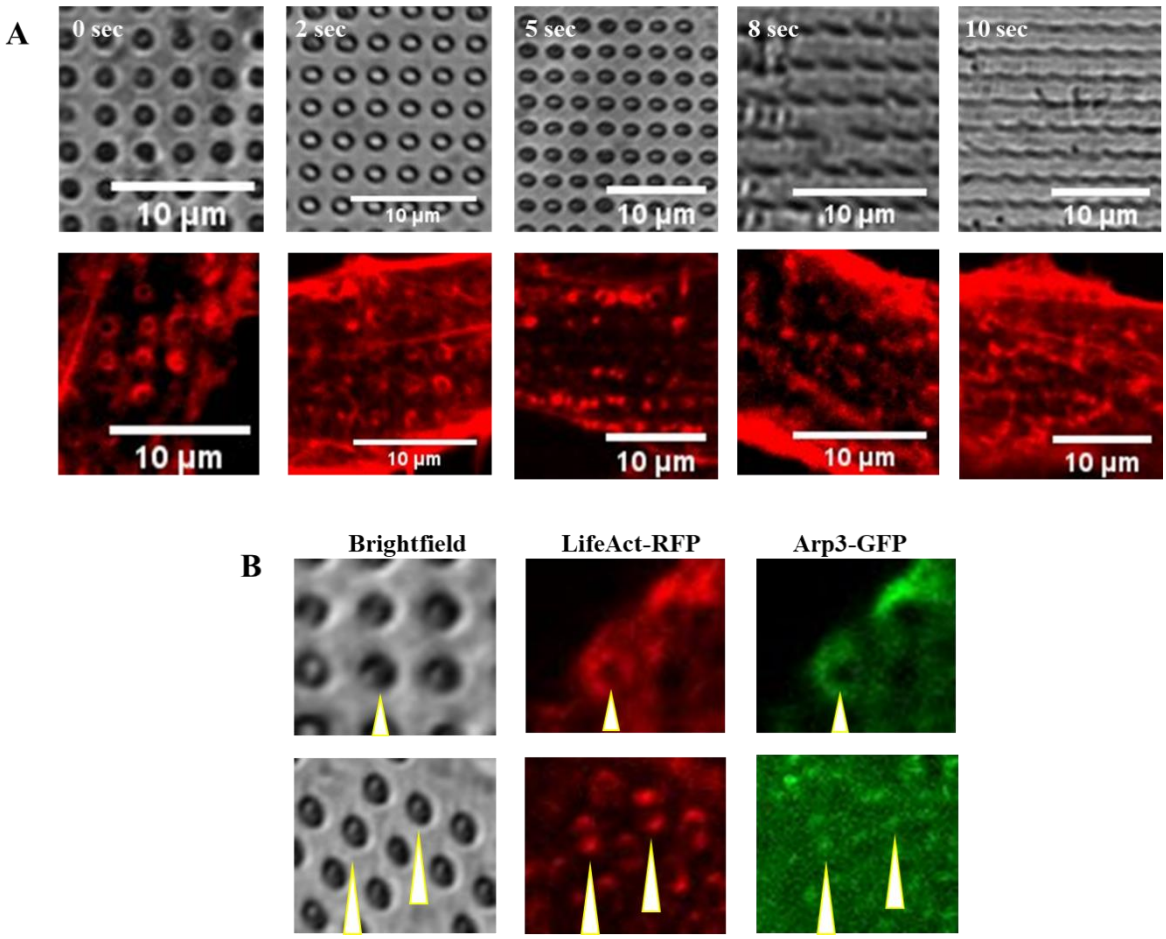

Figure 3.6. A) Upper part, brightfield images of pillar deformation along the polarized laser beam direction at different exposure times. The pillars as fabricated had a diameter of 1 µm, they were slightly elongated (2-5 sec) till a diameter of 2 µm and their inter-pillar distance was significantly reduced (<500nm); a longer illumination (5-8 sec) induced a strongly elongation till to completely merge the structures. Lower part, fluorescent images of Lifeact-RFP on pillars (0 sec) and reshaped structures irradiated for 2 sec, 5 sec, 8 sec and 10 sec. B) (Upper part) Zoom-in of brightfield image of pillars as fabricated and fluorescence images of Lifeact-RFP, Arp3-GFP accumulated around the pillars. (Lower part) Brightfield image of deformed pillars after 5 sec of illumination and fluorescence images of Lifeact-RFP, Arp3-GFP accumulated preferentially at the structure ends (arrows).

The fluorescence intensity of Lifeact-RFP on the reshaped pillar was 1.21 ± 0.04-fold (Standard error of the mean, s.e.m) greater than on the side walls (Figure 3.7 c). A custom-written Matlab code (implemented in Cui's lab) was used to generate square masks located at the ends and sides of bars. For each bar, the fluorescence intensity within the ends and the sides were integrated separately and

divided to calculate the bar-end-to-side ratios). These results confirmed that F-actin accumulation on elongated structures induced strong curvature-dependent F-actin polymerization.

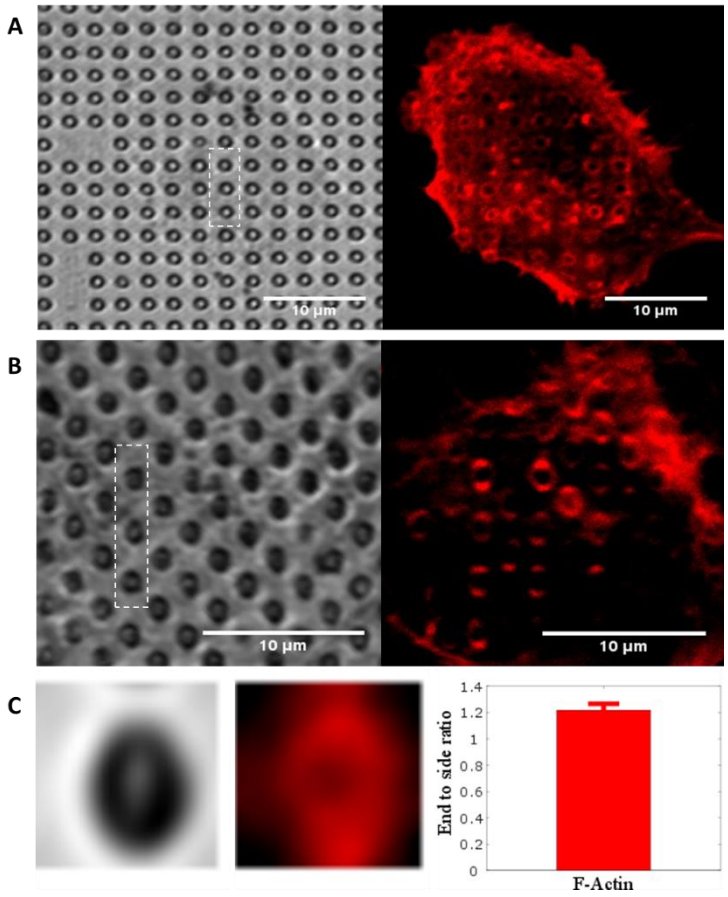

Figure 3.7. A) Brightfield image of pillar (left side) and confocal images of U2OS transfected with LifeAct –RFP (right side). B) Brightfield image of deformed pillar after 5 sec of illumination with a laser at 532 nm (left side) and LifeAct-RFP transfected cell on deformed pillars (right side). C) Brightfield image of elongated pillar (left side), average of intensity of fluorescence (center) and quantified reshaped pillar end-to-side ratios for LifeAct-RFP (right side), n = 137 structure for F-Actin.

We investigated also the behavior of plasma membrane on pillar and ellipsoidal-shape structures, transfecting U2OS cells with CAAX-GFP. We did not observe a considerable wrapping around elongated structures, maybe due to their domes-like structures.

3.3.5 Membrane Curvature-Dependent Actin Polymerization on Dynamic Azopolymer Array

Initially, we evaluated the F-Actin accumulation on reshaped pillars in static condition in order to understand if azopillars were able to induce a membrane curvature-dependent actin polymerization. The positive results brought us to further investigate the effect of *in situ* pillar reshaping on curvature-

dependent F-actin formation. To the best of our knowledge, this is the first work that investigate the reshaped pillar effects on F-actin organization in a dynamic environment. Transfected U2OS cells were seeded on pillar array, after 24 h confocal images of cells that highlighted the F-Actin accumulation as rings on micro-pillars were acquired. This result was confirmed by results published by Cui's lab, in which they reported the observation of ring protein accumulation preferentially on large nanopillars (diameter around 1000 nm) and dots on smaller structures (diameter < 400 nm).[37] Successively, the photo-sensitive pillars were modified by laser illumination with an optical set-up (described in materials and methods) and confocal movies were acquired right after light-deformation. The movies showed a fast reorganization of F-actin accumulation from the region in the surrounding of the pillar to the reshaped structure ends. In Figure 3.8 a, are reported sequential frames of a movie that showed the F-Actin reorganization of U2OS cells transfected with LifeAct-GFP over time. After 5 minutes from pillars' reshaping, the F-actin was still organized as a ring around the pillar, progressively the LifeAct-GFP intensity began to reduce along the lateral side of deformed pillar and accumulate forward the ends (Figure 3.8 b). In average, the F-actin re-organized within 10.14 ± 1.06 min after deformation. The change of intensity profile of Lifeact-GFP along the structure over time is reported in Figure 3.8 c, comparing the F-Actin intensity profile before (0 min) and after 10 min from the light stimulation. While in figure 3.8 d is possible to observe the decrease of intensity along the sidewall and a consequently increase toward the ends of reshaped pillars of F-actin at around 10 min.

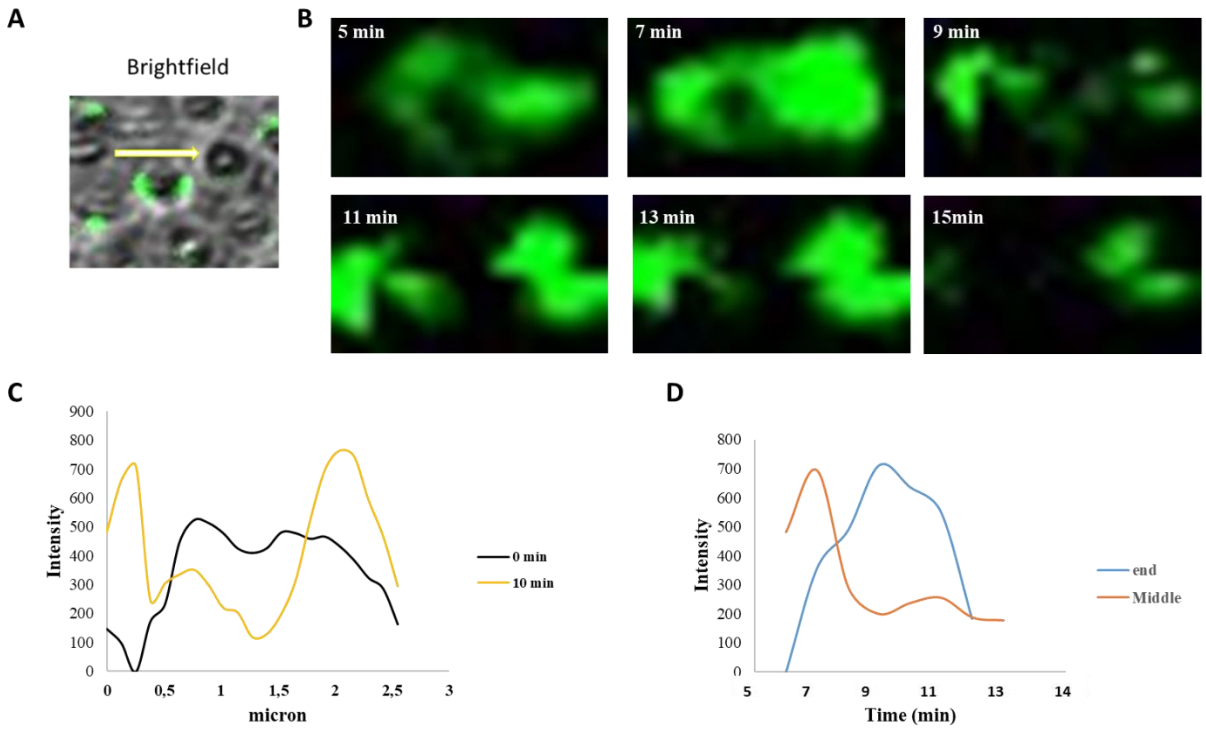

Figure 3.8 U2OS LifeAct-GFP transfected cells on pillar reshaped *in situ*. A) Brightfield and GFP merged channels show the LifeAct-GFP accumulation at the structure ends after 10 minutes from the deformation. The arrow points in the direction of pillar elongation. B) Zoom-in of frames of confocal movie acquired after the light stimulation of azopillars. The frames are acquired at 5 min, 7 min, 9 min, 11 min, 13 min and 15 min after the stimulation. C) Intensity profiles of stack images along time of cell with LifeAct- GFP reported relative to reshaped pillar dimension, before illumination at 0 min (black line) and 10 min after stimulation (yellow line). All the intensity profiles are measured in the same selected ROI and calculated over time with imageJ. D) Intensity of F-Actin accumulation increases over time at reshaped pillar's ends with a maximum at 10 min (blue line) and decreases at middle of structure with a minimum at the same time (orange line).

3.4 Conclusion

In this work, taken advantage from a precise spatial-temporal control of the light induced deformation of azopolymer microstructures, we were able to tune the pillar shape along preferential directions. The surface topography could be controlled at the biointerface in the presence of cells *in real-time*, tuning superficial properties on demand. The reshaped structures were observed to induce a local membrane curvature that consecutively affected the F-actin reorganization inside U2OS cells. When pillar shape was tuned in the presence of cells, the confocal movie recorded after the light-stimulation, showed a rapid actin reorganization. F-Actin labelled with LifeAct-RFP accumulated preferentially on the positive curvature ends of reshaped pillars in about 10 min after light-stimulation. Furthermore, we verified that Arp2/3, a complex to nucleate the formation of branched F-actin, showed the same depended curvature behavior. Previous studies in Cui's lab, have revealed that F-actin accumulation on nanostructures was curvature-dependent. Toca family proteins in particular FBP17, interacted with WASP and cortactin (no membrane curvature depended proteins) and activate Arp2/3-mediated actin polymerization. FBP17 membrane recruitment was highly dynamic and depended on Plasma Membrane (PM) tension.[158] FBP17 was reported as being a PM tensor sensor that activated actin polymerization through the WASP/N-WASP_Arp2/3 complex, thereby increasing PM tension, which in turn promotes its dissociation from the membrane.[158] The correlation between dynamic pillar reshaped and Actin reorganization in our experiments is still under investigation, but our hypothesis is that the light-induced pillar reshaped could dynamically modulate PM tension, which promotes FBP17 and consecutively actin dissociation from the membrane during the reshaped process. So, an increase of PM tension could explain the initial dissociation of actin rings around pillars. After the reshaping, the new pillar shapes could curve the membrane and drive a further recruitment at reshaped pillar ends.

Chapter 4

Hydrogel Scaffolds Containing Azobenzene as Dynamic Cell Culture Systems

Abstract. In this chapter the fabrication of photoresponsive semi-3D gelatin platforms has been investigated with the aim to engineer smart biomaterials that can replicate the dynamic features of ECM. We synthetized hydrogel scaffolds containing azobenzene-based crosslinkers for stem cell culture, overcoming fabrication limit of natural gelatin and taking advantage of azobenzene isomerization to give photo-responsive properties to the materials. High resolution structures have been produced through two-photon polymerization (2PP), a valid technique for fabricating precise micro-nano architectures. As proof of concept, we fabricated gelatin-squared array where hMSCs were physically confined into the channels between the gelatin squares. Photoresponsive scaffolds were deformed by light to tune their mechanical and geometric properties in the presence of cells. Light-triggered expansion of gelatin microstructures induced an in-plane nuclear deformation of physically confined cells. This novel approach propones to pave the way to design dynamic niches to investigate biological responses to environment changes, increasing our understanding on the effects of highly space-time regulated cues on stem cell commitment.

Part of this chapter has been published: Pennacchio, F. A.; Fedele, C.; De Martino, S.; Cavalli, S.; Vecchione, R.; Netti, P. A., 3D Microstructured Azobenzene-Containing Gelatin as Photoactuable Cell Confining System. *ACS applied materials & interfaces* 2017. I contributed principally to the synthetic part (especially related to azobenzene and gelatin-acrylate synthesis). A second part of this chapter is part of manuscript in preparation: De Martino, S.; Fedele, C. Pennacchio; F. A.; Cavalli, S.; Vecchione, R.; Netti, P. A., Photoresponsive hydrogel containing azobenzene photoswitching without UV light. I contributed to the synthetic part, performing biological experiments with stem cells, interpreting results and working on the manuscript.

4.1 Introduction

In the last decade remarkable advancements have been made in the development of smart/stimuli-responsive materials, which can play a significant role for interfacing with biology. In fact, a new challenge arises in designing 3D synthetic materials that can respond to external stimuli with spatial and temporal control and that allows to fine-tune interactions at the cell-material interface, eliciting specific biological responses.[51-52] Up to date, a variety of engineered materials have shown capabilities to control some cell processes and direct their fate, but the knowledge on the basic biological principles that govern cell-material interactions are still limited. In order to overcome these obstacles, scientific research aims at defining platforms with a tight control on their spatial arrangement and temporal evolution to improve understanding on the effects of molecular and physical signals.[159] In this respect, instead of investigate cell behavior on static and planar surface, we have been principally interested to develop "smart" biomaterials able to mimic the complexity of ECM in dynamic and 3D systems. Recently, the use of cell-instructive materials (CIMs) based on light-responsive azopolymers have been constantly increasing. As largely introduced, the azobenzene is one of the most widely used photochromic molecule in this context. Its photo-induced motions can result in relevant morphological and mechanical changes into the polymer matrix.[160] In this thesis's chapter, we report the synthesis of light-responsive hydrogels through the design of an acrylamide-modified gelatin containing azobenzenes as crosslinkers. Part of the results shown here have been previously published by our group.[161] In order to fabricate a scaffold that could emulate properties of the ECM, we combined the hydrogel chemical and mechanical characteristics with light-responsiveness of azobenzene to obtain dynamic semi-3D scaffolds. We employed one of the most promising technique for the fabrication of complex well-defined 3D structures *i.e.* the two-photo-polymerization (2PP). It can trigger highly localized photopolymerization reaction producing complex 3D structures with high resolution. In more details, in our strategy we modified the gelatin and different kind of azobenzene derivatives with acryl-based side groups for light-activated free-radical cross-linking polymerization *via* photoinitiation through 2PP, finalizing the fabrication of three-dimensional (3D) micro- structures.[40] These 3D scaffolds can easily support cell culture because they closely mimic structural features present in the natural extra cellular environment (ECM) with respect to two-dimensional (2D) structures. These photoresponsive high-defined scaffolds allowed to overcome limitations of natural derivate matrices (fibrous collagen or matrigel) modulating the mechanical properties during the fabrication and tuning them on demand with an external trigger. Furthermore, the choice of the type of azobenzene used was crucial in order to obtain a suitable system for cell culture applications. For this reason, we synthesised two azobenzenes both having a half-life

of cis isomers of days, in order to have bistable molecular switches and an “on” and “off” control by the light-stimulation. To sum up, in this chapter we describe the photoinduced deformation observed in azobenzene-containing gelatin and the employment of multiphoton irradiation to manipulate the shape change of scaffolds in the presence of cells. In particular, a light-triggered expansion of these gelatin microstructures induced an in-plane nuclear deformation of physically confined cells. Analysing cell behaviour after the change of their environment by light-stimulation, we could increase our understanding of cell interaction with dynamic artificial materials. Our aim was to take advantage from this innovative scaffold to obtain well-defined dynamic micropatterned cages that could find applications as “engineered stem cell niches”. In fact, they could be used to dynamically tune scaffold dimension and in meantime give a mechanical force to regulate the cytoskeleton and the nucleus of confined stem cells. This mechanical deformation could be translated into cytoskeletal tension that may be a driving factor in stem cell differentiation.[162-163]

4.2 Materials and Methods

4.2.1 Synthesis of Azobenzene-based Crosslinkers

Photophysical and photochemical properties of azobenzene derivatives strongly depend on the substituents on the phenyl groups.[48] Here, we have proposed the synthesis of two different azobenzenes (azo-1 and azo-2), both belong to first class of azobenzene type molecules but with slightly different spectroscopic properties. *Trans→cis* isomerization of azo-1 employed UV light while *cis→trans* occurred with blue light. Azo-2 has methoxy groups in the ortho positions of phenyl rings which modify the spectroscopic properties of azobenzene, so that both isomerizations can be induced in visible range (blue -green light).[62]

4.2.1.1 Azo-crosslinker 1

Azocrosslinker 1 (azo-1) was synthesized by following previous procedure.[34-35] Azo-1 (30 mg, 0.11 mmol) was dissolved in dichloromethane (CH_2Cl_2) with 74 µl of triehtylamine (TEA) at room temperature. 2.4 equiv. of 1-Hydroxybenzotriazole hydrate (HOBt·H_2O), 2.4 equiv. of *N*-(3-dimethylaminopropyl)-*N′*-ethylcarbodiimide hydrochloride (EDC·HCl) and 2.4 equiv. of compound 2 were added to mixture and left reacting overnight. The reaction was followed by thin layer chromatography (TLC) and the product was extracted in dichloromethane. The product was purified by column chromatography and its formation confirmed by Mass Spectrometry. MS (ESI): m/z calculated for $C_{36}H_{54}N_6O_{10}$ 730.39; found: 731.40 $[M+H]^+$. Successively, the compound was treated for 2 h with a solution of 50/50 v/v trifluoroacetic acid (TFA) in CH_2Cl_2 to remove the Boc protecting group, then co-evaporated with toluene and treated with TEA. Finally, Boc-deprotected compound was reacted with 2.4 equiv. of acrylic acid (197 mmol, 14.2 mg), 2.4 equiv. of HOBt·H_2O, 2.4 equiv. of EDC·HCl and 4.8 equiv. of TEA. The reaction was followed by thin layer chromatography (TLC). The product (azo-1-DA) was purified by column chromatography and its formation was confirmed by Mass Spectrometry and characterized by UV/Vis spectrophotometry. MS (ESI): m/z calculated for $C_{32}H_{42}N_6O_8$: 638.39; found: 639.31 $[M+H]^+$.

4.2.1.2 Azo-crosslinker 2

Azo-2, containing methoxy groups on two phenil rings, was synthesized according to the protocol reported by Woolley *et al.* [62] *N*-(3,5-dimethoxyphenyl) acetamide **(1)** (3 g, 19.6 mmol) was dissolved in 50 mL of dry tetrahydrofuran containing 8.2 mL (58.9 mmol) of trimethylamine. 1.5 mL (21.6 mmol) of acetylchloride was slowly added at 5 °C to the solution. The mixture was stirred at room temperature for 20 hours. The triethylamine hydrochloride was filtered off, while the organic phase was concentrated and the product *N*-(3,5-dimethoxyphenyl) acetamide **(2)** was separated by silica gel column chromatography (Biotage KP-SIL 100g, flowrate 50 mL/min) and eluted with 60% EtOAc in petrolatum as a yellow solid (yield: 90%). ^{1}H NMR (600 MHz, $CDCl_3$) δ ppm 2.10 (s, 3 H) 3.72 (s, 6 H) 6.18 (t, J=1.8 Hz, 1 H) 6.68 (d, J=1.8 Hz, 2 H) 7.02 (s, 1 H). ^{13}C NMR (600 MHz, $CDCl_3$) δ ppm 23.80, 54.40, 95.64, 97.03, 138.62, 160.07, 167.16. MS (ESI): calculated for $C_{10}H_{13}NO_3$: 195.09, found m/z 196.10 $[M+H]^+$. A solution of 70% nitric acid (1.2 mL) in 2.2 mL of acetic acid was added dropwise to a solution of **2** (3.4 g, 17.6 mmol) in 200 mL of acetic anhydride at 0 °C. The reaction was stirred for 1 h at a temperature not higher than 7 °C, and then 2 h at room temperature. The solution was cooled, mixed with water saturated with $NaCO_3$ (200 mL) and extracted with EtOAc (3x100 mL). The organic phase was dried with anhydrous Na_2SO_4 and evaporated. The product *N*-(3,5-dimethoxy-4-nitrophenyl) acetamide **(3)** was purified by chromatography on silica gel column chromatography (Biotage KP-SIL 100g, flowrate 50 mL/min) and eluted with 80% EtOAc in petrolatum. Yield: 12 % (0.5 g). 1H NMR (600 MHz, $CDCl_3$) δ ppm 2.20 (s, 3 H) 3.86 (s, 6 H) 6.90 (s, 2 H) 7.20 (s, 1 H). MS (ESI): calculated for ($C_{10}H_{12}N_2O_5$) 240.07, found m/z 241.08 $[M+H]^+$. 0.5 g (2.08 mmol) of **3** was mixed with 60 mL of ammonium hydroxide (30%). To this mixture 2.5 g of Zn dust was added with 1-2 min of vigorous stirring. The mixture was left to stir at 35 °C for 2 h, monitoring the reaction by TLC. Successively, the mixture was filtered through Celite and then the liquid was extracted with CH_2Cl_2 (3 x 100 mL). The organic phase was dried with Na_2SO_4 and evaporated. Further purification was done with silica column chromatography (Biotage ZIP 5 g, flowrate 10 mL/min) and the product *N*-(4-amino-3,5-dimethoxyphenyl) acetamide **(4)** was eluted with 10% of MeOH in CH_2Cl_2 with a yield: 83% (362 mg). 1H NMR (600 MHz, chloroform-d) δ ppm 2.14 (s, 3 H) 3.84 (s, 6 H) 6.73 (s, 2 H) 7.34 (s, 1 H). MS (ESI): calculated for ($C_{10}H_{14}N_2O_3$) 210.10, found m/z 211.11 $[M+H]^+$. 150 mg (0.7 mmol) of **4** was dissolved in 9 mL of dry acetone and to this 0.3 g of AgO was added. The mixture was stirred overnight at room temperature in dark. After this time, it was filtered through Celite and the solid was washed with acetone and MeOH. The solvent was evaporated and the product **Azo-2 (5)** purified on a silica column KP-SIL 10 g and eluted with 10% of MeOH in CH_2Cl_2 and a further purification with SNAP ULTRA 12 g C18 with a gradient

elution using acetonitrile/H_2O (with 0.1% TFA) eluting from 10% acetonitrile. Yield: 13% (0.043 g). 1H NMR (600 MHz, CD3CN) δ ppm 2.02 (s, 6 H) (cis), 2.09 (s, 6 H) (trans), 3.57 (s, 12 H) (cis), 3.75 (s, 12 H) (trans), 6.82 (s, 4 H) (cis), 7.08 (s, 4 H) (trans), 8.26 (s, 2 H) (cis), 8.44 (s, 2 H) (trans). MS (ESI): calculated for ($C_{20}H_{24}N_4O_6$) 416.18, found m/z 417.25 $[M+H]^+$. Successively the azobenzene backbone was further modified to make it photocurable. A mixture of **Azo-2** (16 mg, 0.05 mmol) and thionyl chloride (0.01 mL) was stirred magnetically in 4 mL dry methanol at 40 °C and the progress of the reaction was monitored by TLC. The reaction was stopped after 7 h when the reagent reacted completely. Two products were obtained with a mono-deacetylation **Az-NH_2 (6')** and a bis-deacetylation **Az-2NH_2 (6)**. The products were separated on a SNAP C18 Column. Az-NH_2 was eluted using a gradient of acetonitrile/H_2O (with 0.1% TFA) from 15% acetonitrile to 20% acetonitrile with a flow of 12 mL/min, MS (ESI): m/z calculated for $C_{18}H_{22}N4O_5$: 374.16, found 375.17 $[M+H^+]$ yield 16 % (3 mg, 0.008 mmol). 1H NMR (600 MHz, CD3CN) δ ppm 2.09 (s, 3 H), 3.89 (s, 12 H), 6.15 (s, 2 H), 7.14 (s, 2 H), 8.70 (bs, 1 H). Az-2NH_2, was purified in the same way and it was eluted from 20 % acetonitrile. Yield 60% (10 mg, 0.03 mmol) MS (ESI): calculated for $C_{16}H_{20}N4O_4$: 332.15 Da, found m/z 333.15 $[M+H^+]$, 167.08 $[M+H^+]$. 1H NMR (600 MHz, CD3OD) δ ppm 6.07 (s, 4 H), 3.80 (s, 12 H); 13C NMR (126 MHz, methanol-d4) δ ppm 55.74, 67.68, 90.78, 130.96, 154.25. Then, 10 mg (0.030 mmol) of **6** was treated with TEA and successively dissolved in a mix of DCM/DMF 9/1. Then N-Ethyl-*N*'-(3-dimethylaminopropyl) carbodiimide hydrochloride (EDC HCl; 3 equiv., 17 mg), 1-Hydroxybenzotrazole hydrate (HOBt·H_2O, 3 equiv, 12 mg) and N-Boc-Amido-PEO2-Acid (3 equiv., 25 mg) were dissolved in 1 mL di DMF/DCM and added dropwise to stirred solution of compound **6** containing triethylamine (TEA; 9 equiv). The reaction was left under stirring conditions overnight at room temperature. The solvent was evaporated and the product was purified by C18 column and eluted with 50% of Acetonitrile (ACN) in water (0.1% TFA) to give a purple product **Az-2NH-PEO-BOC (7)** (30%). MS (ESI): m/z calculated for $C_{23}H_{43}N_5O_{10}$: 850.43, found 851.45 $[M+H]^+$. 1H NMR (600 MHz, CD3Cl3) δ ppm 7.44-731(m, 4 H), 3.68 (m, 4 H), 3.63 (m, 4 H), 3.57 (s, 12H), 3.05 (m, 4H), 2.50 (m, 4H), 1.19 (s, 12H); **7** compound was solubilized in a mixture 1:1 of TFA/DCM and left to react for 2 h. Successively, 0.1 ml of water was added to the solution and concentrated under reduced pressure. So, we removed the Boc-, obtaining **Azo-2NH-PEO (8)**. $C_{30}H_{46}N_6O_{10}$: calculated 650.33, found m/z 651.32 $[M+H]^+$, 326.16 $[M+2H]^{2+}$, 217.78 $[M+3H]^{3+}$. 1H NMR (600 MHz, CD3Cl3) δ ppm 7.44-731(m, 4 H), 3.68 (m, 4 H), 3.63 (m, 4 H), 3.57 (s, 12H), 3.05 (m, 4H), 2.50(m, 4H). To a solution of compound **8** and TEA in DCM/DMF (9:1) was added dropwise acrylic acid N-hydroxysuccinimide ester dissolved in DMF. The mixture was stirred overnight to obtain **Az-2NH-PEO-acrylic (Azo-2-DA) (9).** $C_{36}H_{50}N_6O_{12}$: calculated 758.35, found m/z 759.34

$[M+H]^+$, 380,18 $[M+2H]^{2+}$. 1H NMR (600 MHz, CD3OD) δ ppm 7.44-731(m, 4 H), 4.15 (d, 2 H), 4.13 (d, 2 H), 4.05 (dd, 2H), 3.81 (m, 4 H), 3.73 (m, 4 H), 3.60 (s, 12H), 2.66 (m, 4H), 2.34 (m, 4H).

4.2.2 Synthesis of Acrylamide-modified Gelatin B

Acrylic acid *N*-hydroxysuccinimide ester (Aldrich) and 4-Methoxyphenol (MeHQ) (Sigma-Aldrich) were used as received. Gelatin type B (Sigma) was chemically modified with acrylic side groups (Gel-DA). After dissolution of 1 g of gelatin in phosphate buffer (pH 7.8) at 40 °C, 0.76 mmol of acrylic acid *N*-hydroxysuccinimide (NHS)-ester (128.5 mg) and 46 ppm of MeHQ were added to gelatin vigorously stirring. Briefly, after 1 h, the reaction mixture was diluted and dialyzed for 48 h against distilled water at 40 °C. The reaction product was then freeze-dried leading to a white fluffy solid. The degree of substitution was verified using ^{1}H-NMR spectroscopy at 40 °C and quantified by the Habeeb method.[164] A degree of functionalization of 76%, was used for this work.[161]

4.2.3 Gelatin Photoresist Preparation and Two-Photon Polymerization

Acrylamide-modified gelatin B (20 % w/v) was dissolved in a citrate buffer (pH 3.1) at 40 °C for at least 2 h by gently stirring. When the solution became clear, 4 wt% of azo-crosslinker and 3 wt% of Irgacure 369 were added. The gelatin photoresist was heated above the gelation point at 40 °C and then poured on a round glass slide (30 mm diameter, 0.17 mm thickness) and a PDMS reservoir was placed on it. Then the sample was inserted into a two-photon polymerization system (Photonic Professional GT, Nanoscribe GmbH), which uses a 780 nm Ti-Sapphire laser emitting ≈100 fs pulses at 80 MHz with a maximum output power of 150 mW, equipped with a 63x, 1.4 NA oil immersion objective. The system combines a piezo stage and a high-speed galvo mode for faster structuring. For our purposes, a set of squared blocks (30 x 30 x 10 μm^3) with a lateral grating of 3 μm pitch was fabricated. The used parameters were 7500 μm/s as scan speed, 24 mW as output power. The development was carried out stirring the photoresist in hot water (45 °C) for 20 min, that was able to dissolve unreacted material.[161]

4.2.4 Cell Culture Experiments

hMSC cells maintained in growth medium consisting of mesenchymal stem cell basal medium (MSCBM). Cells were incubated at 37 °C in a humidified atmosphere of 95% air and 5% CO_2. Prior to cell seeding, substrates were sterilized in a solution of Pennicillin-Streptomycin (Pen/Strep) in PBS (Phosphate Buffered Saline) (1:2 v/v) for at least 4 h. On each sample 5.000 cell/cm^2 were seeded and left adhering overnight in the incubator.

4.2.4.1 Cell Imaging

At the end of the experiment, cells were fixed with 4% paraformaldehyde for 20 min and permeabilized with 0.1% Triton X−100 in PBS for 3 min. After fixation, cells actin filaments were stained with rhodamin−phalloidin for 30 min at room temperature in the phalloidin solution (dilution 1:200). Successively, cells were incubated for 15 min at 37 °C in Hoechst solution (dilution 1:1000) to stain cell nuclei. Cells were then imaged at the MP (MultiPhoton Microscopy) with a 40x water immersion objective 1.1 NA in z-stack mode.

4.2.4.2 Live/dead Cell Viability Assay

The live/dead assay was used to discriminate live from dead cells by simultaneously staining with green-fluorescent (calcein-AM to indicate intracellular esterase activity) and red-fluorescent (ethidium homodimer-1 to indicate loss of plasma membrane integrity). Calcein AM and EthD-1 have been dissolved in Opti-MEM (Gibco) without FBS at the final concentrations of 2 µM and 4 µM, respectively, after the determination of the optimal non-cytotoxic levels for hMSC cells. 20.000 cells were seeded on each substrate. After 24 hours, the platform was photostimulated with MP at 700 nm for 10 min. Successively, the culture medium was removed, cells were washed twice with PBS and incubated with the staining solution at room temperature for 30 minutes before imaging. Control samples for viable and dead cells were performed by seeding hMSC cells on glass-bottom petri dish. After live cell imaging, cells were treated with the staining solution containing 0.01% Triton as permeabilizing agent.

4.2.5 Photostimulation

The structures containing azo-1 were photostimulated using the MP microscope. A 25x water immersion objective with 6x as zoom factor was used. The MP pulsed laser was tuned at 700 nm and output power was set at 5% (trans and gain) and 42% offset. Four- Regions-of-interest (ROI) of the same size and shape were drawn on the squared gelatin structures, they were contemporary stimulated

for 10 min at 400 Hz scan speed in bidirectional mode, taking 1 frame per second. The structured containing azo-2 were stimulated in the same condition of Azo-1 but with a MP laser tuned at 1000 nm with 20% output power for 15 min.

4.3 Results and Discussion

4.3.1 Hydrogel Scaffold Preparation

ECM-derived biopolymers (i.e. gelatin), represented excellent candidates for the design of cell-compatible biomaterial. Gelatin was widely used as 3D matrices for cell growth due to the similarity of their mechanical and diffusivity properties to the natural cell environment-the extra cellular matrix (ECM).[165] In this work, it was modified with acrylate moieties in order to be photo curable by 2PP (2-photon polymerization) that avoided gelatin processing problems and permitted the obtaining of complex structures with a good resolution. The 3D gelatin scaffold was further modified with azobenzene to make the scaffold photoresponsive. Thus, the customized photoresist used for 3D fabrication, was composed of: Irgacure 369 as PI (Photo initiator) widely used in 2PP, a chemically modified gelatin (gel-DA) and different kind of azobenzene-based bisacrylamide molecule used as crosslinker (Azo-1-DA or Azo-2-DA).

4.3.1.1 Azocrosslinker characterization

The azobenzene moiety that conferred the photoactuability to the gelatin was opportunely designed to act both as photo actuator and as crosslinker in the polymerizable mixture. The azobenzene absorption spectrum had to be compatible with the working conditions of 3D lithography system.[166] The photoresist-containing azobenzene was photo polymerized with 2PP in the near infrared region at 780 nm (the two-photon wavelength at which the Nanoscribe works). The selected azobenzenes (Azo-1-DA or Azo-2-DA) had a valley of absorption around 390 nm, allowing a deeper penetration depth of laser with a negligible power loss. In fact, to induce this isomerization, we selected azobenzene types with absorption bands compatible with our fabrication technique and the half-life of cis isomers stable for days, allowing a temporal tuning of gelatin scaffold properties. Furthermore, because the azobenzene was going to be used as crosslinker, it was further conjugated with a PEO2-linker through the carboxylic acid-amine condensation to dictate a higher molecular flexibility during the isomerization and with acrylamide groups at the end in order to obtain printable molecules. We synthetized and tested two types of azobenzenes (azo-1 and azo-2) that matched all characteristics above described. [161, 167] Azo-1 *trans→cis* isomerization is induced with UV light (in our set-up we used a MP at 700 nm), while the reverse cis-trans isomerization with blue light at 448 nm. Azo-1 backbone synthesis had been already optimized in my research group and it was further modified as reported below to obtain azobenzene-based bisacrylamide crosslinker 1 (Azo-1-DA) (Figure 4.1).

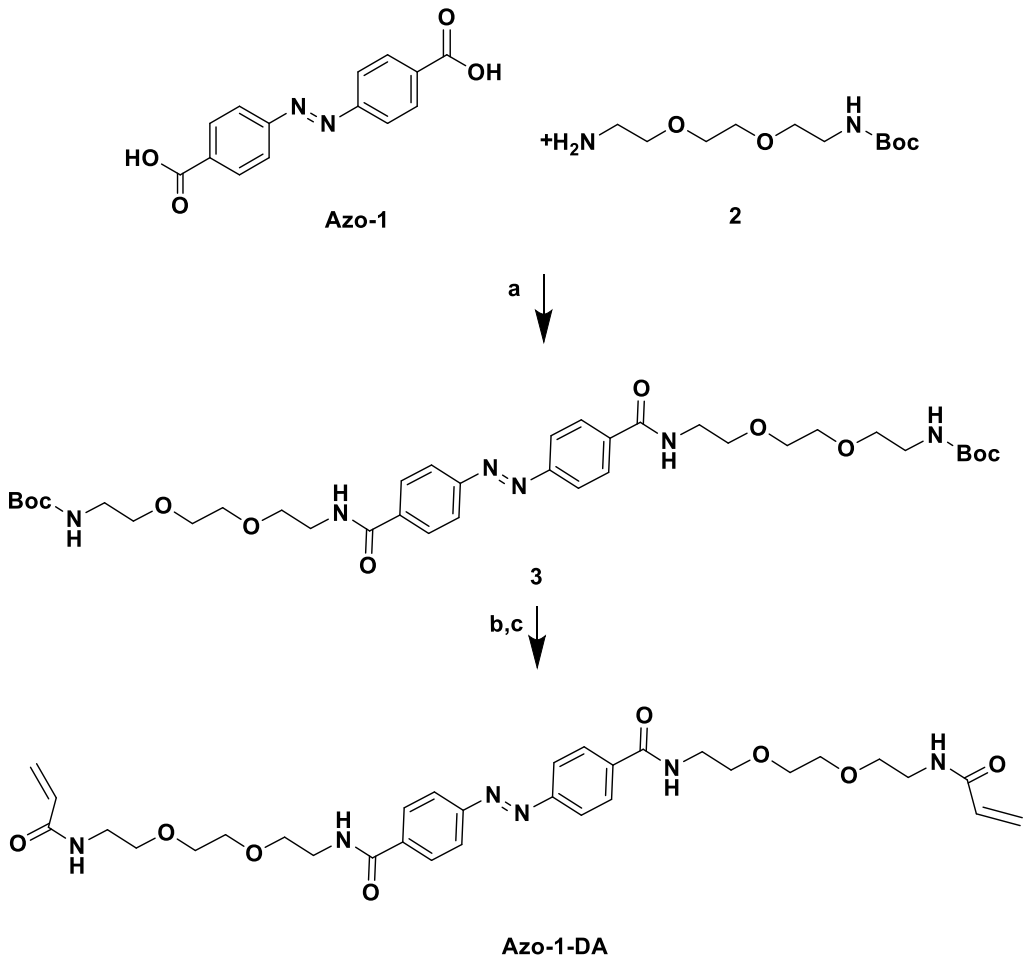

Figure 4.1. Azo-1-DA synthesis. Reaction conditions: a) 0.11 mmol of azo-1, 4.8 equiv. of TEA, 2.4 equiv. of HOBt·H_2O, 2.4 equiv. EDC·HCl and 2.4 equiv. of 2, overnight at room temperature. b) TFA/CH_2Cl_2 50/50 v/v for 2 h to remove the Boc protecting group. After the reaction it was treated with TEA and co-evaporated with toluene. c) Boc-deprotected compound 3 was reacted with 2.4 equiv. of acrylic acid, 2.4 equiv. of HOBt·H_2O, 2.4 equiv. of EDC·HCl and 4.8 equiv. of TEA overnight at room temperature.

The spectroscopic properties of azo-1-DA were verified by spectroscopic analysis. It isomerizes from trans to cis isomers in dimethylformamide (DMF) in about 25 minutes of illumination with UV laboratory lamp (1.2 mW cm^2 of diffused light) and from cis to trans after 1 minute by focusing the light of an halo lamp (filtered for blue light) by a 10x objective. The cis isomer was able to back-isomerize in more than three days in the dark. Figure 4.2 shows the UV/Vis absorption spectra of the azo-crosslinker in solution, subjected to a progressive illumination with UV light (from 1 minute to 25 minutes in total).[161] The black line shows the absorption spectrum of the *trans* isomer (t0 in figure 4.2), while the other colored lines represent the spectra of the mixture subjected to increasing illumination time with a UV lamp at 356 nm.

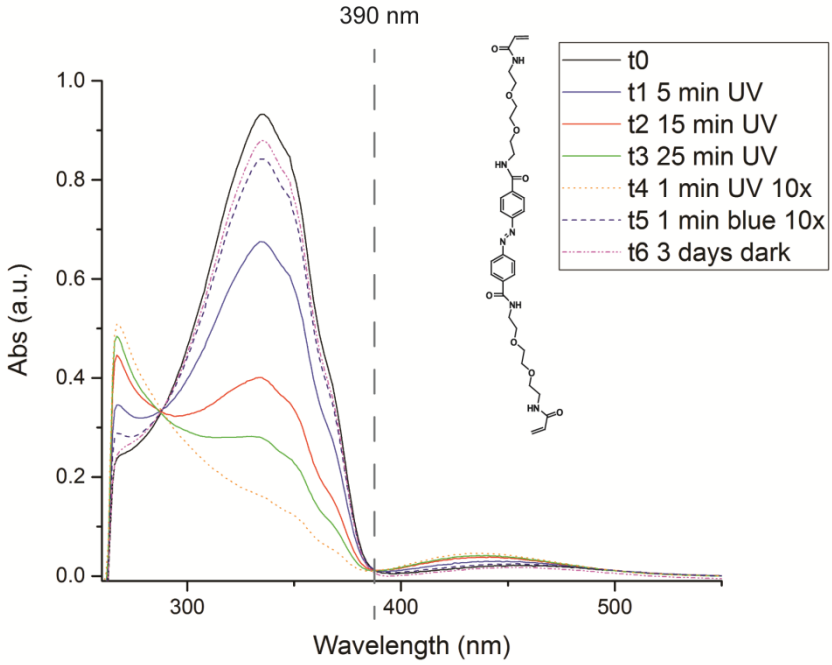

Figure 4.2. UV/Vis absorption spectra of Azo-crosslinker in DMF in different illumination conditions. The dashed light gray line indicates the molecule absorption at the wavelength (390 nm) of the focal volume of the two-photon polymerization system. In the legend "UV" indicates the diffused light of a laboratory lamp at 365 nm, while "UV 10x" stays for the light of a mercury lamp focused by a 10x objective and filtered in the UV region. Finally, "blue 10x" represents the same light source filtered in the blue region. (Reprinted from Applied Materials & interfaces, 2018, reference 161).

Azo-2 has methoxy groups in the ortho positions of the two phenyl rings, resulting in a splitting of n→π* absorption bands of *trans* and *cis* isomers, that allows to use green and blue light to induce *trans*→*cis* and *cis*→*trans* isomerization respectively. In addition, this azobenzene shows interesting properties: a long half-life of the cis isomer (in order of days); multiple rounds of photoisomerization, and even constant high-intensity irradiation with green light without evidence of photobleaching or photo-oxidation. These properties made of it an ideal candidate for our applications. In order to use direct laser writing technique to fabricate 3D scaffolds, azo-2 backbone was modified with PEO and acrylamide side groups (Azo-2-DA) and was subsequently cross-linked by two-photon polymerization *via* photoinitiator. Azo-2 was synthetized as reported by Woolley and co-worker.[62] The deacylation of Azo-2 was efficiently promoted by $SOCl_2$ as catalyst in dry methanol at reflux temperature and the progress of the reaction was monitored by TLC. Deacetylation of Azo-2 with the addition of $SOCl_2$ proceeded with excellent yield compared to direct use of conc. HCl as the catalyst that caused the degradation of the product. AZ-NH_2 was modified in both *para* positions with PEO spacers (N-Boc-Amido-PEO2-Acid). AZ-NH_2 was treated with TEA then EDC HCl, HOBt·H_2O and N-Boc-Amido-PEO2-ACID were added dropwise to stirred solution of compound AZ-NH_2. The

result was then purified by chromatography. After removal of the BOC with strong acids (trifluoroacetic acid/dichloromethane 1:1), the product was acrylated. So, a diacrylate symmetric azomonomer (Azo-2-DA) that could be used as crosslinker was synthesized (Figure 4.3)**.**

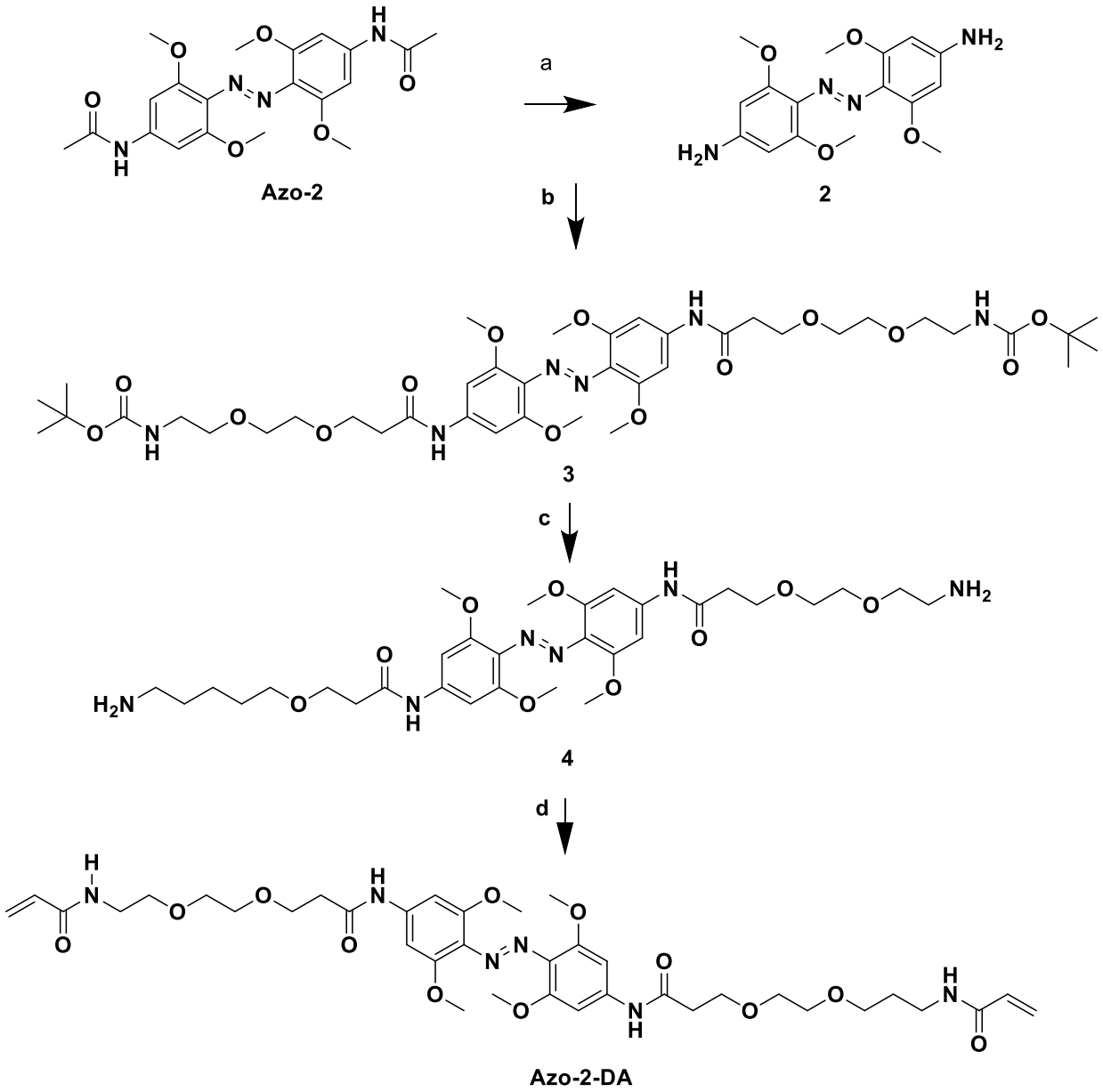

Figure 4.3. Reagents and conditions for the synthesis of Azo-2-DA. (a) Azo-2, $SOCl_2$ in MeOH. (b) **2**, (1.5 equiv), N-Boc-AmidoPEO2-Acid. (c) **3**, 50% of TFA in DCM 2 h at RT. (d) **4**, (2 equiv) Acrylic Acid N-Hydroxysuccinimide ester, overnight at RT.

The UV/Vis spectrum of Azo-2-DA **(**Figure 4.4 b) was confirmed to be similar to that of the backbone azo-2 (Figure 4.4 a**).**

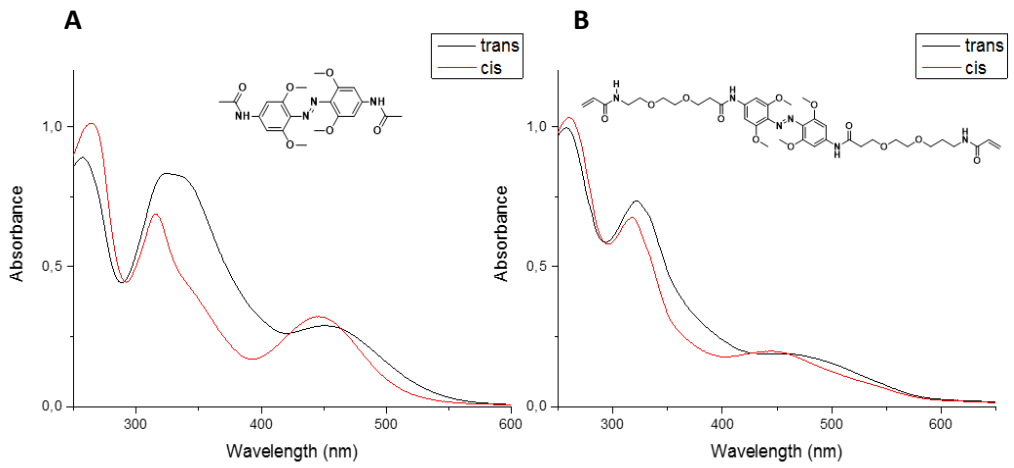

Figure 4.4. UV/Vis spectra of A) Azo-2 and B) Azo-2-DA in methanol at 25 °C. Spectra of trans (solid black trace) and cis (red black trace) isomers. Cis state is obtained after irradiation at 514 nm with a 10x

Irradiation of Azo-2 with green light (514 nm) induced a *trans→cis* isomerization while the cis isomer could be switched back to the trans state with blue light (~71,8%, calculated by NMR) (at 25 °C). The spectroscopic properties of azo-2-DA were verified by spectroscopic analysis. *Cis*-Azo-2-DA was thermally stable for days, recovering completely the more stable trans state after about 4 days in the dark. Rates of thermal *cis-to-trans* isomerization at 25 °C was measured by acquiring absorption spectra in function of time after 1, 2, 3 days **(**Figure 4.5**)**. A slow thermal relaxation was an advantage for own purposes because the light could be used for photoswitching without thermal relaxation interference. Both photochromic moieties (Azo-1-DA, Azo-2-DA) were tested into gelatin matrix as "probes" enabled to trigger photoinduced deformation.

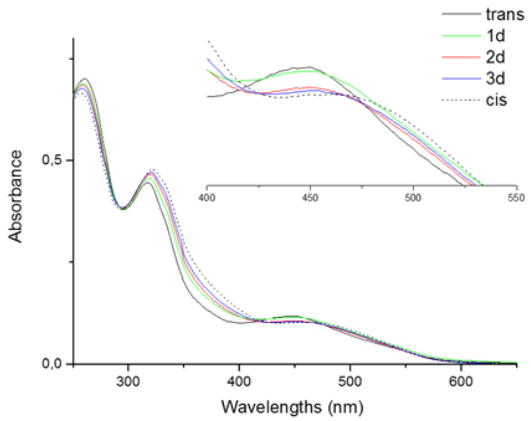

Figure 4.5. Thermal relaxation of cis to trans isomers of Azo-2-DA in the dark, cis (dashed black trace), after 1 day (cyan trace), 2 days (red trace), 3 days (blue trace) and 4 days (solid black trace) at 25°C.

4.3.1.2 Acrylamide Modified Gelatin Hydrogels characterization

In the light of foregoing information, we have proponed in this work to combine the natural advantages of gelatin scaffold with high resolution fabrication of 2PP to obtain 3D gelatin scaffold. Hydrogels have been largely used as components of cell scaffolds being three-dimensional polymeric networks with a strong hydrophilicity, able to mimic the mechanical properties of natural tissues. As introduced, the gelatin being a derivative of collagen is a desirable candidate for the development of biomaterials for tissue engineering thanks to its appealing advantages such as cell-adhesive properties, low cost, high biocompatibility, biodegradability and low immunogenicity. Nevertheless, the fabrication of well-defined gelatin microstructures resulted challenging, and as a consequence, the application of gelatin in the production of advanced cell instructive platforms is limited. Its use is restricted principally because of its relatively low melting point that is not compatible with physiological conditions. In order to overcome this limitation and taking advantage by gelatin diverse and accessible functional groups allowed for chemical modifications, a variety of chemically crosslinking approach have been developed over the years.[168,169] Among these, two-photon photopolymerization (2PP) has gained growing interest and was adopted in this work. Gelatin was chemically modified by substituting amine side groups with acrylamide moieties as described by Van Den Bulcke.[170] Gelatin is a protein built up of a variety of amino acids *e.g.*, lysine (Lys), hydroxylysine (Hly), ornithine (Orn), containing free amines, that are the reactive sites modified in our apprach.[171] First of all, gelatin was dissolved in phosphate buffer (pH 7.8) at 40 °C and successively 2 equiv of acrylic acid *N*-hydroxysuccinimide ester was added to the gelatin mixture to obtain a degree of substitution (DS) of 76 %. The amount of incorporated cross-linkable side groups defined the mechanical properties of the resulting hydrogel. The substitution degree was verified using ^{1}H-NMR spectroscopy at 40 °C and quantified by the Habeeb method (Figure 4.6), furthermore it could be simply adjusted varying the amount of acrylic acid added during the synthesis.[171] The unpolymerizated gel acrylated was removed after the fabrication by washing the samples 3 times in distilled water at 55 °C.

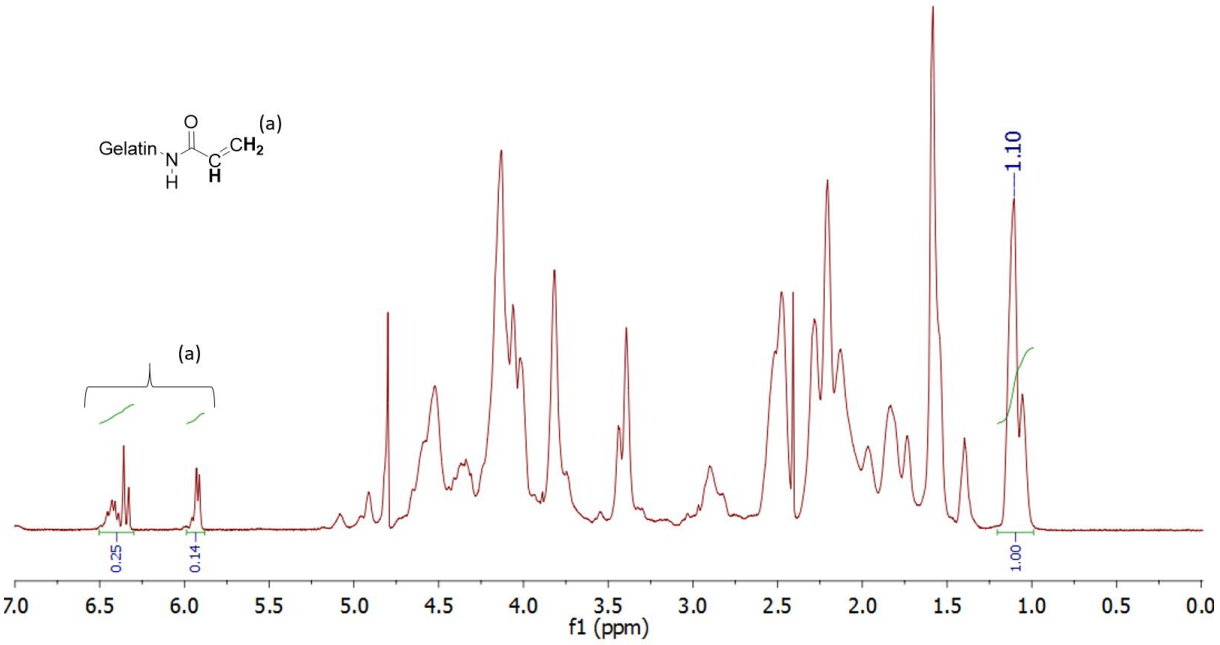

Figure 4.6. 1H NMR spectrum of modified gelatin B. (Reprinted from Applied Materials & interfaces, 2018, reference 161).

4.3.2 Fabrication of 3D Scaffolds

The gelatin modification with photo-sensitive moieties allowed to have curable molecules so that the 2PP radical polymerization could take place. Furthermore, it allowed to tune mechanical properties of the final polymeric scaffold in relationship to the degree of acrylic acid incorporated. Furthermore, the addition of Azo-1-DA crosslinker in the mixture increased the structural properties and mechanical stability of the scaffold. The polymerization of acrylamide modified gelatin (20% w/v acrylamide-modified gelatin chains,) and Azo-1-DA (4% w/w respect to gelatin) was performed by direct laser writing using 2PP with a femtosecond laser emitting at ∼780 nm. The absorption spectrum of both azobenzene crosslinkers with a valley of absorbance at ~ 390 nm were matched well with the half-wavelength of the applied laser radiation and avoided the overlapping of the absorption peak of the photoinitiator (PI) used in the two-photon polymerization (Irgacure 369, 3% w/w). The photoinitiator (PI) exposed at a high intensity laser underwent to the absorption of two photons mediated by a virtual state that allowed the access to an excited triplet state, so producing active species able to initiate the polymerization reaction. The absorption of two photons shows a non-linear (quadratic) dependence to the intensity, resulting in a highly localized excitation and thus a potentially highly resolved polymerization. The azo-crosslinker improved the CAD reproducibility and the structural stability of the fabricated microstructures, two critical issues in the photopatterning of gelatin by means of DLW-2PP technique (Figure 4.7). It gave the possibility to considerably increase the control over the micro feature resolution, resulting in the creation of very complex three-dimensional structures, just by laser scanning. Effectively, we proved that the introduction of azocrosslinker could both made the material photosensitive and increase its structural properties, as shown in Figure 4.7 by the comparison between scaffold with azobenzene as crosslinker (Figure 4.7 d) and without azocrosslinker (figure 4.7 c).

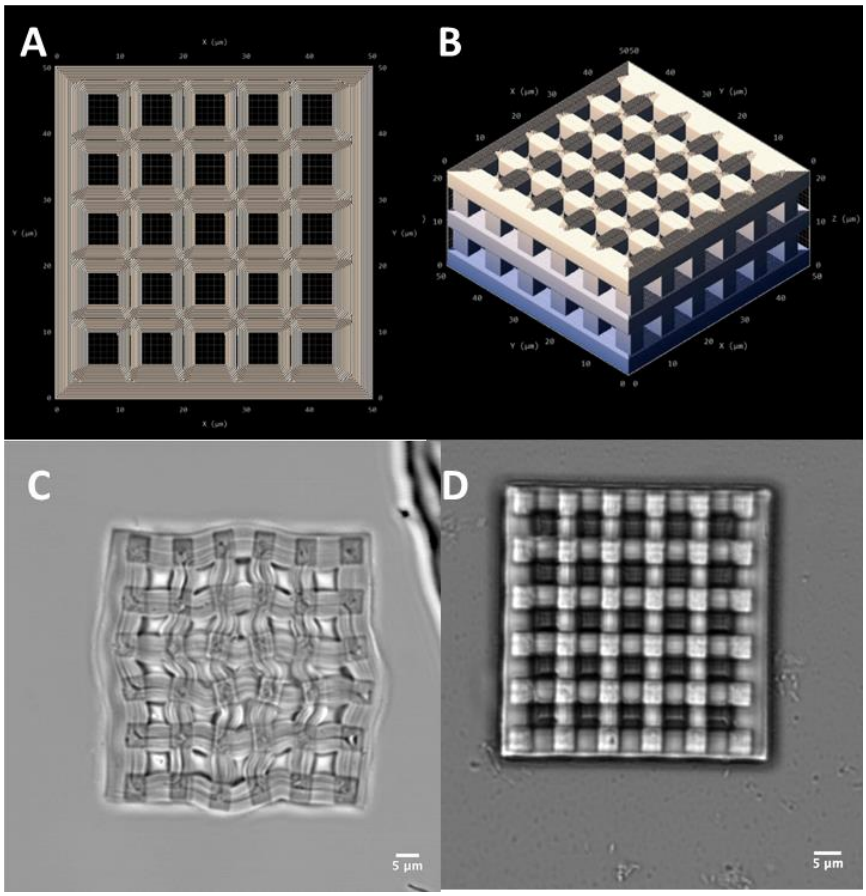

Figure 4.7. A) CAD structures of a 3D platform in x,y plane and B) in 3-dimension. Confocal images of 2PP-produced gelatin scaffolds fabricated C) without and with D) azobenzene crosslinker. Scale bar of 5 µm

As proof of concept, we focused on a network of interconnected channels to obtain geometrical confinement for stem cell. We fabricated an array of acrylate gelatin parallelepipeds (30 x 30 x 10 μm^3) directly attached to a glass substrate, laterally patterned with 3 µm pitch gratings and distanced of 20 µm and 30 µm (Figure 4.8 a).

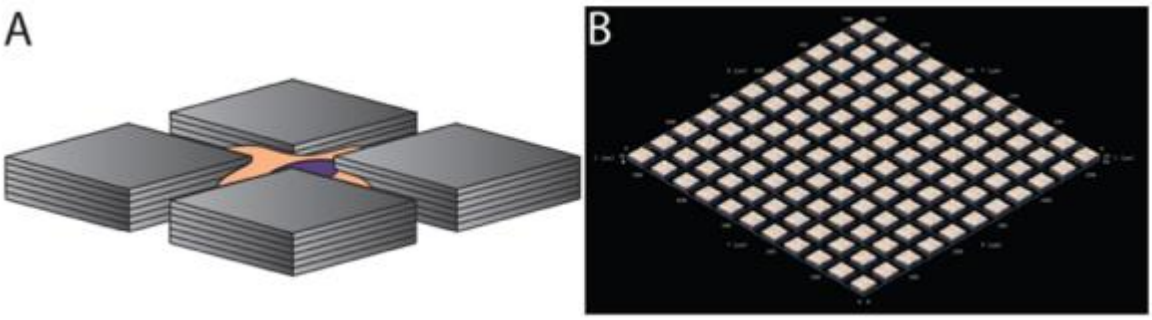

Figure 4.8. A) Graphical representation of Gelatin Scaffold B) CAD structure of entire platform. (Reprinted from Applied Materials & interfaces, 2018, reference 161).

4.3.3 Photostimulation of the gelatin squared structures

The photodeformation of gelatin microstructures was studied employing the multiphoton laser (MP) of a confocal microscope. Gelatin blocks were employed as simple test structures, used as modular elements for cell stimulation. The microscope laser was not only a finely tunable irradiation tool for the photoactuation, but also a powerful system to observe, record and evaluate *in real-time* the material microdeformations with spatial-temporal accuracy, even in the presence of living cells. The squared hydrogel structures were stimulated at 700 nm (in order to excite the azobenzene isomerization at 350 nm) at a fixed z position for 10 minutes. The light stimulation translated into a mechanical expansion of the structures in x and y of about 10%, as shown in Figure 4.9. As introduced, the isomerization induces changes in geometry and dipole moments of the azobenzene, that can induce a change of hydrophilicity of the hydrogels upon *trans-cis* isomerization and the swelling of the structures. Moreover, from preliminary AFM analysis, the material showed a variation in stiffness, in fact, the Young modulus decreased from 6.5 to 3.9 kPa in response to the light stimulus.[161]

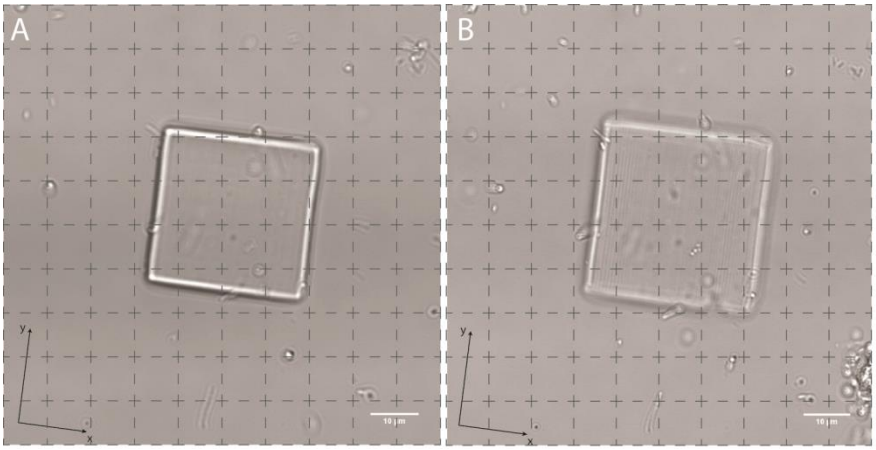

Figure 4.9. Deformation of the gelatin squared structures upon MP illumination at 700 nm for 10 minutes. A) Before illumination and B) after illumination. (Reprinted from Applied Materials & interfaces, 2018, reference 161).

We attributed the hydrogel expansion only to azobenzene isomerization and not to other side effects. To prove this hypothesis, we illuminated the azobenzene-containing structures for 10 min at 780 nm (a voxel wavelength of 390 nm), a wavelength at which the azobenzene molecule presents an adsorption valley and does not isomerize. Actually, no expansion was observed in this condition showing that the hydrogel response was due solely to azobenzene isomerization. Furthermore, in the set experimental condition, we were able to precisely localize the UV absorption with the use of the multiphoton laser that moreover was suitable for the biological studies. In fact, because UV light is

known to be harmful for cells, this method minimized cytotoxic effects, while maximizing the light penetration depth. So, to improve the biocompatibility of our platforms, we focused both on MP source able to reduce cytotoxic effects and on employment of azobenzene able to isomerize in visible range avoiding the side effects of UV illumination. As described previously, Woolley's group reported an interesting azobenzene derivative, able to photoswitch in the visible range. We synthetized this azobenzene (Azo-2) in which four methoxy groups introduced in the *ortho*-positions led to a 36 nm splitting of *trans* and *cis* isomers' n→π* bands, so that green and blue light can be used to induce isomerizations.[62] Employing this azobenzene, we did not observe an engrossing light response of structures, likely because photoconversion was not enough high to lead a relivable photomechanical effect. Only a little expansion ~ 2% of gelatin structures was observed after the illumination for 15 min at 1000 nm by MP, the wavelength able to induce the *trans→cis* isomerization (data not shown). Also in this case, the gelatin platform response could be attributed solely to azo-isomerization because the structures did not show any modification after illumination at 633 nm, a wavelength at which Azo-2 did not absorb. The Azo-1 employed in the photopolymerizable mixture gave us more evident results relative to Azo-2 and for this reason, the biological investigation was carried out with gelatin containing Azo-1. In the meantime, for future experiments we propone to synthetize other azobenzenes to include in hydrogels matrices with a higher efficiency to convert light into mechanical energy. In this respect in material science, a variety of azobenzenes with high conversion efficiency isomerizable in the visible range have been identified (*e.g.*, an azobenzene covalently bridged in *ortho*-positions by an ethylene linker and azobenzene functionalized with *ortho*-fluorine atoms).[58-59]

4.3.4 Biological Investigation

Our aim was to fabricate 3D structures that could mimic the cell natural environment simultaneous in term of topographic cues (high-defined 3D structures by 2PP), biological cues (cell adhesion property of gelatin scaffold), and mechanical cues (cell compression during azobenzene gelatin expansion upon light illumination). Thus, we fabricated well-defined semi-3D scaffolds, with topographic and mechanical cues tunable by light on demand. As proof of concept, we investigated the nuclei deformation of cell confining structures *in real-time*. Our preliminary studies were carried out with NIH-3T3 to prove the potentiality of the platform and successively with hMSCs with the goal in future to analyze effects of dynamic cues on stem cell differentiation. Despite it has been proved that the dynamicity of cellular responses to changes in the microenvironment is a fundamental

property during tissue development or renewal,[172] there are in literature, only few examples of studies in dynamic conditions. In a recent key study, Kurpinski *et al.* suggested that mechanical strain plays an important role in MSC differentiation and proliferation. MSCs were induced to distinctly differentiate along the myogenic pathway when cultured on the substrates with the uniaxial strain but along the osteogenic pathway with uniform biaxial stretch, marking the importance of external stresses in MSC differentiation.[173] Also Gong and co-workers evaluated the effects of tunable geometric microwells and the resulting mechanical force to guide the rat bone marrow mesenchymal stem cells (rBMSCs) differentiation.[124] Tuning the shape of micro-well substrates, which were made of the six-arm poly(ethylene glycol)-poly(ε-caprolactone) (6A PEGPCL) polymer with thermally activated shape memory function, revealed that cells cultured in various dynamic micro-wells had differentiated along adipogenesis and osteogenesis pathways.[124] Also our approach was proposed to set a platform able, at the same time, to impose a specific shape to cell through gelatin-microarray confinement and to induce a mechanical force on cell during gelatin structures expansion under light illumination. The mechanical cue, associated with a geometry- confined cell, could enhance the stem cell commitment in a specific cell lineage.

A preliminary analysis was done to design the channel size for the localization and manipulation of single cells, changing the space between gelatin-blocks from 20 μm to 30 μm (Figure 4.10).

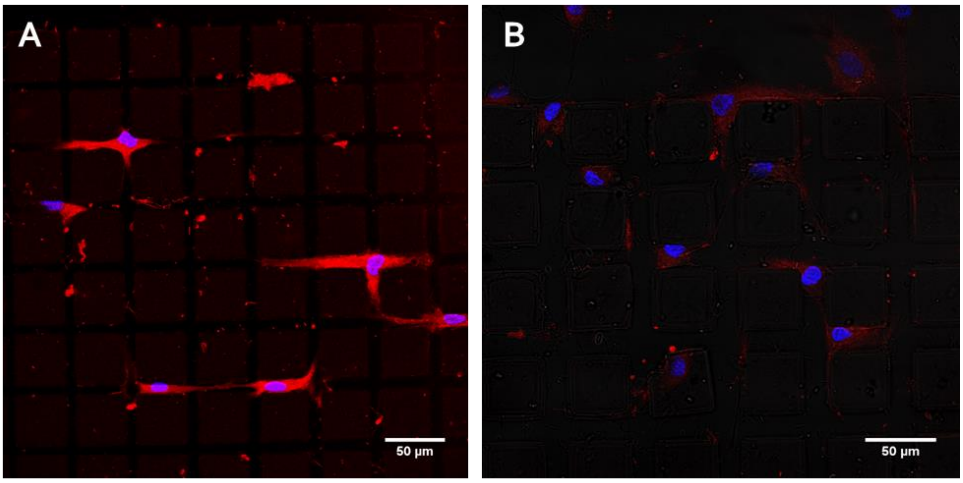

Figure 4.10. hMSC seeded in the channel between squared structures A) 30 x 30 x 10 μm^3 spacing 20 μm and B) spacing 30 μm. Scale bar of 50 μm. hMSCs were stained with the vital CellTracker Deep Red for the cell body and Hoechst for the nucleus. Images of cells were collected by using a 40x objective on a confocal microscope A TCS SP5 multiphoton (MP) microscope (Leica Microsystems).

The cell relegation inside channels were further favored by a grating (3 μm pitch) on the later walls of the squared structures. In fact, in Figure 4.11 it is shown the cell cytoskeleton strongly stretched and furthermore wrapped around sides of structures.

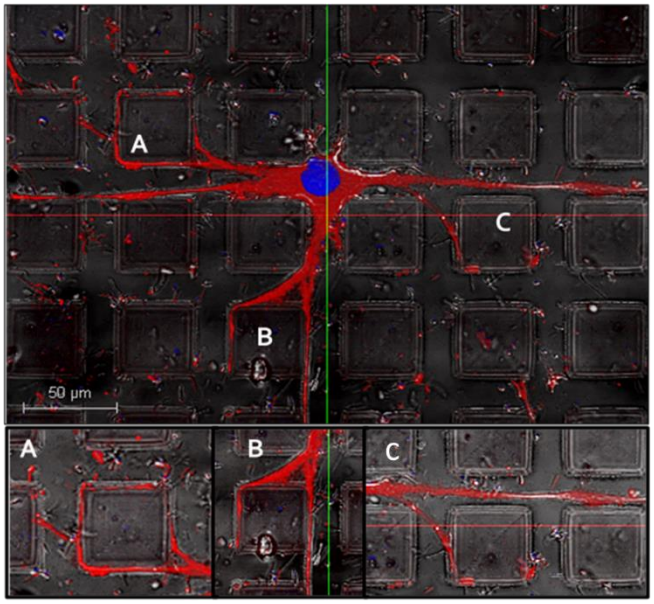

Figure 4.11. hMSC localized in channels of 20 µm. The cell was stained with the vital CellTracker Deep Red for the cell body, while Hoechst was used for nucleus staining. Scale bar 50 µm.

Our system was able to deform cell nuclei at single cell level, allowing for a high localization of the external light trigger to the material parts, activating the laser only into region of interest (ROIs), drawn on gelatin blocks. Biocompatibility of the platform was tested with live/dead assay that showed (Figure 4.12) cell viability on the material after the light stimulation.

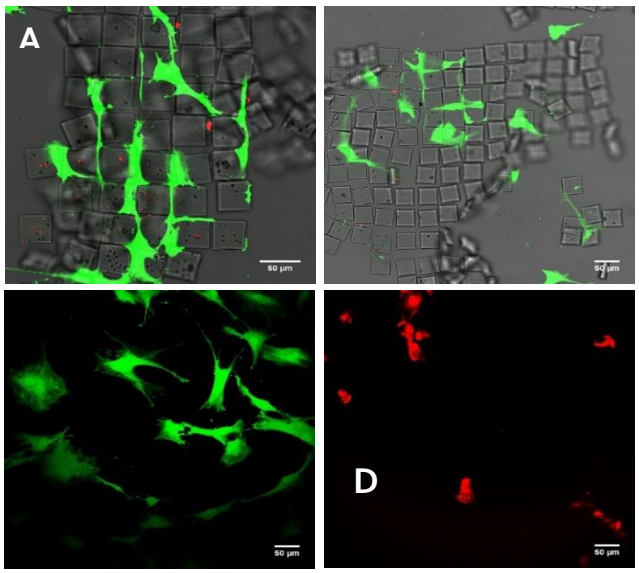

Figure 4.12. Confocal images of Live/Dead assay on gelatin structures. A) hMSC after illumination with a MP at 1000 nm for 15 minutes. B) hMSC after illumination with a MP at 700 nm for 10 minutes. Images represent a merge of the two channels for fluorescent calcein AM (green) and ethidium homodimer-1 (red), C) Positive control of live cells on a glass-bottom petri dish, and D) negative control for dead cells after treatment with triton 0.01%. Scale bars are 50 µm.

The local MP stimulation avoided unwanted interactions between high power laser and living cells. In fact, since UV light is known to be harmful for cells, this method minimizes cytotoxic effect, maximizing the light penetration depth. In our already published paper these photoresponsive hydrogels were tested with NIH-3T3 cell line, we showed a correlation between cell deformation after stimulation and initial nuclei polarization of cell confined into the channels. In more details, higher polarization of the nucleus was associated with a lower cellular compliance.[161] So for these experiments, we selected channels of 20 μm that allowed a good cell confined without excessive nucleus polarization of hMSC. Also these results, showed that an initial high cell polarization (I_{max}/I_{min} ~ 5) induced a contraction of nuclei deformation in the range of 1-2 %, while higher contraction (5-15%) was observed when I_{max}/I_{min} ~ 2-3. The variation in the nuclear area was quantified by comparing the fluorescent signal of the nucleus before and after the stimulation, and the initial polarization degree of the nucleus was calculated as the ratio between its two main axes (I_{max}/I_{min}). We evaluated not only the nuclei deformation of hMSC in x-y plane but the change of entire nuclei volume in x,y and z. In figure 4.13, we reported a representative example of cell volume contraction during the structure stimulation. Initially the stem cell confined into the channel had a volume of 1488,8 μm^3 that appeared reduced of 34% (Vf 987,8 μm^3) after the expansion of structures with a concomitant reduction of channel size. In this way, we proved the tunability of platform's physical properties (e.g., stiffness and geometry) by light. A change of stiffness, for example, can strongly affect the cell behavior, principally during the differentiation of stem cells, as reported by Rosales *et al.*[174] Furthermore, the mechanical cue, associated with a geometry- confined cell, could enhance the stem cell commitment in a specific cell lineage.

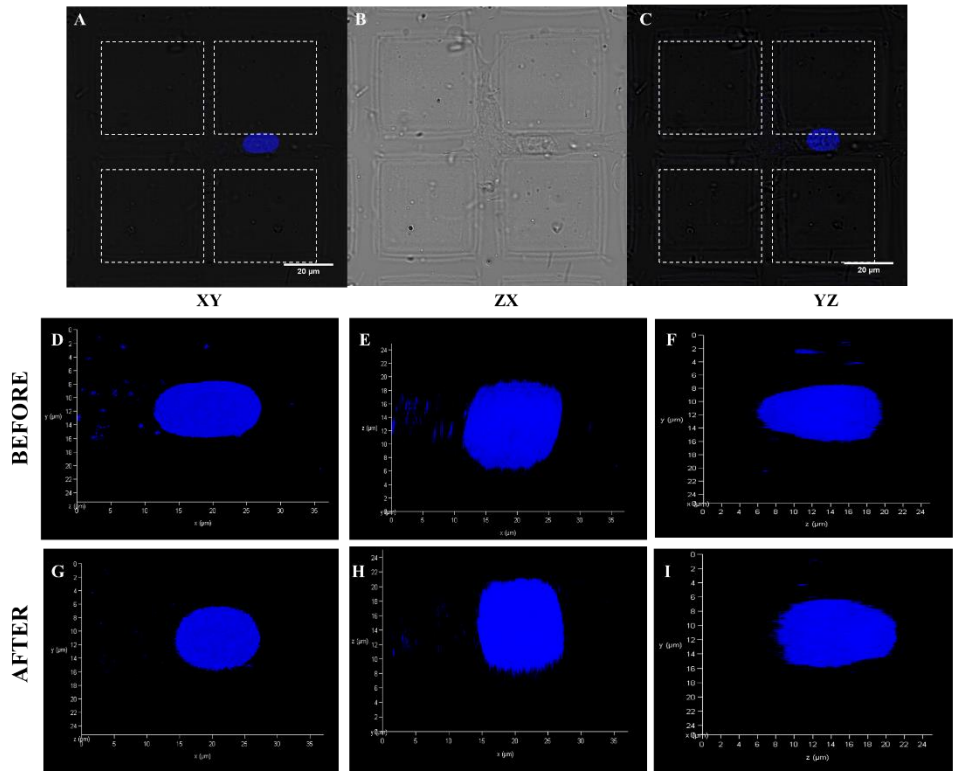

Figure 4.13. Images of hMSC nuclei deformation confined between gelatin microchannels upon gelatin photostimulation. A) cell nucleus before light illumination, B) brightfield image of a stem cell confined into the channel, C) cell nucleus after light stimulation. Nuclei are stained in blue with hoechst. D), E), F) Nuclei projections before and after G), H), I) stimulation of the gelatin platform in xy, xz and zy respectively.

In fact, this paves the way to envelope light-tunable platforms that can directly influence stem cell fate acting alone or in combination with chemical cues. Furthermore, we observed that the material did not compromise cellular viability even after longer culture timing (25 days), thus showing the potential use of these platforms for differentiation process (21 days). In fact, we can consider this system as a starting point to envelope light-tunable platforms and a novel method to investigate the effects of physical signals (cell special constrains) and the dynamic force (gelatin swelling and consequently nucleus squeezing) in determining MSC lineage commitment.

4.4 Conclusion

The fabrication of light-responsive photocurable hydrogels that could be used as stem cell caging platforms, has been proposed in this chapter. The gelatin-based photoresist has been synthetized through a chemical modification of side chain functions of both gelatin and azobenzene into a photopolymerizable mixture. Two-photo-polymerization has enabled to obtain well-defined microstructures that can confine and deliver a local mechanical stimulation at a single-cell level. In particular, the introduction of azobenzene-based crosslinkers into the photoresist mixture has allowed to add a light-responsive functionality to the material and increased the resolution of hydrogel structures. The stimulation with a multiphoton laser in the range of azobenzene isomerization provoked an in-plane deformation of the designed structures, with a concomitant change in mechanical properties. Choosing the multiphoton laser of a confocal microscope as light source, we were able to selectively deform the single cell (hMSC) with high spatial-temporal accuracy in a biocompatible environment. Our results evidenced that the photostimulation was efficiently transferred from the structures to the cell nuclei, provoking a decrease of the cell nuclear area. These findings demonstrate the applicability of these platforms as dynamic 3D scaffolds suitable for future application with the aim to guide the stem cell differentiation tuning topographic and mechanical properties on demand.

Conclusion and Future Perspectives

The work described in this thesis intends to design and to use azobenzene-based platforms for cell culture to investigate cell-dynamic material interaction at the biointerface. Recently, a great challenge in tissue engineering lies in the dynamic modulation of the cell-material interaction to recapitulate the dynamic crosstalk between cells and the physiological extracellular microenvironment. Engineered materials can control a variety of cellular processes (adhesion, migration, proliferation etc.) but, recent researches have also highlighted how the lack of a spatial-temporal control offered by static material surfaces limits a comprehensive recapitulation of the ECM structure. Although, static cues (topography, stiffness, biochemical cues), represent the first step towards the understanding of cell-material crosstalk, to move one step further, we focused on dynamic materials, such as azobenzene-based polymers, that can exhibit on demand surface changes under external stimuli (i.e., light exposure). This can represent a powerful system to investigate cell behavior in a more biomimetic way and overcoming the limit of static systems.

In this thesis, we focused mainly on the variation of topographic cues in the presence of cells either at a single-cell level or in multicellular systems. In particular, we investigated the impact of dynamic cues on different biological processes spanning from actin re-organization to cell differentiation. We designed various platforms in terms of material geometry (e.g., ridge/groove, squared blocks and pillar) and employed azopolymers (pDR1m or modified hydrogel containing azobenzene). In more details, in **Chapter 1** an overview of cell−material interaction, properties of azopolymers and their biological applications was given. In particular, we focused on the recent use of azopolymers as dynamic cell instructive materials. The aim was to investigate the crosstalk between cell and a dynamic environment and in particular to study the effect of topographic variations on biological processes (e.g., adhesion, contact guidance, differentiation). In **Chapter 2**, we discussed an optical technique that allowed spatial-temporal modulation of topographic features on cell-populated surfaces. By means of a laser-based confocal microscope, we photo-patterned an azopolymer thin films (creating groove/ridge patterns) through a mass migration phenomenon in the presence of human mesenchymal stem cells (hMSCs). The topography was successively modified *in situ*, obtaining different topographic features. This technique showed the possibility to tune the topography of the material on demand over time without any toxicity effects on cells. In more details, we investigated stem cells response after the change of topographic cues both in term of cell cytoskeletal re-organization and cell differentiation. hMSCs that initially were aligned and elongated on ridges/grooves pattern, reorganized themselves rapidly during the topographic change and appeared

randomly spread on a grid surface after the dynamic switch. In addition to the cell morphology analysis, the effect on gene expression was evaluated. In particular, we analyzed the expression of some osteogenic markers (RUNX2 and BGLAP) expressed after 21 days of culture with rtPCR both in static and dynamic conditions. After the material photoswitching, the transcription of genes involved in the osteogenic pathway seemed to be inhibited. Indeed, we can suppose that the dynamic change of topography can modify the tension and the arrangement of cytoskeletal fibers, affecting signal transduction and inhibiting ostegenesis. Our hypothesis needs to be confirmed by further analysis at different switching points in differentiation phases to understand the correlation between the time in which the topography is changed and osteogenic gene expression profile. Moreover, we asked whether epigenetic effect induced by changes in the biophysical properties of the substrate over time would redirect the expression of lineage specific markers, explaining the osteogenic inhibition. We can conclude that the presented photoswitchable platform can be a suitable tool for investigating the effect of dynamic cues on stem cell differentiation. Furthermore, we propose to improve this platform and deeply investigate the effect of dynamic cues at different phases of stem cell development into specialized cell types. In **Chapter 3**, we presented an array of azopolymer pillars made-up by soft lithography that could be re-shaped by light. The external trigger induced an athermal photofluidization of the polymer able to deform the initial pillar shapes. Pillars were re-shaped along the direction of laser polarization, resulting in elongated structures with controllable eccentricity. Under these conditions, our platforms were used to control and modulate cellular processes at the interface over time/space. Human bone osteosarcoma epithelial cells (U2OS) transfected with LifeAct-RFP were used to investigate the F-Actin organization during the transition from circular pillar to ellipsoidal shape over time. We observed that initially the F-Actin accumulated around the pillar, forming a ring-like morphology and this actin assembly was rapidly damaged during the light stimulation. The F-actin appeared accumulated preferentially at the structure ends, where the cell membrane generated local curvature, when pillars were reshaped in elongated structures (ellipsoidal-shape). The F-Actin re-organization occurred in less than 10 min from stimulation. The reshaped process was rapid and anisotropic, two factors that can have important effects on speed and directionality of cell migration. Thus, we propose for our future experiments to investigate how the curvature-dependent F-actin accumulation triggered by dynamic reshaped pillars can influence cell migration process in term of speed and cell migration direction along a photoinduced direction. In **Chapter 4**, we fabricated semi-3D hydrogel platforms containing azobenzene as photoactuable cell confining systems. An acrylamide-modified gelatin containing azobenzene-based cross linker was used to microfabricate well-defined semi-3D photo-responsive structures by means of two-photon lithography (2PP). We fabricated an array of squared structures where cells were physically confined

between adjacent gelatin blocks. The array was stimulated via a multiphoton laser in the range of azobenzene isomerization provoking an in-plane deformation of the designed structures, with a subsequent change in mechanical properties (swelling and decrease of stiffness). Our results evidence that the photostimulation was efficiently transferred from the structures to the stem cell nuclei, provoking a decrease of the cell nuclear area. As outlook we propose to synthetize other azobenzenes, isomerizable in the visible range, with high conversion efficiency that can improve the hydrogel photomechanical response. Our future perspective is to investigate the photomechanical effects on stem cell commitment after the change of mechanical and geometrical properties of these hydrogel blocks under light illumination. Furthermore, we consider the possibility to fabricated complex 3D architectures so that, this platform could find future applications as “engineered stem cell niche”.

Taken all together, these findings demonstrate that the proposed systems may have a great impact on creating smart platforms for cell culture. This study paves the way to the use of similar 2D and semi-3D dynamic cell−instructive biomaterials to investigate many processes involved in dynamic cell−biomaterial interaction. In particular, we propose to use these platforms to evaluate the impact of dynamic cues on commitment and differentiation of stem cells for future important application in the use of synthetic niches for stem cell therapy and as powerful tools for basic cell studies as well as promising biomedical applications.

References

1. Mason, C.; Dunnill, P., A brief definition of regenerative medicine. **2008**.

2. Bean, A. C.; Tuan, R. S., Stem cells and nanotechnology in tissue engineering and regenerative medicine. *Micro and Nanotechnologies in Engineering Stem Cells and Tissues* **2013**, 1-26.

3. Bowers, S. L.; Banerjee, I.; Baudino, T. A., The extracellular matrix: at the center of it all. *Journal of molecular and cellular cardiology* **2010,** *48* (3), 474-482.

4. Park, J.; Lakes, R. S., *Biomaterials: an introduction*. Springer Science & Business Media: 2007.

5. Stabenfeldt, S. E.; Brown, A. C.; Barker, T. H., Engineering ECM complexity into biomaterials for directing cell fate. In *Biomaterials as Stem Cell Niche*, Springer: 2010; pp 1-18.

6. Ventre, M.; Causa, F.; Netti, P. A., Determinants of cell–material crosstalk at the interface: towards engineering of cell instructive materials. *Journal of the Royal Society Interface* **2012**, rsif20120308.

7. Lutolf, M.; Hubbell, J., Synthetic biomaterials as instructive extracellular microenvironments for morphogenesis in tissue engineering. *Nature biotechnology* **2005,** *23* (1), 47.

8. Ventre, M.; Netti, P. A., Engineering cell instructive materials to control cell fate and functions through material cues and surface patterning. *ACS applied materials & interfaces* **2016,** *8* (24), 14896-14908.

9. Jansen, K. A.; Donato, D. M.; Balcioglu, H. E.; Schmidt, T.; Danen, E. H.; Koenderink, G. H., A guide to mechanobiology: where biology and physics meet. *Biochimica et Biophysica Acta (BBA)-Molecular Cell Research* **2015,** *1853* (11), 3043-3052.

10. Uto, K.; Tsui, J. H.; DeForest, C. A.; Kim, D.-H., Dynamically tunable cell culture platforms for tissue engineering and mechanobiology. *Progress in polymer science* **2017,** *65*, 53-82.

11. Bökel, C.; Brown, N. H., Integrins in development: moving on, responding to, and sticking to the extracellular matrix. *Developmental cell* **2002,** *3* (3), 311-321.

12. Khalili, A. A.; Ahmad, M. R., A review of cell adhesion studies for biomedical and biological applications. *International journal of molecular sciences* **2015,** *16* (8), 18149-18184.

13. Daley, W. P.; Peters, S. B.; Larsen, M., Extracellular matrix dynamics in development and regenerative medicine. *Journal of cell science* **2008,** *121* (3), 255-264.

14. Kim, J.; Hayward, R. C., Mimicking dynamic in vivo environments with stimuli-responsive materials for cell culture. *Trends in biotechnology* **2012,** *30* (8), 426-439.

15. Custódio, C. A.; Reis, R. L.; Mano, J. F., Engineering biomolecular microenvironments for cell instructive biomaterials. *Advanced healthcare materials* **2014,** *3* (6), 797-810.

16. Jung, D.; Kapur, R.; Adams, T.; Giuliano, K.; Mrksich, M.; Craighead, H.; Taylor, D., Topographical and physicochemical modification of material surface to enable patterning of living cells. *Critical reviews in biotechnology* **2001,** *21* (2), 111-154.

17. Curtis, A.; Wilkinson, C., Topographical control of cells. *Biomaterials* **1997,** *18* (24), 1573-1583.

18. Hulshof, F. F.; Zhao, Y.; Vasilevich, A.; Beijer, N. R.; de Boer, M.; Papenburg, B. J.; van Blitterswijk, C.; Stamatialis, D.; de Boer, J., NanoTopoChip: High-throughput nanotopographical cell instruction. *Acta biomaterialia* **2017,** *62*, 188-198.

19. Kingham, E.; White, K.; Gadegaard, N.; Dalby, M. J.; Oreffo, R. O., Nanotopographical cues augment mesenchymal differentiation of human embryonic stem cells. *Small* **2013,** *9* (12), 2140-2151.

20. McNamara, L. E.; McMurray, R. J.; Biggs, M. J.; Kantawong, F.; Oreffo, R. O.; Dalby, M. J., Nanotopographical control of stem cell differentiation. *Journal of tissue engineering* **2010,** *1* (1), 120623.

21. Ventre, M.; Natale, C. F.; Rianna, C.; Netti, P. A., Topographic cell instructive patterns to control cell adhesion, polarization and migration. *Journal of the royal society Interface* **2014,** *11* (100), 20140687.

22. Yim, E. K.; Reano, R. M.; Pang, S. W.; Yee, A. F.; Chen, C. S.; Leong, K. W., Nanopattern-induced changes in morphology and motility of smooth muscle cells. *Biomaterials* **2005,** *26* (26), 5405-5413.

23. Bettinger, C. J.; Langer, R.; Borenstein, J. T., Engineering substrate topography at the micro- and nanoscale to control cell function. *Angewandte Chemie International Edition* **2009,** *48* (30), 5406-5415.

24. Yao, X.; Peng, R.; Ding, J., Cell–material interactions revealed via material techniques of surface patterning. *Advanced materials* **2013,** *25* (37), 5257-5286.

25. Watari, S.; Hayashi, K.; Wood, J. A.; Russell, P.; Nealey, P. F.; Murphy, C. J.; Genetos, D. C., Modulation of osteogenic differentiation in hMSCs cells by submicron topographically-patterned ridges and grooves. *Biomaterials* **2012,** *33* (1), 128-136.

26. Dillow, A.; Lowman, A., *Biomimetic materials and design: biointerfacial strategies, tissue engineering and targeted drug delivery*. CRC Press: 2002.

27. Masters, K. S.; Anseth, K. S., Cell–material interactions. *Advances in Chemical Engineering* **2004,** *29*, 7-46.

28. Brunette, D., Fibroblasts on micromachined substrata orient hierarchically to grooves of different dimensions. *Experimental cell research* **1986,** *164* (1), 11-26.

29. Hamilton, D. W.; Oates, C. J.; Hasanzadeh, A.; Mittler, S., Migration of periodontal ligament fibroblasts on nanometric topographical patterns: influence of filopodia and focal adhesions on contact guidance. *PLoS One* **2010,** *5* (12), e15129.

30. Ahn, E. H.; Kim, Y.; An, S. S.; Afzal, J.; Lee, S.; Kwak, M.; Suh, K.-Y.; Kim, D.-H.; Levchenko, A., Spatial control of adult stem cell fate using nanotopographic cues. *Biomaterials* **2014,** *35* (8), 2401-2410.

31. Dalby, M. J.; Gadegaard, N.; Tare, R.; Andar, A.; Riehle, M. O.; Herzyk, P.; Wilkinson, C. D.; Oreffo, R. O., The control of human mesenchymal cell differentiation using nanoscale symmetry and disorder. *Nature materials* **2007,** *6* (12), 997.

32. Santos, E.; Hernández, R. M.; Pedraz, J. L.; Orive, G., Novel advances in the design of three-dimensional bio-scaffolds to control cell fate: translation from 2D to 3D. *Trends in biotechnology* **2012,** *30* (6), 331-341.

33. Liu, H.; Lin, J.; Roy, K., Effect of 3D scaffold and dynamic culture condition on the global gene expression profile of mouse embryonic stem cells. *Biomaterials* **2006,** *27* (36), 5978-5989.

34. Tibbitt, M. W.; Anseth, K. S., Hydrogels as extracellular matrix mimics for 3D cell culture. *Biotechnology and bioengineering* **2009,** *103* (4), 655-663.

35. Barry III, R. A.; Shepherd, R. F.; Hanson, J. N.; Nuzzo, R. G.; Wiltzius, P.; Lewis, J. A., Direct-write assembly of 3D hydrogel scaffolds for guided cell growth. *Advanced materials* **2009,** *21* (23), 2407-2410.

36. Kang, J. H.; Moon, J. H.; Lee, S. K.; Park, S. G.; Jang, S. G.; Yang, S.; Yang, S. M., Thermoresponsive Hydrogel Photonic Crystals by Three-Dimensional Holographic Lithography. *Advanced Materials* **2008,** *20* (16), 3061-3065.

37. Abagnale, G.; Steger, M.; Nguyen, V. H.; Hersch, N.; Sechi, A.; Joussen, S.; Denecke, B.; Merkel, R.; Hoffmann, B.; Dreser, A., Surface topography enhances differentiation of mesenchymal stem cells towards osteogenic and adipogenic lineages. *Biomaterials* **2015,** *61*, 316-326.

38. Murphy, S. V.; Atala, A., 3D bioprinting of tissues and organs. *Nature biotechnology* **2014,** *32* (8), 773.

39. Klein, F.; Richter, B.; Striebel, T.; Franz, C. M.; Freymann, G. v.; Wegener, M.; Bastmeyer, M., Two-component polymer scaffolds for controlled three-dimensional cell culture. *Advanced materials* **2011,** *23* (11), 1341-1345.

40. Ovsianikov, A.; Deiwick, A.; Van Vlierberghe, S.; Dubruel, P.; Möller, L.; Dräger, G.; Chichkov, B., Laser fabrication of three-dimensional CAD scaffolds from photosensitive gelatin for applications in tissue engineering. *Biomacromolecules* **2011,** *12* (4), 851-858.

41. Ovsianikov, A.; Gruene, M.; Pflaum, M.; Koch, L.; Maiorana, F.; Wilhelmi, M.; Haverich, A.; Chichkov, B., Laser printing of cells into 3D scaffolds. *Biofabrication* **2010,** *2* (1), 014104.

42. Murphy, W. L.; McDevitt, T. C.; Engler, A. J., Materials as stem cell regulators. *Nature materials* **2014,** *13* (6), 547.

43. Lam, M. T.; Clem, W. C.; Takayama, S., Reversible on-demand cell alignment using reconfigurable microtopography. *Biomaterials* **2008,** *29* (11), 1705-1712.

44. Guvendiren, M.; Burdick, J. A., Stem cell response to spatially and temporally displayed and reversible surface topography. *Advanced healthcare materials* **2013,** *2* (1), 155-164.

45. Kirschner, C. M.; Anseth, K. S., In situ control of cell substrate microtopographies using photolabile hydrogels. *small* **2013,** *9* (4), 578-584.

46. Le, D. M.; Kulangara, K.; Adler, A. F.; Leong, K. W.; Ashby, V. S., Dynamic Topographical Control of Mesenchymal Stem Cells by Culture on Responsive Poly (ϵ-caprolactone) Surfaces. *Advanced materials* **2011,** *23* (29), 3278-3283.

47. Davis, K. A.; Burke, K. A.; Mather, P. T.; Henderson, J. H., Dynamic cell behavior on shape memory polymer substrates. *Biomaterials* **2011,** *32* (9), 2285-2293.

48. Yakacki, C. M.; Shandas, R.; Lanning, C.; Rech, B.; Eckstein, A.; Gall, K., Unconstrained recovery characterization of shape-memory polymer networks for cardiovascular applications. *Biomaterials* **2007,** *28* (14), 2255-2263.

49. Wang, G.; Zhang, J., Photoresponsive molecular switches for biotechnology. *Journal of Photochemistry and Photobiology C: Photochemistry Reviews* **2012,** *13* (4), 299-309.

50. Fedele, C.; Netti, P.; Cavalli, S., Azobenzene-based polymers: emerging applications as cell culture platforms. *Biomaterials science* **2018**.

51. Goulet-Hanssens, A.; Barrett, C. J., Photo-control of biological systems with azobenzene polymers. *Journal of Polymer Science Part A: Polymer Chemistry* **2013,** *51* (14), 3058-3070.

52. Mahimwalla, Z.; Yager, K. G.; Mamiya, J.-i.; Shishido, A.; Priimagi, A.; Barrett, C. J., Azobenzene photomechanics: prospects and potential applications. *Polymer bulletin* **2012,** *69* (8), 967-1006.

53. Kumar, G. S.; Neckers, D., Photochemistry of azobenzene-containing polymers. *Chemical Reviews* **1989,** *89* (8), 1915-1925.

54. El Halabieh, R. H.; Mermut, O.; Barrett, C. J., Using light to control physical properties of polymers and surfaces with azobenzene chromophores. *Pure and applied chemistry* **2004,** *76* (7-8), 1445-1465.

55. Rau, H., Photoisomerization of azobenzenes. *Photochemistry and photophysics* **1990,** *2*, 119-141.

56. Natansohn, A.; Rochon, P., Photoinduced motions in azo-containing polymers. *Chemical reviews* **2002,** *102* (11), 4139-4176.

57. Wegner, H. A., Azobenzenes in a New Light—Switching In Vivo. *Angewandte Chemie International Edition* **2012,** *51* (20), 4787-4788.

58. Bléger, D.; Schwarz, J.; Brouwer, A. M.; Hecht, S., o-Fluoroazobenzenes as readily synthesized photoswitches offering nearly quantitative two-way isomerization with visible light. *Journal of the American Chemical Society* **2012,** *134* (51), 20597-20600.

59. Siewertsen, R.; Neumann, H.; Buchheim-Stehn, B.; Herges, R.; Näther, C.; Renth, F.; Temps, F., Highly efficient reversible Z− E photoisomerization of a bridged azobenzene with visible light through resolved S1 (nπ*) absorption bands. *Journal of the American Chemical Society* **2009,** *131* (43), 15594-15595.

60. Knie, C.; Utecht, M.; Zhao, F.; Kulla, H.; Kovalenko, S.; Brouwer, A. M.; Saalfrank, P.; Hecht, S.; Bléger, D., ortho-Fluoroazobenzenes: Visible Light Switches with Very Long-Lived Z Isomers. *Chemistry–A European Journal* **2014,** *20* (50), 16492-16501.

61. Samanta, S.; McCormick, T. M.; Schmidt, S. K.; Seferos, D. S.; Woolley, G. A., Robust visible light photoswitching with ortho-thiol substituted azobenzenes. *Chemical Communications* **2013,** *49* (87), 10314-10316.

62. Beharry, A. A.; Sadovski, O.; Woolley, G. A., Azobenzene photoswitching without ultraviolet light. *Journal of the American Chemical Society* **2011,** *133* (49), 19684-19687.

63. Cojocariu, C.; Rochon, P., Light-induced motions in azobenzene-containing polymers. *Pure and applied chemistry* **2004,** *76* (7-8), 1479-1497.

64. Kumar, K.; Knie, C.; Bléger, D.; Peletier, M. A.; Friedrich, H.; Hecht, S.; Broer, D. J.; Debije, M. G.; Schenning, A. P. H. J., A chaotic self-oscillating sunlight-driven polymer actuator. *Nature Communications* **2016,** *7*, 11975.

65. Weis, P.; Tian, W.; Wu, S., Photoinduced Liquefaction of Azobenzene-Containing Polymers. *Chemistry-A European Journal* **2017**.

66. Yager, K. G.; Barrett, C. J., Light-induced nanostructure formation using azobenzene polymers. *Polymeric Nanostructures and Their Applications 0* **2006**, 1-38.

67. Barrett, C. J.; Mamiya, J.-i.; Yager, K. G.; Ikeda, T., Photo-mechanical effects in azobenzene-containing soft materials. *Soft Matter* **2007,** *3* (10), 1249-1261.

68. Ikeda, T.; Nakano, M.; Yu, Y.; Tsutsumi, O.; Kanazawa, A., Anisotropic Bending and Unbending Behavior of Azobenzene Liquid-Crystalline Gels by Light Exposure. *Advanced Materials* **2003,** *15* (3), 201-205.

69. Yamada, M.; Kondo, M.; Miyasato, R.; Naka, Y.; Mamiya, J.-i.; Kinoshita, M.; Shishido, A.; Yu, Y.; Barrett, C. J.; Ikeda, T., Photomobile polymer materials—various three-dimensional movements. *Journal of Materials Chemistry* **2009,** *19* (1), 60-62.

70. Finkelmann, H.; Nishikawa, E.; Pereira, G.; Warner, M., A new opto-mechanical effect in solids. *Physical Review Letters* **2001,** *87* (1), 015501.

71. Yin, R.; Xu, W.; Kondo, M.; Yen, C.-C.; Mamiya, J.-i.; Ikeda, T.; Yu, Y., Can sunlight drive the photoinduced bending of polymer films? *Journal of Materials Chemistry* **2009,** *19* (20), 3141-3143.

72. Yadavalli, N. S.; Loebner, S.; Papke, T.; Sava, E.; Hurduc, N.; Santer, S., A comparative study of photoinduced deformation in azobenzene containing polymer films. *Soft Matter* **2016,** *12* (9), 2593-2603.

73. Saphiannikova, M.; Toshchevikov, V.; Ilnytskyi, J., Photoinduced deformations in azobenzene polymer films. *Nonlinear Opt., Quantum Opt* **2010,** *41*, 27-57.

74. Karageorgiev, P.; Neher, D.; Schulz, B.; Stiller, B.; Pietsch, U.; Giersig, M.; Brehmer, L., From anisotropic photo-fluidity towards nanomanipulation in the optical near-field. *Nature materials* **2005,** *4* (9), 699.

75. Rochon, P.; Batalla, E.; Natansohn, A., Optically induced surface gratings on azoaromatic polymer films. *Applied Physics Letters* **1995,** *66* (2), 136-138.

76. Kim, D.; Tripathy, S.; Li, L.; Kumar, J., Laser-induced holographic surface relief gratings on nonlinear optical polymer films. *Applied Physics Letters* **1995,** *66* (10), 1166-1168.

77. Ahmadi-Kandjani, S.; Tajalli, P.; Khoshsima, H.; Barille, R.; Nunzi, J.-M.; Kucharski, S.; Tajalli, H., Birefringence properties and surface relief grating formation on methylacrylate polymers with photochromic side chains. **2010**.

78. Kim, D.; Li, L.; Shivshankar, V.; Kumar, J.; Tripathy, S. *Polarized Laser Induced Holographic Surface Relief Gratings on Polymer Films*; MASSACHUSETTS UNIV LOWELL DEPT OF CHEMISTRY: 1995.

79. Jeng, R.; Chen, Y.; Kumar, J.; Tripathy, S., Novel crosslinked guest-host system with stable second-order nonlinearity. *Journal of Macromolecular Science—Pure and Applied Chemistry* **1992,** *29* (12), 1115-1127.

80. Hurduc, N.; Donose, B. C.; Macovei, A.; Paius, C.; Ibanescu, C.; Scutaru, D.; Hamel, M.; Branza-Nichita, N.; Rocha, L., Direct observation of athermal photofluidisation in azo-polymer films. *Soft Matter* **2014,** *10* (26), 4640-4647.

81. Bian, S.; Williams, J. M.; Kim, D. Y.; Li, L.; Balasubramanian, S.; Kumar, J.; Tripathy, S., Photoinduced surface deformations on azobenzene polymer films. *Journal of Applied Physics* **1999,** *86* (8), 4498-4508.

82. Bian, S.; Li, L.; Kumar, J.; Kim, D.; Williams, J.; Tripathy, S., Single laser beam-induced surface deformation on azobenzene polymer films. *Applied Physics Letters* **1998,** *73* (13), 1817-1819.

83. Grosjean, T.; Courjon, D., Photopolymers as vectorial sensors of the electric field. *Optics Express* **2006,** *14* (6), 2203-2210.

84. Noga, J.; Sobolewska, A.; Bartkiewicz, S.; Virkki, M.; Priimagi, A., Periodic Surface Structures Induced by a Single Laser Beam Irradiation. *Macromolecular Materials and Engineering* **2017,** *302* (2).

85. Ishitobi, H.; Tanabe, M.; Sekkat, Z.; Kawata, S., The anisotropic nanomovement of azo-polymers. *Optics express* **2007,** *15* (2), 652-659.

86. Ishitobi, H.; Shoji, S.; Hiramatsu, T.; Sun, H.-B.; Sekkat, Z.; Kawata, S., Two-photon induced polymer nanomovement. *Optics Express* **2008,** *16* (18), 14106-14114.

87. Rianna, C.; Rossano, L.; Kollarigowda, R. H.; Formiggini, F.; Cavalli, S.; Ventre, M.; Netti, P. A., Dynamic Cell Substrates: Spatio-Temporal Control of Dynamic Topographic Patterns on Azopolymers for Cell Culture Applications (Adv. Funct. Mater. 42/2016). *Advanced Functional Materials* **2016,** *26* (42), 7743-7743.

88. Ambrosio, A.; Camposeo, A.; Carella, A.; Borbone, F.; Pisignano, D.; Roviello, A.; Maddalena, P., Realization of submicrometer structures by a confocal system on azopolymer films containing photoluminescent chromophores. *Journal of Applied Physics* **2010,** *107* (8), 083110.

89. Hubert, C.; Fiorini-Debuisschert, C.; Maurin, I.; Nunzi, J. M.; Raimond, P., Spontaneous Patterning of Hexagonal Structures in an Azo-Polymer Using Light-Controlled Mass Transport. *Advanced Materials* **2002,** *14* (10), 729-732.

90. Galinski, H.; Ambrosio, A.; Maddalena, P.; Schenker, I.; Spolenak, R.; Capasso, F., Instability-induced pattern formation of photoactivated functional polymers. *Proceedings of the National Academy of Sciences* **2014,** *111* (48), 17017-17022.

91. Kang, H. S.; Lee, S.; Park, J. K., Monolithic, Hierarchical Surface Reliefs by Holographic Photofluidization of Azopolymer Arrays: Direct Visualization of Polymeric Flows. *Advanced Functional Materials* **2011,** *21* (23), 4412-4422.

92. Lee, S.; Shin, J.; Lee, Y.-H.; Fan, S.; Park, J.-K., Directional photofluidization lithography for nanoarchitectures with controlled shapes and sizes. *Nano letters* **2009,** *10* (1), 296-304.

93. Lee, S.; Kang, H. S.; Ambrosio, A.; Park, J.-K.; Marrucci, L., Directional superficial photofluidization for deterministic shaping of complex 3d architectures. *ACS applied materials & interfaces* **2015,** *7* (15), 8209-8217.

94. Pirani, F.; Angelini, A.; Frascella, F.; Rizzo, R.; Ricciardi, S.; Descrovi, E., Light-Driven Reversible Shaping of Individual Azopolymeric Micro-Pillars. *Scientific reports* **2016,** *6*.

95. Lee, S.; Kang, H. S.; Park, J. K., Directional photofluidization lithography: micro/nanostructural evolution by photofluidic motions of azobenzene materials. *Advanced Materials* **2012,** *24* (16), 2069-2103.

96. Pirani, F.; Angelini, A.; Frascella, F.; Rizzo, R.; Ricciardi, S.; Descrovi, E., Light-driven reversible shaping of individual azopolymeric micro-pillars. *Scientific reports* **2016,** *6*, 31702.

97. Oscurato, S. L.; Borbone, F.; Maddalena, P.; Ambrosio, A., Light-driven wettability tailoring of azopolymer surfaces with reconfigured three-dimensional posts. *ACS applied materials & interfaces* **2017,** *9* (35), 30133-30142.

98. Pirani, F.; Angelini, A.; Ricciardi, S.; Frascella, F.; Descrovi, E., Laser-induced anisotropic wettability on azopolymeric micro-structures. *Applied Physics Letters* **2017,** *110* (10), 101603.

99. Choi, J.; Cho, W.; Jung, Y. S.; Kang, H. S.; Kim, H.-T., Direct fabrication of micro/nano-patterned surfaces by vertical-directional photofluidization of azobenzene materials. *ACS nano* **2017,** *11* (2), 1320-1327.

100. Ubukata, T.; Isoshima, T.; Hara, M., Wavelength-Programmable Organic Distributed-Feedback Laser Based on a Photoassisted Polymer-Migration System. *Advanced Materials* **2005,** *17* (13), 1630-1633.

101. Hurduc, N.; Macovei, A.; Paius, C.; Raicu, A.; Moleavin, I.; Branza-Nichita, N.; Hamel, M.; Rocha, L., Azo-polysiloxanes as new supports for cell cultures. *Materials Science and Engineering: C* **2013,** *33* (4), 2440-2445.

102. Baac, H.; Lee, J.-H.; Seo, J.-M.; Park, T. H.; Chung, H.; Lee, S.-D.; Kim, S. J., Submicron-scale topographical control of cell growth using holographic surface relief grating. *Materials Science and Engineering: C* **2004,** *24* (1-2), 209-212.

103. Barille, R.; Janik, R.; Kucharski, S.; Eyer, J.; Letournel, F., Photo-responsive polymer with erasable and reconfigurable micro-and nano-patterns: an in vitro study for neuron guidance. *Colloids and Surfaces B: Biointerfaces* **2011,** *88* (1), 63-71.

104. Koçer, G.; ter Schiphorst, J.; Hendrikx, M.; Kassa, H. G.; Leclère, P.; Schenning, A. P.; Jonkheijm, P., Light-Responsive Hierarchically Structured Liquid Crystal Polymer Networks for Harnessing Cell Adhesion and Migration. *Advanced materials* **2017,** *29* (27).

105. Martella, D.; Paoli, P.; Pioner, J. M.; Sacconi, L.; Coppini, R.; Santini, L.; Lulli, M.; Cerbai, E.; Wiersma, D. S.; Poggesi, C., Liquid crystalline networks toward regenerative medicine and tissue repair. *Small* **2017,** *13* (46), 1702677.

106. Pittenger, M. F.; Mackay, A. M.; Beck, S. C.; Jaiswal, R. K.; Douglas, R.; Mosca, J. D.; Moorman, M. A.; Simonetti, D. W.; Craig, S.; Marshak, D. R., Multilineage potential of adult human mesenchymal stem cells. *science* **1999,** *284* (5411), 143-147.

107. Lagunas, A.; Caballero, D.; Samitier, J., Influence of Controlled Micro-and Nanoengineered Environments on Stem Cell Fate. *Advanced Surfaces for Stem Cell Research* **2016**, 87-141.

108. McBeath, R.; Pirone, D. M.; Nelson, C. M.; Bhadriraju, K.; Chen, C. S., Cell shape, cytoskeletal tension, and RhoA regulate stem cell lineage commitment. *Developmental cell* **2004,** *6* (4), 483-495.

109. Kilian, K. A.; Bugarija, B.; Lahn, B. T.; Mrksich, M., Geometric cues for directing the differentiation of mesenchymal stem cells. *Proceedings of the National Academy of Sciences* **2010,** *107* (11), 4872-4877.

110. Woodbury, D.; Schwarz, E. J.; Prockop, D. J.; Black, I. B., Adult rat and human bone marrow stromal cells differentiate into neurons. *Journal of neuroscience research* **2000,** *61* (4), 364-370.

111. Yim, E. K.; Pang, S. W.; Leong, K. W., Synthetic nanostructures inducing differentiation of human mesenchymal stem cells into neuronal lineage. *Experimental cell research* **2007,** *313* (9), 1820-1829.

112. Chen, A.; Lieu, D. K.; Freschauf, L.; Lew, V.; Sharma, H.; Wang, J.; Nguyen, D.; Karakikes, I.; Hajjar, R. J.; Gopinathan, A., Shrink-film configurable multiscale wrinkles for functional alignment of human embryonic stem cells and their cardiac derivatives. *Advanced Materials* **2011,** *23* (48), 5785-5791.

113. Anselme, K.; Ploux, L.; Ponche, A., Cell/material interfaces: influence of surface chemistry and surface topography on cell adhesion. *Journal of Adhesion Science and Technology* **2010,** *24* (5), 831-852.

114. Dalby, M. J.; McCloy, D.; Robertson, M.; Agheli, H.; Sutherland, D.; Affrossman, S.; Oreffo, R. O., Osteoprogenitor response to semi-ordered and random nanotopographies. *Biomaterials* **2006,** *27* (15), 2980-2987.

115. Rianna, C.; Calabuig, A.; Ventre, M.; Cavalli, S.; Pagliarulo, V.; Grilli, S.; Ferraro, P.; Netti, P. A., Reversible holographic patterns on azopolymers for guiding cell adhesion and orientation. *ACS applied materials & interfaces* **2015,** *7* (31), 16984-16991.

116. Rianna, C.; Rossano, L.; Kollarigowda, R. H.; Formiggini, F.; Cavalli, S.; Ventre, M.; Netti, P. A., Spatio-Temporal Control of Dynamic Topographic Patterns on Azopolymers for Cell Culture Applications. *Advanced Functional Materials* **2016,** *26* (42), 7572-7580.

117. Guilak, F.; Cohen, D. M.; Estes, B. T.; Gimble, J. M.; Liedtke, W.; Chen, C. S., Control of stem cell fate by physical interactions with the extracellular matrix. *Cell stem cell* **2009,** *5* (1), 17-26.

118. Mathieu, P. S.; Loboa, E. G., Cytoskeletal and focal adhesion influences on mesenchymal stem cell shape, mechanical properties, and differentiation down osteogenic, adipogenic, and chondrogenic pathways. *Tissue Engineering Part B: Reviews* **2012,** *18* (6), 436-444.

119. Lagunas, A.; Caballero, D.; Samitier, J., Influence of Controlled Micro-and Nanoengineered Environments on Stem Cell Fate. *Advanced Surfaces for Stem Cell Research* **2016**, 87-141.

120. Burdick, J. A.; Vunjak-Novakovic, G., Engineered microenvironments for controlled stem cell differentiation. *Tissue Engineering Part A* **2008,** *15* (2), 205-219.

121. Yang, Y.; Wang, K.; Gu, X.; Leong, K. W., Biophysical regulation of cell behavior—cross talk between substrate stiffness and nanotopography. *Engineering* **2017,** *3* (1), 36-54.

122. Ebara, M.; Akimoto, M.; Uto, K.; Shiba, K.; Yoshikawa, G.; Aoyagi, T., Focus on the interlude between topographic transition and cell response on shape-memory surfaces. *Polymer* **2014,** *55* (23), 5961-5968.

123. Gong, T.; Zhao, K.; Yang, G.; Li, J.; Chen, H.; Chen, Y.; Zhou, S., The control of mesenchymal stem cell differentiation using dynamically tunable surface microgrooves. *Advanced healthcare materials* **2014,** *3* (10), 1608-1619.

124. Gong, T.; Lu, L.; Liu, D.; Liu, X.; Zhao, K.; Chen, Y.; Zhou, S., Dynamically tunable polymer microwells for directing mesenchymal stem cell differentiation into osteogenesis. *Journal of Materials Chemistry B* **2015,** *3* (46), 9011-9022.

125. Russew, M. M.; Hecht, S., Photoswitches: from molecules to materials. *Advanced Materials* **2010,** *22* (31), 3348-3360.

126. Abdallah, B.; Kassem, M., Human mesenchymal stem cells: from basic biology to clinical applications. *Gene therapy* **2008,** *15* (2), 109.

127. Engler, A. J.; Sen, S.; Sweeney, H. L.; Discher, D. E., Matrix elasticity directs stem cell lineage specification. *Cell* **2006,** *126* (4), 677-689.

128. Lee, J.; Abdeen, A. A.; Kilian, K. A., Rewiring mesenchymal stem cell lineage specification by switching the biophysical microenvironment. *Scientific reports* **2014,** *4*, 5188.

129. Itano, N.; Okamoto, S.-i.; Zhang, D.; Lipton, S. A.; Ruoslahti, E., Cell spreading controls endoplasmic and nuclear calcium: a physical gene regulation pathway from the cell surface to the nucleus. *Proceedings of the National Academy of Sciences* **2003,** *100* (9), 5181-5186.

130. Hui-Chun Ho, J.; Ma, W. H.; Su, Y.; Tseng, K. C.; Kwang-Chun Kuo, T.; Kuang-Sheng Lee, O., Thymosin beta-4 directs cell fate determination of human mesenchymal stem cells through biophysical effects. *Journal of Orthopaedic Research* **2010,** *28* (1), 131-138.

131. Rochon, P.; Gosselin, J.; Natansohn, A.; Xie, S., Optically induced and erased birefringence and dichroism in azoaromatic polymers. *Applied Physics Letters* **1992,** *60* (1), 4-5.

132. Lee, M. R.; Kwon, K. W.; Jung, H.; Kim, H. N.; Suh, K. Y.; Kim, K.; Kim, K.-S., Direct differentiation of human embryonic stem cells into selective neurons on nanoscale ridge/groove pattern arrays. *Biomaterials* **2010,** *31* (15), 4360-4366.

133. Zanchetta, E.; Guidi, E.; Della Giustina, G.; Sorgato, M.; Krampera, M.; Bassi, G.; Di Liddo, R.; Lucchetta, G.; Conconi, M. T.; Brusatin, G., Injection molded polymeric micropatterns for bone regeneration study. *ACS applied materials & interfaces* **2015,** *7* (13), 7273-7281.

134. Pajerowski, J. D.; Dahl, K. N.; Zhong, F. L.; Sammak, P. J.; Discher, D. E., Physical plasticity of the nucleus in stem cell differentiation. *Proceedings of the National Academy of Sciences* **2007,** *104* (40), 15619-15624.

135. Treiser, M. D.; Yang, E. H.; Gordonov, S.; Cohen, D. M.; Androulakis, I. P.; Kohn, J.; Chen, C. S.; Moghe, P. V., Cytoskeleton-based forecasting of stem cell lineage fates. *Proceedings of the National Academy of Sciences* **2010,** *107* (2), 610-615.

136. Anselme, K., Osteoblast adhesion on biomaterials. *Biomaterials* **2000,** *21* (7), 667-681.

137. Natale, C. F.; Ventre, M.; Netti, P. A., Tuning the material-cytoskeleton crosstalk via nanoconfinement of focal adhesions. *Biomaterials* **2014,** *35* (9), 2743-2751.

138. Henderson, E.; Haydon, P.; Sakaguchi, D., Actin filament dynamics in living glial cells imaged by atomic force microscopy. *Science* **1992,** *257* (5078), 1944-1946.

139. Iannone, M.; Ventre, M.; Formisano, L.; Casalino, L.; Patriarca, E. J.; Netti, P. A., Nanoengineered surfaces for focal adhesion guidance trigger mesenchymal stem cell self-organization and tenogenesis. *Nano letters* **2015,** *15* (3), 1517-1525.

140. Lam, M. T.; Sim, S.; Zhu, X.; Takayama, S., The effect of continuous wavy micropatterns on silicone substrates on the alignment of skeletal muscle myoblasts and myotubes. *Biomaterials* **2006,** *27* (24), 4340-4347.

141. Martinez, E.; Engel, E.; Planell, J.; Samitier, J., Effects of artificial micro-and nano-structured surfaces on cell behaviour. *Annals of Anatomy-Anatomischer Anzeiger* **2009,** *191* (1), 126-135.

142. Kilian, K. A.; Bugarija, B.; Lahn, B. T.; Mrksich, M., Geometric cues for directing the differentiation of mesenchymal stem cells. *Proceedings of the National Academy of Sciences* **2010**.
143. Lin, G. L.; Hankenson, K. D., Integration of BMP, Wnt, and notch signaling pathways in osteoblast differentiation. *Journal of cellular biochemistry* **2011,** *112* (12), 3491-3501.
144. Augello, A.; De Bari, C., The regulation of differentiation in mesenchymal stem cells. *Human gene therapy* **2010,** *21* (10), 1226-1238.
145. Wang, L.; Li, Z.-y.; Wang, Y.-p.; Wu, Z.-h.; Yu, B., Dynamic expression profiles of marker genes in osteogenic differentiation of human bone marrow-derived mesenchymal stem cells. *中国医学科学杂志* **2015,** *30* (2), 108-113.
146. Lee, J.; Abdeen, A. A.; Kilian, K. A., Rewiring mesenchymal stem cell lineage specification by switching the biophysical microenvironment. *Scientific reports* **2014,** *4*.
147. Lee, E. M. Influence of static and dynamic topography on osteoblast proliferation and maturation. Georgia Institute of Technology, 2016.
148. Carvalho, A.; Pelaez-Vargas, A.; Hansford, D. J.; Fernandes, M. H.; Monteiro, F. J., Effects of line and pillar array microengineered SiO2 thin films on the osteogenic differentiation of human bone marrow-derived mesenchymal stem cells. *Langmuir* **2016,** *32* (4), 1091-1100.
149. Hanson, L.; Lin, Z. C.; Xie, C.; Cui, Y.; Cui, B., Characterization of the cell–nanopillar interface by transmission electron microscopy. *Nano letters* **2012,** *12* (11), 5815-5820.
150. Hanson, L.; Zhao, W.; Lou, H.-Y.; Lin, Z. C.; Lee, S. W.; Chowdary, P.; Cui, Y.; Cui, B., Vertical nanopillars for in situ probing of nuclear mechanics in adherent cells. *Nature nanotechnology* **2015,** *10* (6), 554-562.
151. Ebara, M.; Uto, K.; Idota, N.; Hoffman, J. M.; Aoyagi, T., The taming of the cell: shape-memory nanopatterns direct cell orientation. *International journal of nanomedicine* **2014,** *9* (Suppl 1), 117.
152. Lou, H.-Y.; Zhao, W.; Zeng, Y.; Cui, B., The Role of Membrane Curvature in Nanoscale Topography-Induced Intracellular Signaling. *Accounts of chemical research* **2018,** *51* (5), 1046-1053.
153. Bandara, H. D.; Burdette, S. C., Photoisomerization in different classes of azobenzene. *Chemical Society Reviews* **2012,** *41* (5), 1809-1825.
154. Cui, B. a. c., Unpublished results.
155. Zhao, W.; Hanson, L.; Lou, H.-Y.; Akamatsu, M.; Chowdary, P.; Santoro, F.; Marks, J.; Grassart, A.; Drubin, D.; Cui, Y., Nanoscale manipulation of membrane curvature for probing endocytosis in live cells. *bioRxiv* **2017**, 122275.

156. McMahon, H. T.; Gallop, J. L., Membrane curvature and mechanisms of dynamic cell membrane remodelling. *Nature* **2005,** *438* (7068), 590.

157. Lee, S.; Kang, H. S.; Park, J. K., High-Resolution Patterning of Various Large-Area, Highly Ordered Structural Motifs by Directional Photofluidization Lithography: Sub-30-nm Line, Ellipsoid, Rectangle, and Circle Arrays. *Advanced Functional Materials* **2011,** *21* (10), 1770-1778.

158. Tsujita, K.; Takenawa, T.; Itoh, T., Feedback regulation between plasma membrane tension and membrane-bending proteins organizes cell polarity during leading edge formation. *Nature cell biology* **2015,** *17* (6), 749.

159. Dhowre, H. S.; Rajput, S.; Russell, N. A.; Zelzer, M., Responsive cell-material interfaces. *Nanomedicine* **2015,** *10* (5), 849-871.

160. Viswanathan, N.; Kim, D.; Tripathy, S., Surface relief structures on azo polymer films. *Journal of Materials Chemistry* **1999,** *9* (9), 1941-1955.

161. Pennacchio, F. A.; Fedele, C.; De Martino, S.; Cavalli, S.; Vecchione, R.; Netti, P. A., 3D Microstructured Azobenzene-Containing Gelatin as Photoactuable Cell Confining System. *ACS applied materials & interfaces* **2017**.

162. Galli, C.; Piemontese, M.; Lumetti, S.; Ravanetti, F.; Macaluso, G.; Passeri, G., Actin cytoskeleton controls activation of Wnt/β-catenin signaling in mesenchymal cells on implant surfaces with different topographies. *Acta biomaterialia* **2012,** *8* (8), 2963-2968.

163. Sun, Y.; Chen, C. S.; Fu, J., Forcing stem cells to behave: a biophysical perspective of the cellular microenvironment. *Annual review of biophysics* **2012,** *41*, 519-542.

164. Habeeb, A. S. A., Determination of free amino groups in proteins by trinitrobenzenesulfonic acid. *Analytical biochemistry* **1966,** *14* (3), 328-336.

165. Ovsianikov, A.; Mühleder, S.; Torgersen, J.; Li, Z.; Qin, X.-H.; Van Vlierberghe, S.; Dubruel, P.; Holnthoner, W.; Redl, H.; Liska, R., Laser photofabrication of cell-containing hydrogel constructs. *Langmuir* **2013,** *30* (13), 3787-3794.

166. Nguyen, L.; Straub, M.; Gu, M., Acrylate-Based Photopolymer for Two-Photon Microfabrication and Photonic Applications. *Adv. Funct. Mater.* **2005,** *15* (2), 209-216.

167. Vaselli, E.; Fedele, C.; Cavalli, S.; Netti, P. A., "On–Off" RGD Signaling Using Azobenzene Photoswitch-Modified Surfaces. *ChemPlusChem* **2015,** *80* (10), 1547-1555.

168. Liang, H. C.; Chang, W. H.; Liang, H. F.; Lee, M. H.; Sung, H. W., Crosslinking structures of gelatin hydrogels crosslinked with genipin or a water-soluble carbodiimide. *Journal of Applied Polymer Science* **2004,** *91* (6), 4017-4026.

169. Deiber, J. A.; Ottone, M. L.; Piaggio, M. V.; Peirotti, M. B., Characterization of cross-linked polyampholytic gelatin hydrogels through the rubber elasticity and thermodynamic swelling theories. *Polymer* **2009,** *50* (25), 6065-6075.

170. Van Den Bulcke, A. I.; Bogdanov, B.; De Rooze, N.; Schacht, E. H.; Cornelissen, M.; Berghmans, H., Structural and rheological properties of methacrylamide modified gelatin hydrogels. *Biomacromolecules* **2000,** *1* (1), 31-38.

171. Billiet, T.; Gasse, B. V.; Gevaert, E.; Cornelissen, M.; Martins, J. C.; Dubruel, P., Quantitative Contrasts in the Photopolymerization of Acrylamide and Methacrylamide-Functionalized Gelatin Hydrogel Building Blocks. *Macromolecular bioscience* **2013,** *13* (11), 1531-1545.

172. Lu, P.; Takai, K.; Weaver, V. M.; Werb, Z., Extracellular matrix degradation and remodeling in development and disease. *Cold Spring Harbor perspectives in biology* **2011,** *3* (12), a005058.

173. Kurpinski, K.; Chu, J.; Hashi, C.; Li, S., Anisotropic mechanosensing by mesenchymal stem cells. *Proceedings of the National Academy of Sciences* **2006,** *103* (44), 16095-16100.

174. Rosales, A. M.; Mabry, K. M.; Nehls, E. M.; Anseth, K. S., Photoresponsive elastic properties of azobenzene-containing poly (ethylene-glycol)-based hydrogels. *Biomacromolecules* **2015,** *16* (3), 798-806.